EV BATTERIES AND CHARGING SOLUTIONS

D 4.1: EV batteries and charging solutions models. (M14)

Date: **30/03/2021**
Author(s): **Natascia Andrenacci (ENEA)**
Co-author(s): **Manlio Pasquali, Federico Haig Karagulian, Antonino Genovese (ENEA)**

This project has received funding from the European Union's Horizon 2020 research and innovation programme under grant agreement No [875187]

Deliverable details

Project number	Project acronym	Project title
875187	USER-CHI	Innovative solutions for USER centric Charging Infrastructure

Title	WP	Version
EV batteries and charging solutions models	4	1.0

Contractual delivery date	Actual delivery date	Delivery type*
M14 (March 2021)	M14 (March 2021)	R

*Delivery type: **R**: Document, report; **DEM**: Demonstrator, pilot, prototype; **DEC**: Websites, patent fillings, videos, etc; **OTHER**; **ETHICS**: Ethics requirement; **ORDP**: Open Research Data Pilot.

Author(s)	Organisation
Natascia Andrenacci	ENEA

Document history

Version	Date	Person	Action	Status*	Dissemination level**
V0.1	11/03/2021	Natascia Andrenacci (ENEA)	Document ready for review	Draft	CO
V0.2	22/03/2021	Maria Tomás (ETRA I+D)	Peer-review	Draft	CO
V1.0	26/03/2021	Natascia Andrenacci (ENEA)	Final version	Final	PU

*Status: Draft, Final, Approved, Submitted (to European Commission).

Dissemination Level: **PU: Public; **CO**: Confidential, only for members of the consortium (including the Commission Services); **EU-RES** Classified Information - restraint UE; **EU-CON**: Classified Information - confidential UE; **EU-SEC**: Classified Information - secret UE

Abstract

One of the objectives of the USER-CHI project is the implementation of a smart grid integration module (SMAC, Product P6) minimising the grid impact associated to the implementation of charging infrastructure while providing high-value services for citizens and cities.

In this work we illustrate the results regarding models of charging infrastructures for electric vehicles that adequately define and formalise their flexibility, control and response capabilities to be integrated into the smart grid. The report analyses various insights of the charging infrastructure, such as the components for an optimal investment starting from real data on electric charging events of the demo-cities. In particular, the economic and functional impact of the introduction of renewable energy sources and battery energy storage systems dedicated to shaving load peaks was assessed. In addition, we illustrated algorithms and models for describing the response of electric vehicle batteries and the charging infrastructure for optimal charging and discharging actions.

Keywords

Charging infrastructure, battery modeling, power fluxes analysis, charging algorithm.

Copyright statement

Executive summary

The purpose of the USER-CHI deliverable D4.1 “EV batteries and charging solutions models” is to illustrate the results of task T4.1, “Modelling of EV batteries and charging solutions” which is devoted to model the different aspects and interactions involved in the charging process.

The document begins with data analysis of demo-cities datasets for charging events representing the benchmark for our analysis. Charging strategies are presented and validated using appropriate models for electric vehicles battery. The document includes the planning of a charging infrastructure integrated with a PV-battery system, considering costs and operational aspects, including V2G aspects.

The USER-CHI task T4.1 is part of the WP 4 which is devoted to the development of the product P6 SMAC, implemented in tasks T4.2-T4.4.

Table of contents

List of figures

List of tables

1. Introduction

1.1 Scope of the document

This report illustrates the results of the work carried out in activity T4.1 "Modelling of EV batteries and charging solutions", aimed at identifying the main characteristics of a charging structure and its interaction with users and the electricity grid. It contains the analysis of data on charging events carried out in 2019 in some of the cities participating in the USER-CHI project. The data are intended to numerically validate the models created in the activities of the task.

To evaluate the operation of a charging station, the power flows were identified, as well as the main characteristics of the components of the charging process, including the batteries of electric vehicles. In this regard, different models were compared concerning the response of variables of interest.

Approaches for charging algorithms have also been proposed to shave the peak demand at the station, including the possibility of bidirectional power flows with the vehicle batteries. The effects on the charging profile, and the feasibility from the point of view of the user, are analysed.

Finally, a system for the optimal sizing and management of a charging infrastructure equipped with a photovoltaic and battery stationary storage system has been evaluated on the case studies of some demo-cities.

1.2 Structure of the document

The document is structured as follows. After the Introduction, Chapter 2 is dedicated to the analysis of data on charging events in 2019 from the cities of Turku, Rome, and the metropolitan area of the city of Barcelona.

Chapter 3 is dedicated to the modelling of automotive batteries to evaluate their response to different algorithms, strategies, and proposed profiles. It also illustrates a fuzzy-type approach to manage recharges in a hypothetical charging station.

Chapter 4 focuses on the design, economic and technical feasibility of a charging station integrated with a renewable energy source and storage system. From the sizing we move to the evaluation of the power flows typical of the operating station.

Chapter 5 contains the conclusions. Annex A collects a review of electrochemical energy storage technologies, while Annex B illustrates some aspects related to battery aging. Annex C reports the answers to a questionnaire submitted to cities on some issues relating to the charging infrastructures in their territory.

2. Charging events datasets and analysis

The available datasets came from the Municipal Area of Barcelona (AMB) and from the city of Turku, and have the following structures:

- AMB data set:
    - "HISTORIC DATA 2019 ELECTROLINERES AMB.xlsx" with the following records: CHARGING POINT; CONNECTOR; START TIME; STOP TIME; DURATION (min); VEHICLE; MODEL
    - "STATIC INFORMATION CHARGING POINTS AMB 29042020.xlsx", with the following records: Location, longitude, latitude, Schuko 3kW 16A mode 1, Mennekes 7 kW 16A mode 3, Mennekes 43 kW 63A mode 3, CHAdeMO 55kW 125A mode 4, Observations, Maker
- Turku data set: "Lataustapahtumat, julkiset latauslaitteet 2019.xlsx" with records: Created, Station ID, Station name, Start time, Stop time, Duration, Energy (Wh), Plug Type (AC/DC), Cumulative energy (Wh)

In AMB data, "normal" chargers include 3 kW and 7 kW, while "quick" refers to 43 kW and 55 kW. In Turku dataset, AC refers to 22 kW and DC to 50 kW.

We also analyze the Rome data set, but the results are not used, since this data set contains only aggregated information.

2.1 AMB

From the original AMB dataset (38219 charging registrations), we removed 1806 records with zero energy exchange (around 4.7% of the dataset). The average parking time duration of these records is 45.96 minutes, ranging from 5 minutes up to about 10 days.

Moreover, we disregard 220 records in which the average charging power (energy/duration(h)) is greater than the maximum nominal power of the charging point (as obtained from registrations in AMB dataset").

After the above filtering, we obtained a dataset of 36193 records with an average charging duration of 45.67 minutes and a standard deviation of 704.5 minutes, while the average energy delivered is 10 kWh with a standard deviation of 7.7 kWh.

When selecting only normal chargers (slow: 3kW or 7kW), we obtain 3155 records with an average charging duration of 223.6 minutes and a standard deviation of 2377.7, while the average energy delivered is 4.1 kWh with a standard deviation of 4.9 kWh. However, we disregard a record with a charging duration of over 92 days referred to the charging point “FLNR Sant Andreu da la Barca: Pg. Rafael de Casanova FGC”, which is the only one with 7kW power delivered. On the other hands, 8 records exceeding the 24 hours duration are included. The relevant statistical parameters for the AMB dataset (mean value and standard deviation) are reported in Table 1.

Table 1: Statistical parameters for AMB datasets

Dataset	Mean duration (min)	St. dev duration (min)	Mean energy (kWh)	St. dev energy (kWh)
Entire	41.99	90.37	10.09	7.76
Normal	181.56	262.96	4.11	4.91
Quick	28.67	17.57	10.66	7.74

Table 2 reports some figures on the usage of the CPs based on their typology such as the average number of charges during the year and in a day. Last two columns report the value for the most and less crowded CPs. In Table 3 it is reported the number of charges for each location, for normal and quick chargers.

Table 2: Usage of charging points for different typology

Charge typology	No. charge/year	No. charge/day	Max charge/day	Min charge/day
Normal	286.7	0.79	1.69	0.15
Quick	3302.9	9.05	14.03	3.78

Table 3: Usage of charging points for each location

Location	Normal CP Id	No. Of charges (year)	Quick CP Id	No. Of charges (year)	Total no. Of charges (year)
Sant Andreu da la Barca: Pg. Rafael de Casanova FGC	1	280			280
Badalona: C. Anna Tugas - Pg. Olof Palmer	2	269	12	1582	1851
Barberà del Vallés: C. Arquímedes, 8	3	55	13	2399	2454

Location	Normal CP Id	No. Of charges (year)	Quick CP Id	No. Of charges (year)	Total no. Of charges (year)
Cornellà de Llobregat: Carrer de Baltasar Oriol i Mercer	4	315	14	4679	4994
El Prat de Llobregat: Pl. Volateria (Mas Blau)	5	72	15	3704	3776
Gavà: C. del Progres, 54	6	616	16	5121	5737
L'Hospitalet de Ll.: C. Salvador Espriu - Gran Via de les Corts Catalanes	7	257	17	3824	4081
Montcada i Reixac: C. Tarragona - C. Pla de Matabous	8	171	18	1378	1549
Pallejà: Rda. Santa Eulalia - C. Joan Maragall	9	397	19	2389	2786
Sant Cugat del Vallès: Av. Via Augusta, 3	10	201	20	4305	4506
Sant Joan Despí: C. TV3 - C. Jacint Verdaguer	11	521	21	3648	4169

In Figure 1, the mean value of the energy and standard deviation for normal charges are presented.

Figure 1: Mean value and standard deviation of the energy delivered during the charge of normal chargers (3 and 7 kW).

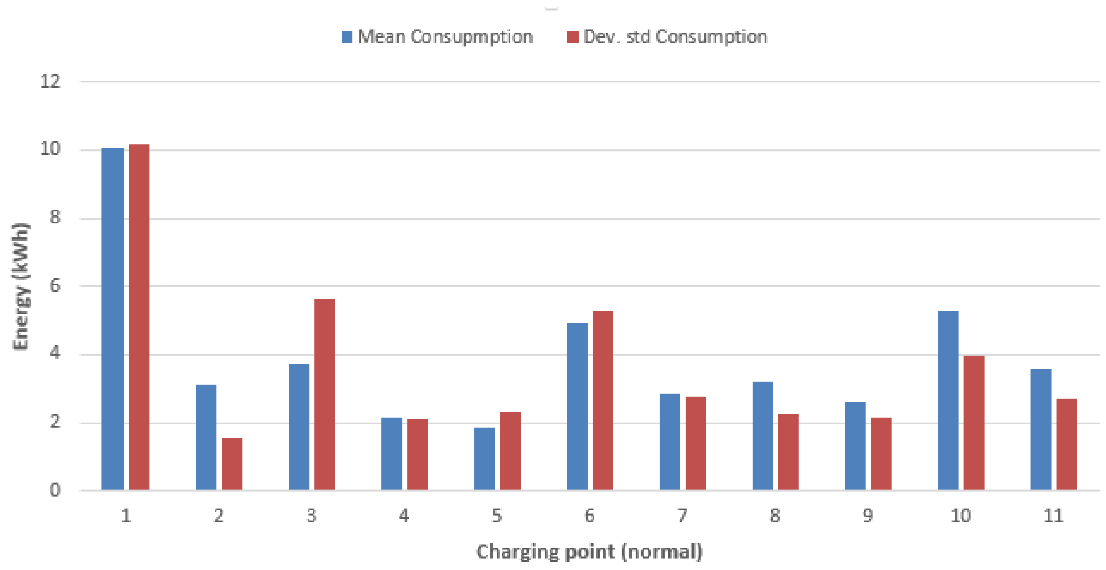

Figure 2 shows the mean charging duration, along with its standard deviation. The mean duration is around 100 minutes for the largest part of the charging points, while the larger standard deviation is observed for the charging point n.8 (PdRL Montcada i Reixac: C. Tarragona - C. Pla de Matabous) for which several records have a duration of more than one day.

Figure 2: Mean value and standard deviation of the charge duration for normal chargers (3 and 7 kW).

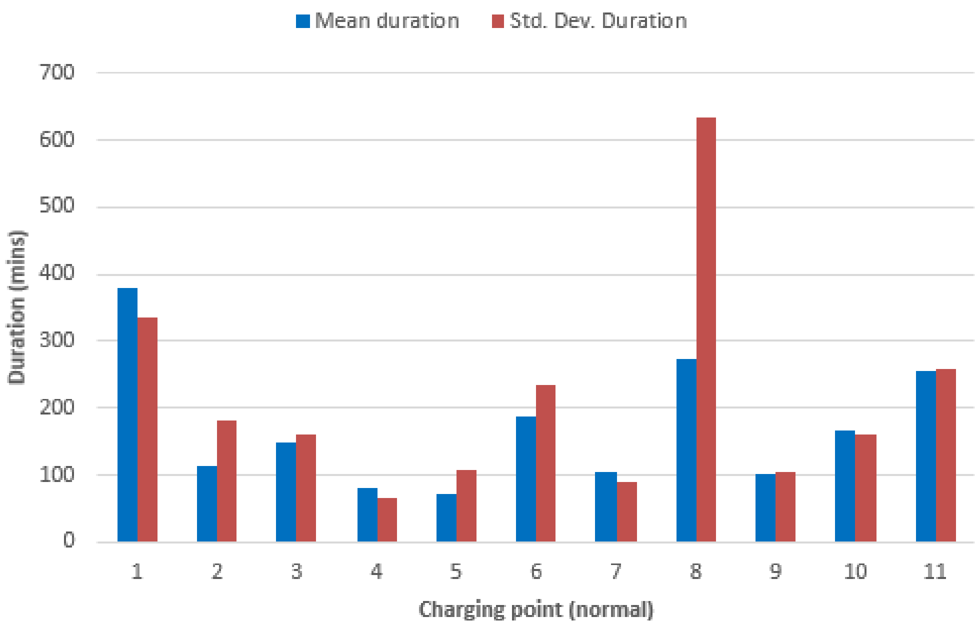

Figure 3 reports the total number of charging events in the year. The graph shows that only 3 charging points (CP) register more than 1 charge per day (CP 6, 9 and 11). The most popular charging point is the n.6 (PdRL Gavà: C. del Progres, 54),

Figure 3: Number of charging events (yearly) for normal chargers (3 and 7 kW).

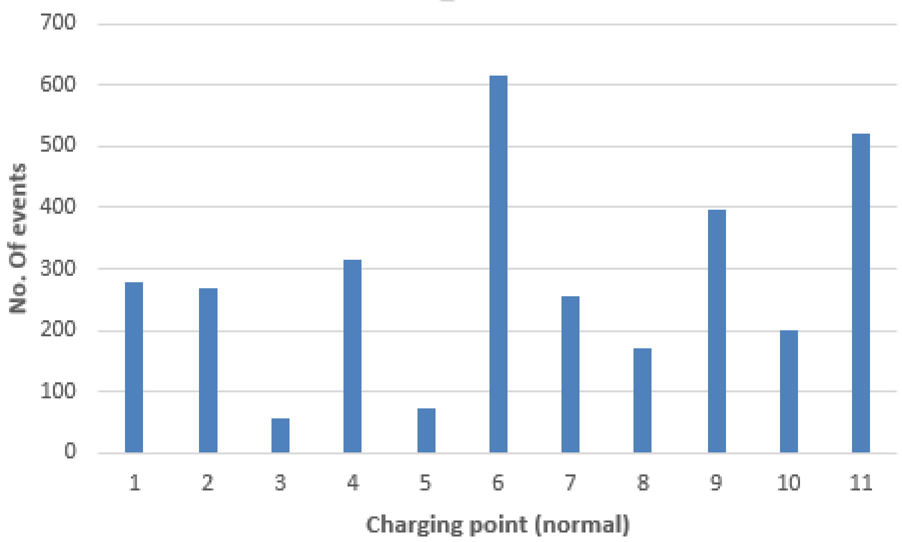

When only quick chargers are selected (43kW or 44kW), we obtain 33029 records with an average charging duration of 28.7 minutes and a standard deviation of 17.6, while the average energy delivered is 10.7 kWh with a standard deviation of 7.7 kWh. The median value is 26 minutes

Bar charts reported in Figure 4 and Figure 5 show that the "quick" charging dataset is more homogeneous than the "normal" charging ones in terms of energy distribution, and duration, probably because this type of refilling reflects a use more similar to that of petrol stations, where refueling is done along the way.

Figure 4: Mean values and standard deviation of the energy delivered for quick charging points.

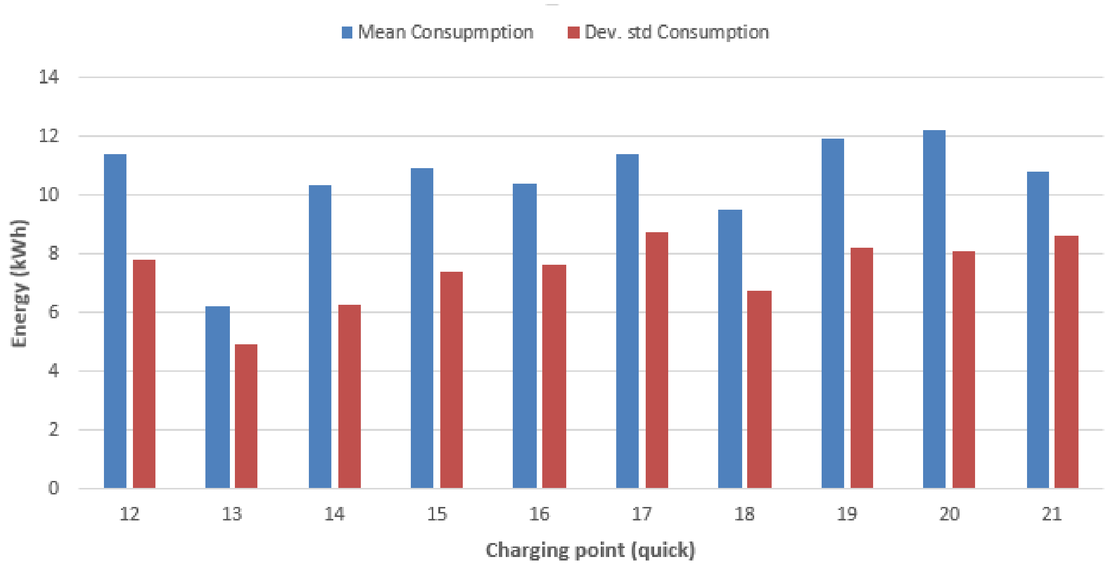

Figure 5: Mean values and standard deviation of the charge duration for quick charging points.

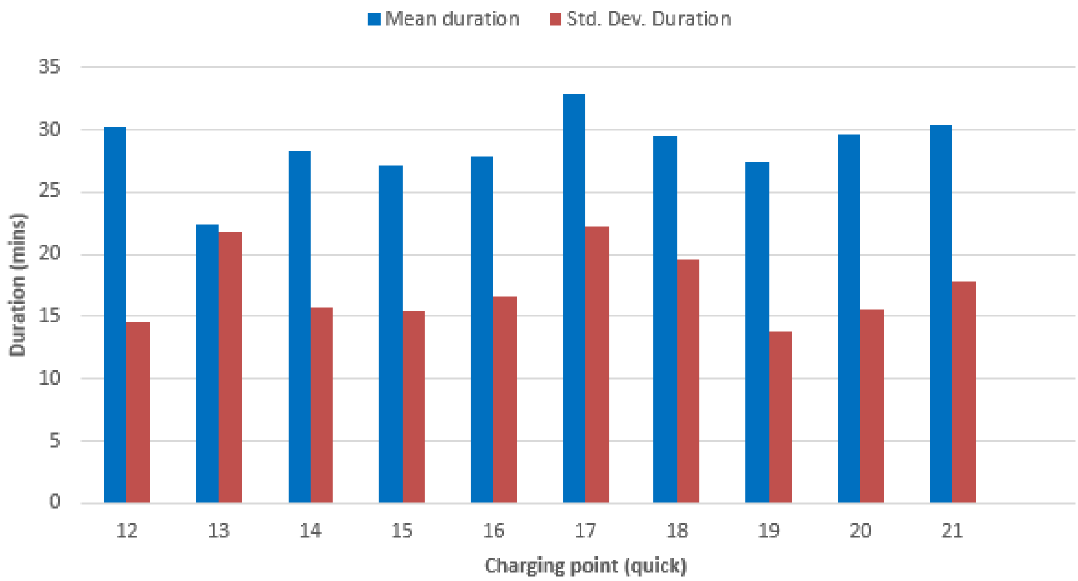

Figure 6 reports the number of annual charge events for each charging point. In this case, on average, all the CPs have at least more than 3 charges per day.

Figure 6: Number of charging events for quick charging points.

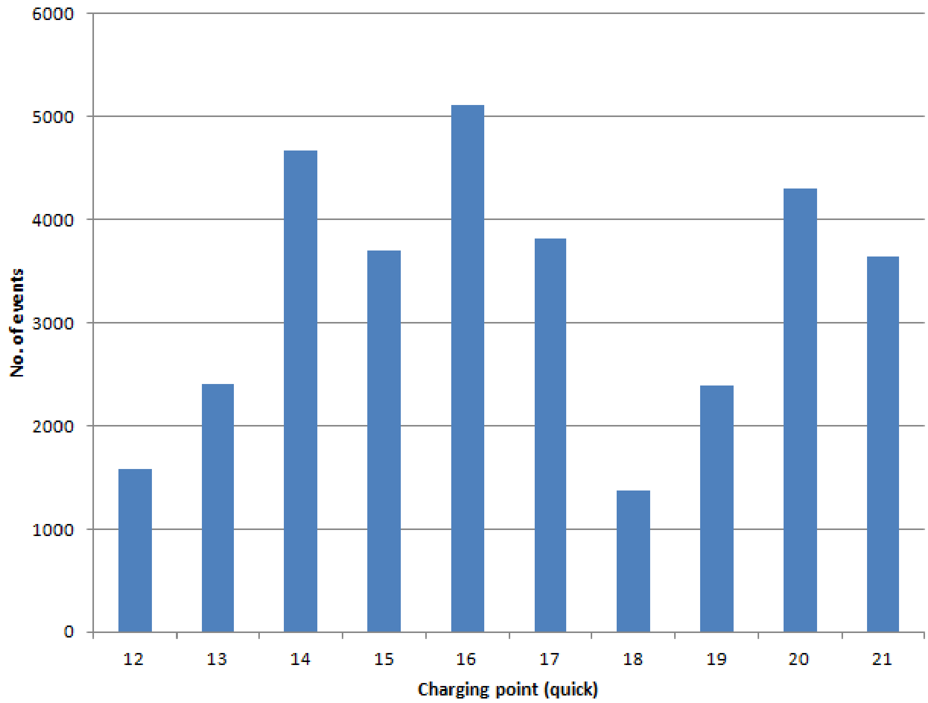

2.1.1 Distribution of charges during weekdays

Figure 7(a) reports the distribution of the hourly number of charging events while Figure 7(b) reports the mean hourly duration of charges during a weekday.

Figure 7: Hourly distribution of number and average duration of charges during a typical weekday.

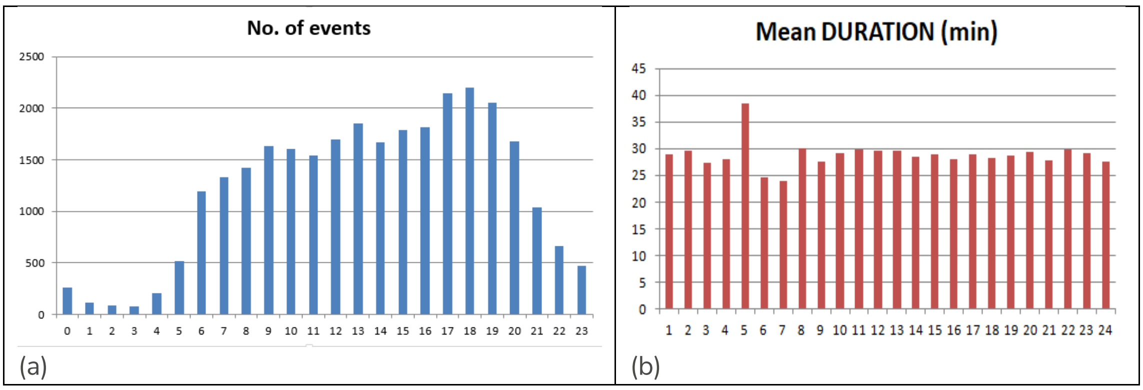

Figure 8 shows the analysis of the previous parameters for normal chargers during working days (Monday to Friday) and during weekends (Saturday and Sunday). In Figure 8 (a) we report the average number of charges that start at a given hour during the working days and the weekend. In the weekdays, normal charges start prevalently at 5 pm lasting until 7pm, with secondary peaks at 1 pm. On the other hand, during weekends the distribution of the start time is flatter, with two peaks at 1pm and at 7pm. Also, the number of charges per day is smaller for the weekends. The mean charge duration does not show distinctive patterns, even though it tends to be longer in the nighttime in both cases.

Figure 8: Hourly distribution of average number (a) and average duration (b) of charges for Normal chargers during of a working day and during weekends.

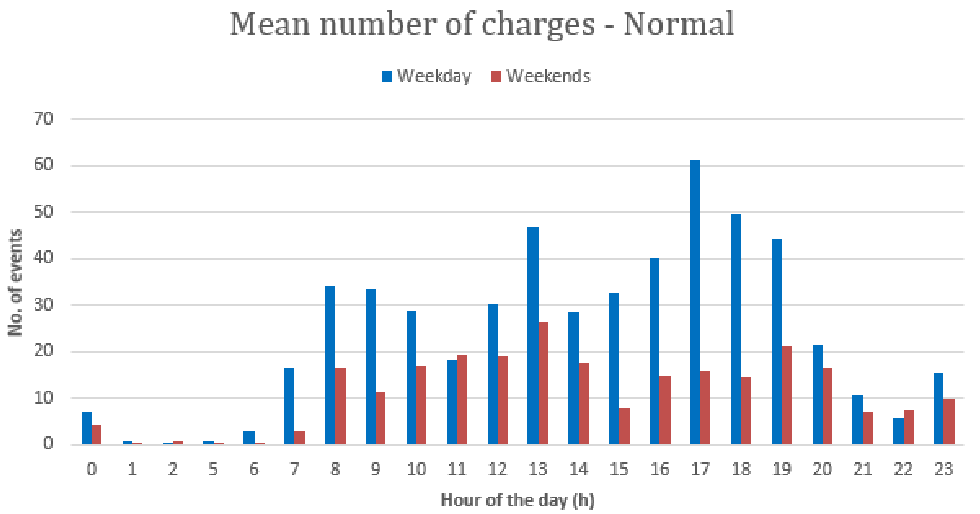

(a)

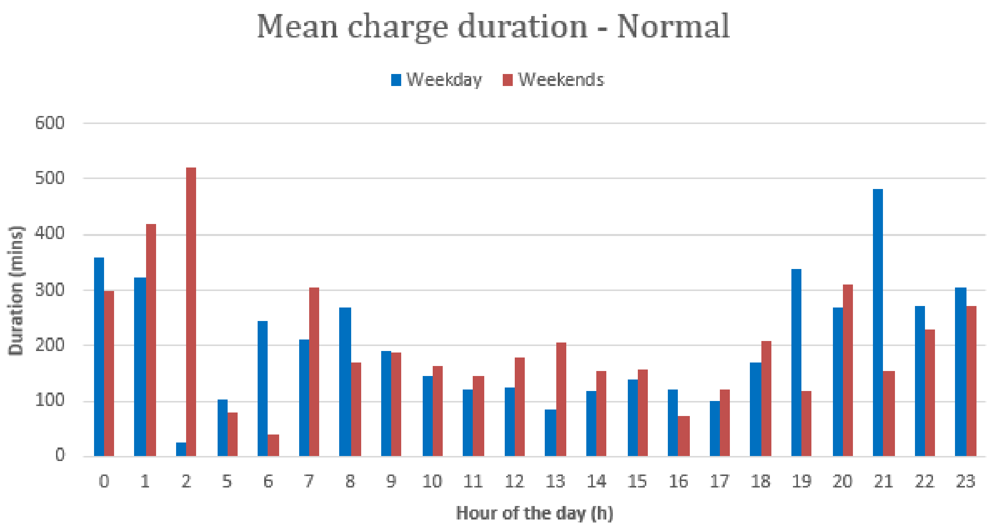

(b)

Figure 9 (a) reports the *average* number of events *per charging point*[1] for quick charges. Besides that, the number of quick charges is much larger during weekdays than during weekends, the hourly distribution is similar, even though during weekday there is an increase around 6 pm, while

1 Total number of events/total number of quick chargers

during weekends there are two different peaks, around 12 am and 7 pm. The mean charge duration, Figure 9 (b), is quite homogeneous for different hours and days, with a slight increase during nighttime of working days (12 pm – 5 am). This supports the hypothesis that fast charging is perceived in a similar way of refueling at the station.

Figure 9: Hourly distribution of the average number (a) and average duration (b) of charges for quick chargers during weekdays and during weekends.

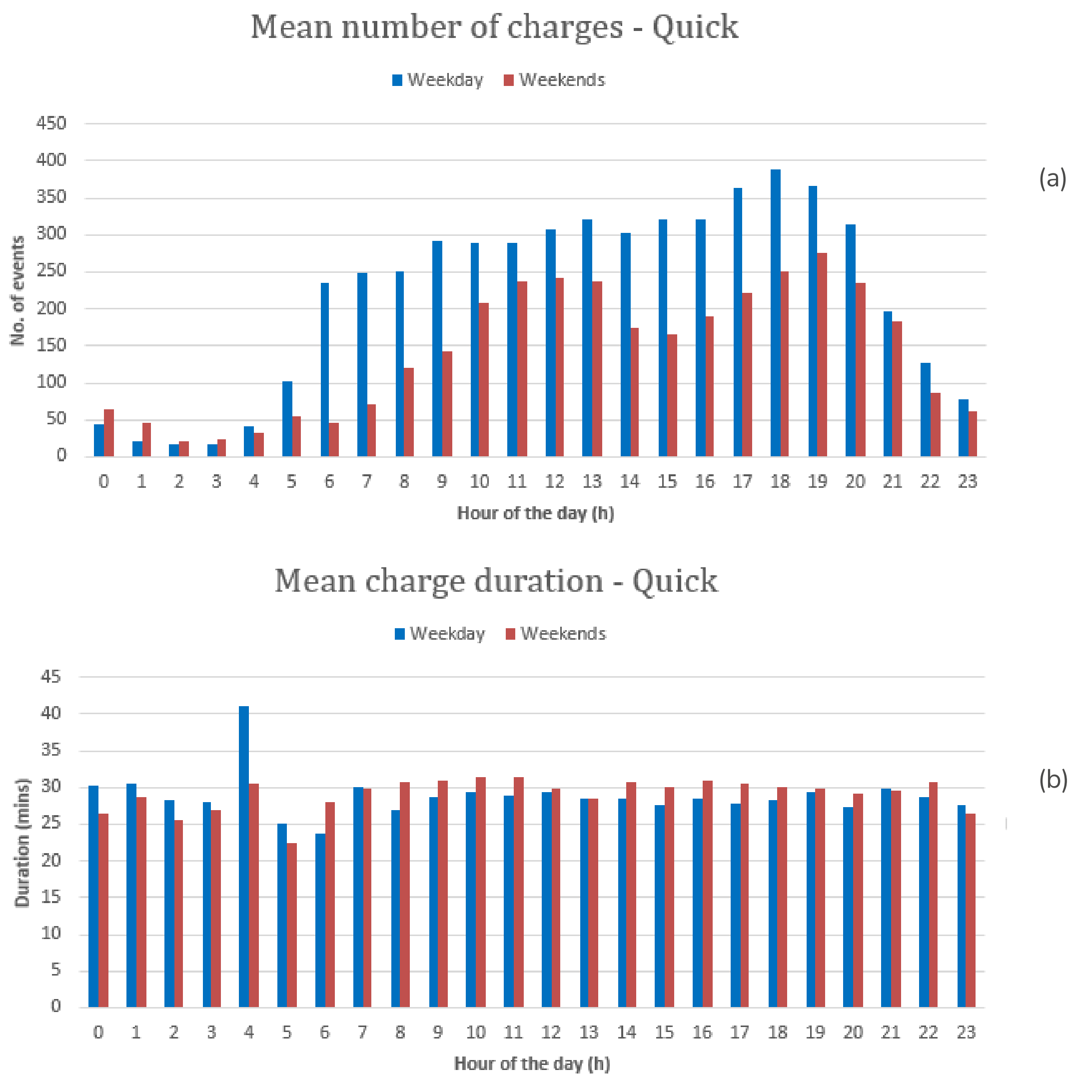

Table 4 reports some parameters for the yearly dataset referred to weekends and working days. The number of quick charges during weekends and working days (per day and per charging point) is the 91% and 93% of the total number of charges, respectively.

Table 4: Average parameter for weekend and working days.

Dataset AMB	No. of events/CP Mon-Fri	No. of events/CP Sat & Sun	Mean duration Mon-Fri (min)	Mean duration Sat & Sun	Mean energy Mon-Fri (kWh)	Mean energy Sat & Sun (kWh)
Normal	247.5	48.36	228.01	176.92	4.18	3.97
Quick	2634.4	681.4	28.42	29.87	10.59	11.86

Figure 10 reports the mean duration and mean energy consumption of quick and normal charges for the period of (1) December, January and February; (2) March, April and May; (3) June, July and August; (4) September, October and November.

Figure 10: Seasonal influence on some charge parameter: (a) mean charge duration, (b) mean charged energy for the following periods: 1: December, January and February; 2: March, April and May; 3: June, July and August; 4: September, October and November.

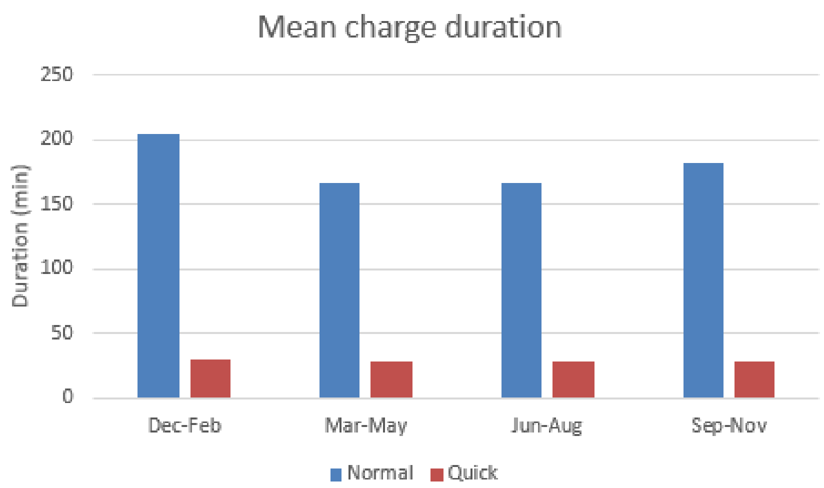

(a)

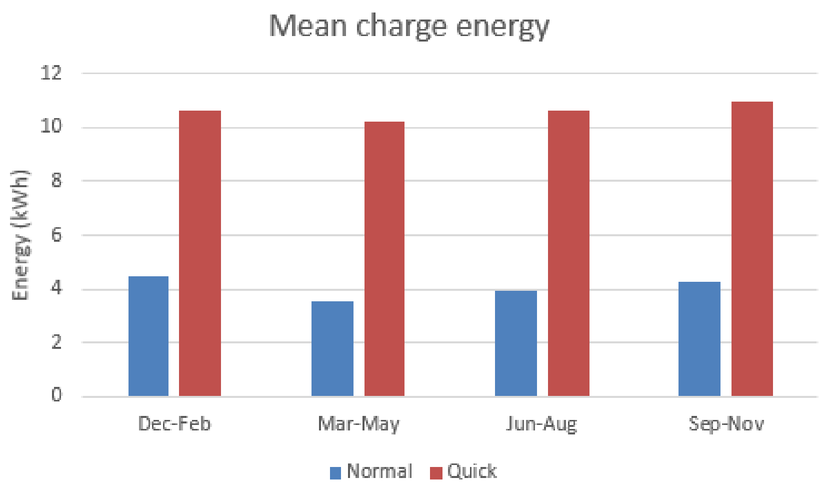

(b)

Figure 10 clearly shows there are no significant differences among the seasons with the exception of a longer duration for normal charges during the winter compared to the rest of the year, and a slight increase of the energy delivered.

In the dataset, there is some information about the EV models having benefited from the charge, but this is scarce and is recorded in the database without a predefined format. However, we can try to infer some information about the battery by cross-referencing the charging data, the vehicle model, and the information provided by car manufacturers. The smallest battery size is 3.1 kWh for the Volta BNC. However, there are some discrepancies among data. For example, 287 registrations declare an amount of energy delivered greater than the battery capacity (up to 7 times, as retrieved from datasheets or from literature, normally available for the latest models. There are also some EVs models that can have onboard batteries of different size). However, these discrepancies have not be taken into account in the data selection since we cannot be sure about the real capacity of the EV battery actually connected (we are not aware how the EV model information has been acquired during the charging registration and the real battery size).

If we exclude these records, we can attempt analyzing the relationship between charge duration and the fraction of energy delivered with respect to the battery size. The dataset including normal and quick charges has a linear correlation coefficient (Lcc) of 0.3206 (weak linear correlation). Its graphical representation is reported in Figure 11. If only normal charges are considered, the Lcc is 0.5494, while it becomes 0.4061 for quick charges. The best correlation for normal charging may be that it is used routinely. In fact, normal refills show more regular start and end times, which can be linked to arrival and departure from a usual parking lot, such as the workplace or home. Since these are regular trips, the initial and final battery charge state is more or less the same for each day.

Figure 11: Charge duration of quick and normal charges.

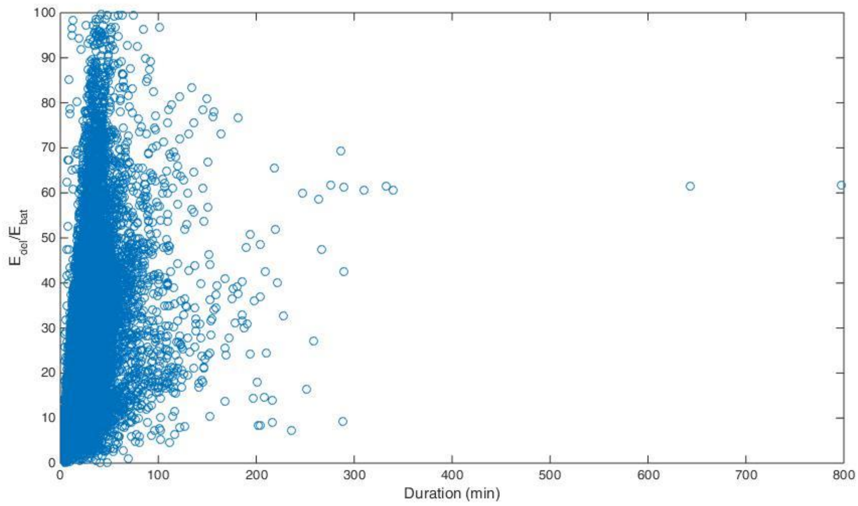

The correlation factors among other parameters of the dataset can be calculated. Table 5 and Table 6 show that no correlation exists among the starting time of the charge and the duration or the energy delivered. In addition, a very low correlation exists between the energy delivered and duration, both for 3 kW and quick chargers.

Table 5: Correlation factors for 3kW chargers.

Normal	Duration (min)	Energy (kWh)	Start time of the day
Duration (min)	1	0.4642	0.0215
Energy (kWh)	0.4642	1	-0.0414
Start time of the day	0.0215	-0.0414	1

Table 6: Correlation factors for Quick chargers.

Quick	Duration (min)	Energy (kWh)	Start time of the day
Duration (min)	1	0.5705	0.0067
Energy (kWh)	0.5705	1	0.0566
Start time of the day	0.0067	0.0566	1

The usage of the charging points during the year is reported in Figure 12-Figure 14. For the charging station of 7 kW (4 CPs) we can observe, after an idle time of nearly 4 months, a period of use with a very low energy delivered (Figure 12). This may refers to long parking events or errors in the registration system of the chargers.

From Figure 13 it is evident that the chargers at the quick stations are never fully deployed, as the occupancy is never greater than one even though there are 3 CPs in each station. The occupancy for normal stations sometimes saturates the number of CPs (2 for each station, Figure 14), but this could be due to a parking time longer than the charging time.

Figure 12: Number of users and energy delivered at the charging point FLNR Sant'Andreu da la Barca.

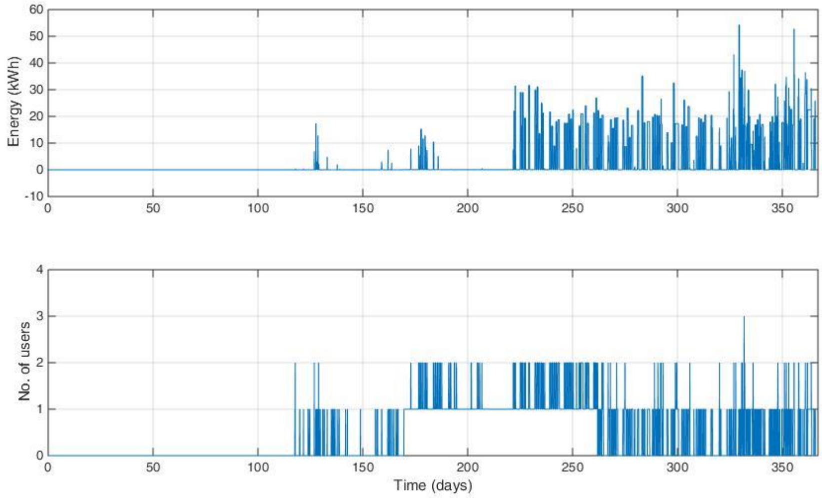

Figure 13: Number of users at quick charging points.

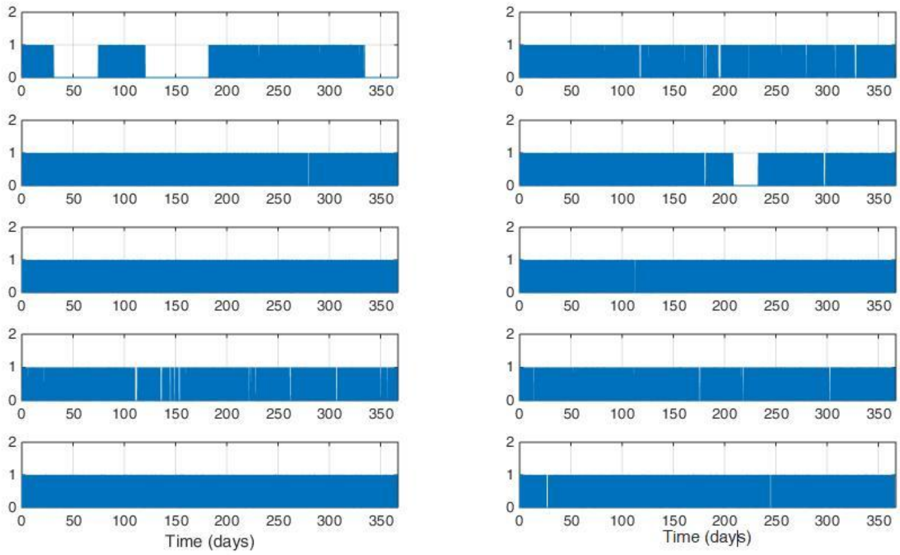

Figure 14: Number of users at normal charging points (from station 2 to 11).

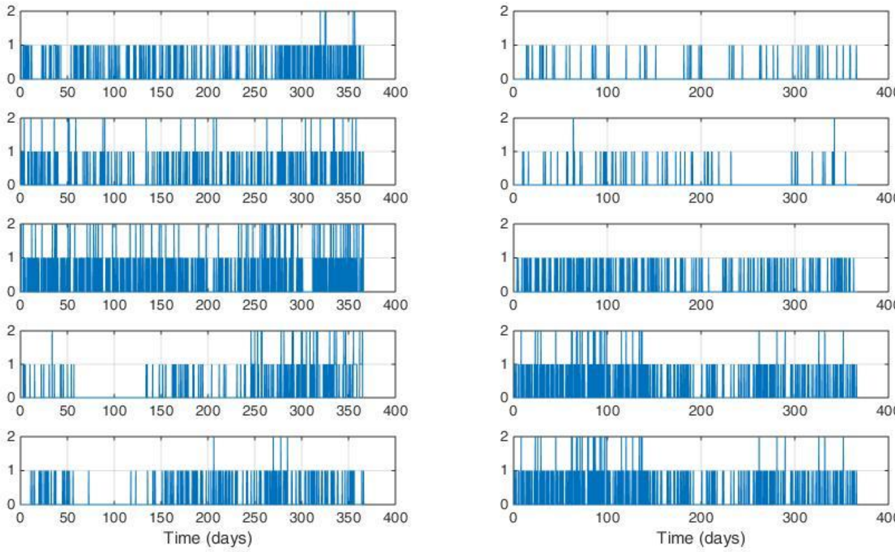

Figure 15 shows the frequency distribution of the charging power to the various types of stations. It can be observed that, for the 7kW station, most of the charging events take place at very low power. This is actually due to the very long parking times of the cars which show charging times of even days compared to a small amount of charged energy. For the "quick" and 3kW stations, the frequency distribution is more centered on values compatible with the rated powers of the CPs. In particular, for "quick" recharges the modal value is around 17 kW, while for "slow" recharges it is around 2 kW.

Figure 15: Average power delivered during charge (a) at the 7kW station, (b) at quick stations, (c) at 3 kW stations.

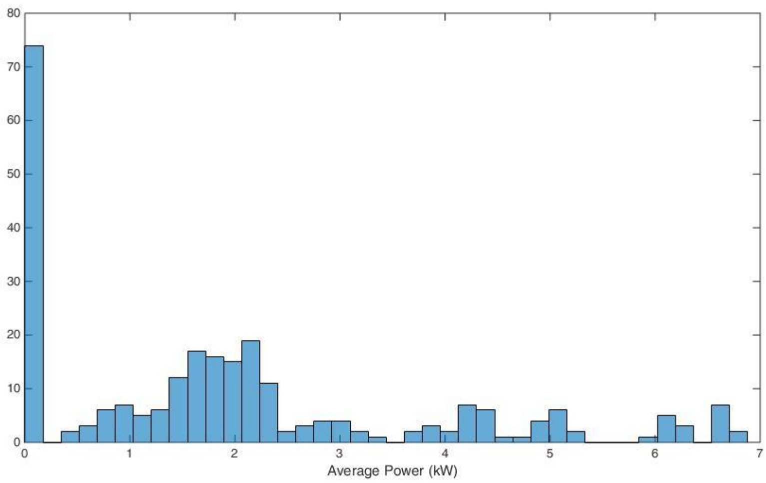

(a)

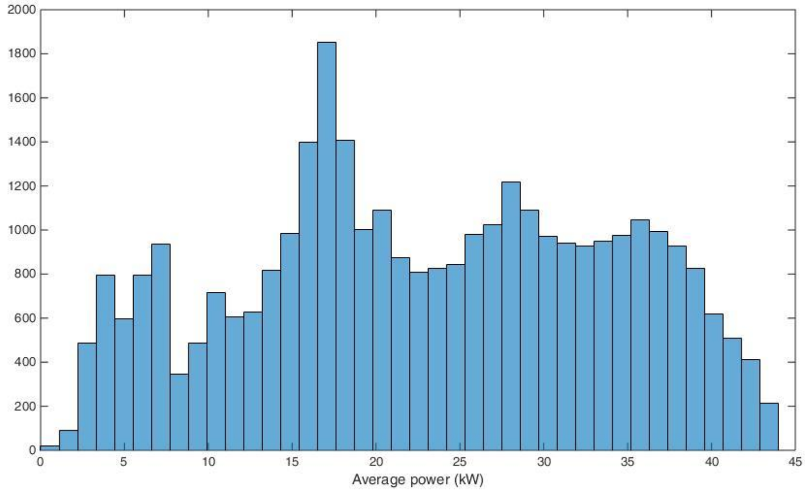

(b)

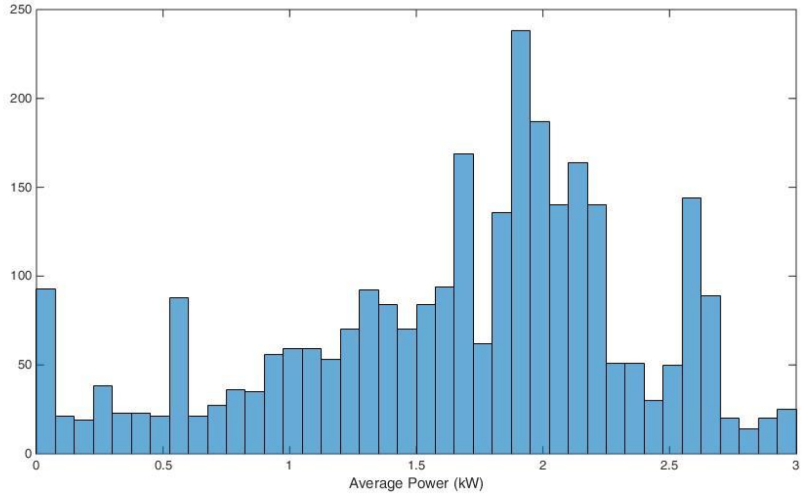

(c)

.

2.1.2 Inferences on dynamic information

The information in the dataset is only related to the charging events but it does not contain any dynamic information on the demand (waiting time, distances, etc.). Therefore, we can try inferring some information by analyzing the time interval between two consecutive charging events:

$$(Idle\ time)cp, x = (start\ time)x\ - (stop\ time)x - 1$$

The distribution for CP is shown in Figure 16.

Figure 16: Distribution of the minimum idle time.

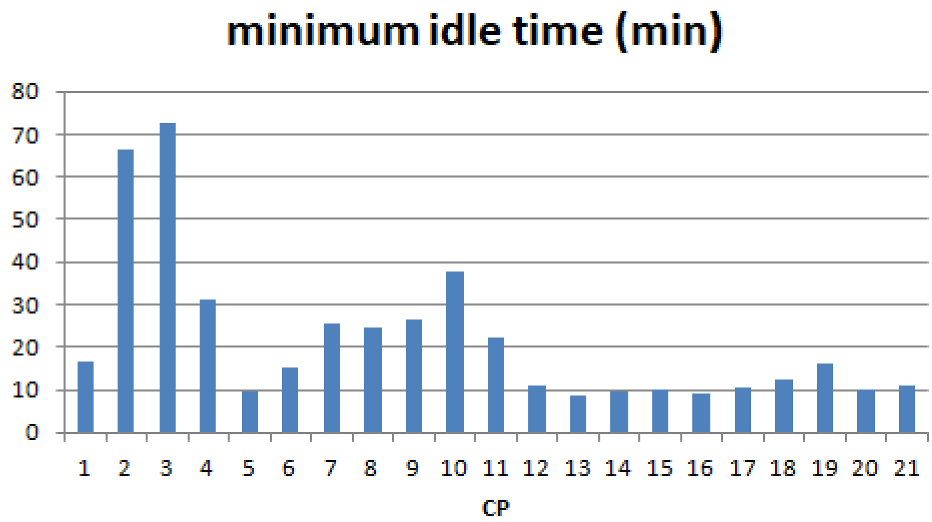

As it can be seen, the idle time is shorter for quick chargers, as can be also inferred from the average number of charges per day. The mean value of the idle time over the year is showed in Figure 17 where it is possible to observe the occurrences of short idle time are fewer for "normal" charger points (CPs)

Figure 17: Mean idle time for CP.

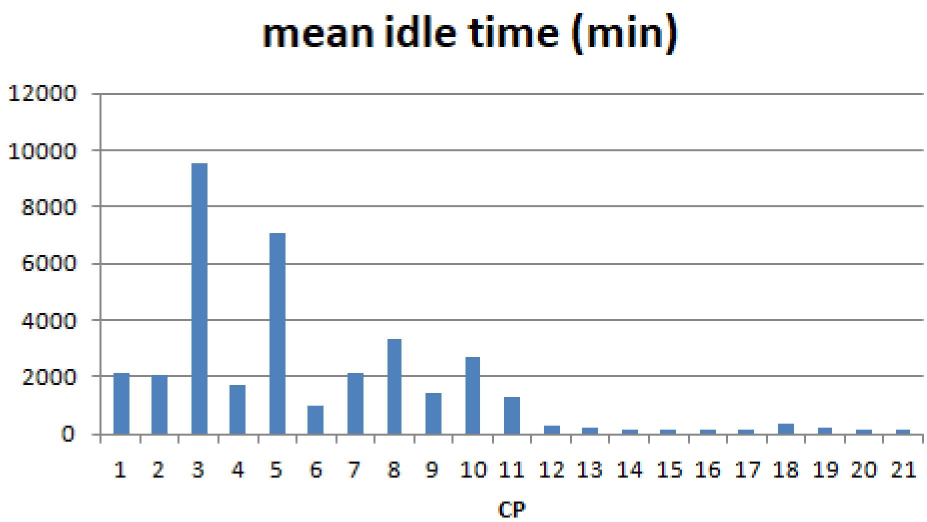

This confirms that, for "normal" charging, there is a high possibility to keep the parking lot occupied even when the charge is ended.

2.2 Turku

For the city of Turku, the original dataset is composed of 7737 records. We do not consider records with energy and/or charge duration less or equal to zero. The dataset is then reduced to 6536 records. The relevant statistical parameters for charge duration and energy delivered are reported in Table 7.

Table 7: Mean values and standard deviations for different datasets referring to Turku.

Dataset	Mean duration (min)	Stdev duration (min)	Mean energy (kWh)	Stdev energy (kWh)	Mean number of charges/day
Entire	195.31	502.38	6.31	6.64	0.99
AC	232.28	574.33	5.77	5.45	0,92
DC	25.58	25.88	8.80	10.14	1.6

We can see there is a relevant dispersion in all the data sets. In particular, for the AC the dispersion is quite relevant for the charge duration, while for the DC charges the dispersion is more relevant for the energy delivered.

Graphs in Figure 18 to Figure 21 show the same statistical parameters reported in Table 7 for each charging types. In particular, in Figure 18 we report the mean value and the standard deviation of the energy delivered by AC chargers. It is interesting to observe that some charging stations differ from the average behavior. In particular, CP no. 6441 delivers a relevant quantity of energy in a relatively low usage rate, as can be seen from Figure 19, where the mean charge duration, its standard deviation are shown, along with the total number of events over the year.

Figure 18: Mean value and standard deviation of energy (in kWh) for AC chargers (22 kW) [2].

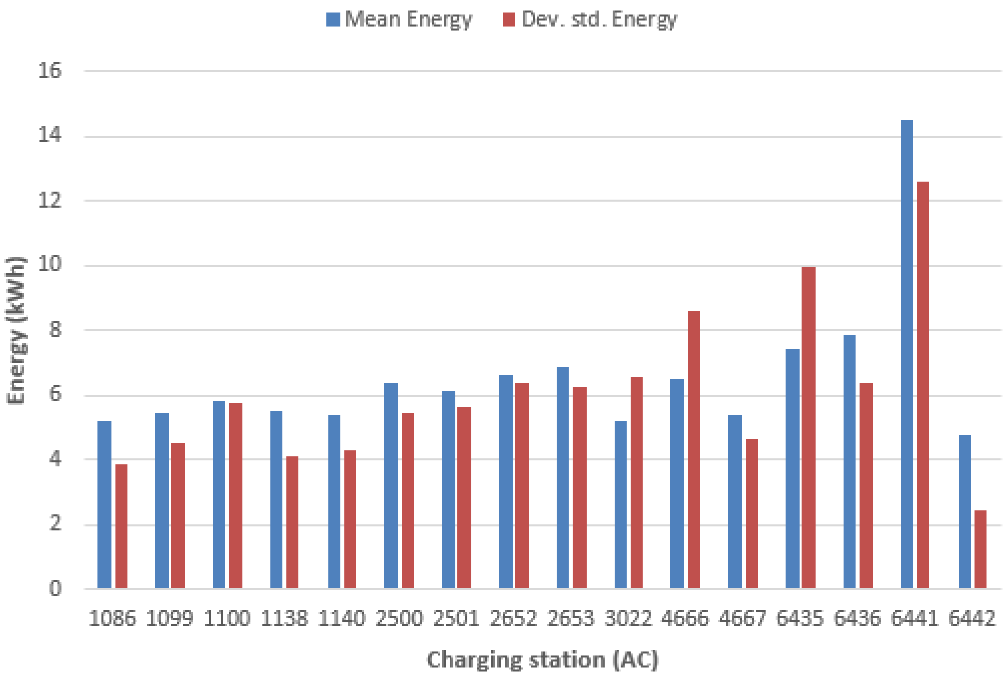

The distribution of the charge duration shows two tendencies: most of the charge durations are between two and three hours, while some charging stations show average durations above the eight hours. However, these stations show huge deviations, so probably there are few events of very long duration.

2 Inferred from data: to be confirmed by Turku

Figure 19: Number of yearly charging events, mean value and standard deviation of the duration (min) for AC chargers.

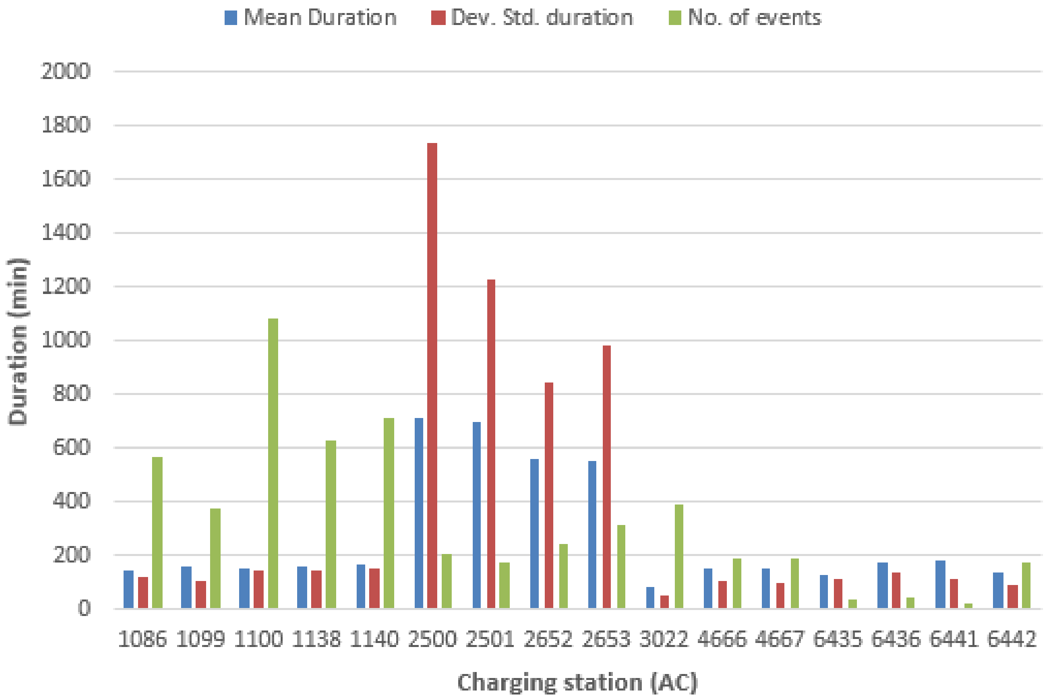

Very little can be said on DC charging events because of their relatively low numbers. Indeed, there are only 2 DC charger station in the entire dataset, and their average daily use is around 1.6 user per day (see Table 7). Although the set is small, some information can be obtained from the data. Figure 20 shows the mean value and the standard deviation for the energy delivered during the charges. The mean values are very similar for the two stations. It can also be seen that the mean energy is quite small, so it can hypothesize that fast charge are used for small recharges (biberonage).

Figure 20: Mean value and standard deviation of energy (in kWh) for DC chargers.

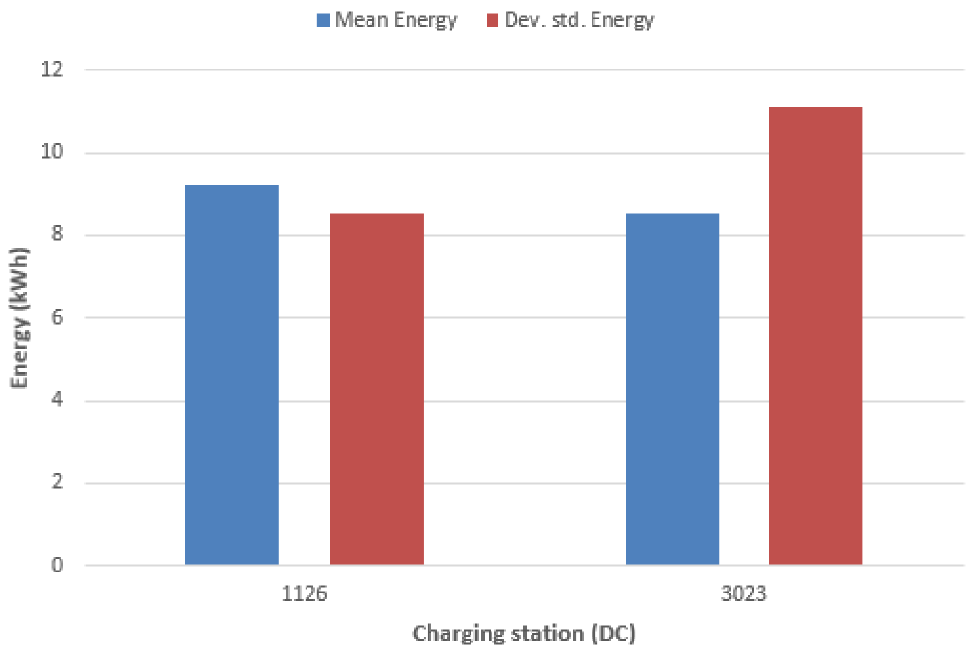

The DC charge durations (Figure 21) are close to the typical charge durations found in literature.

Figure 21: Mean value and standard deviation for the duration (min) of charges at the DC chargers.

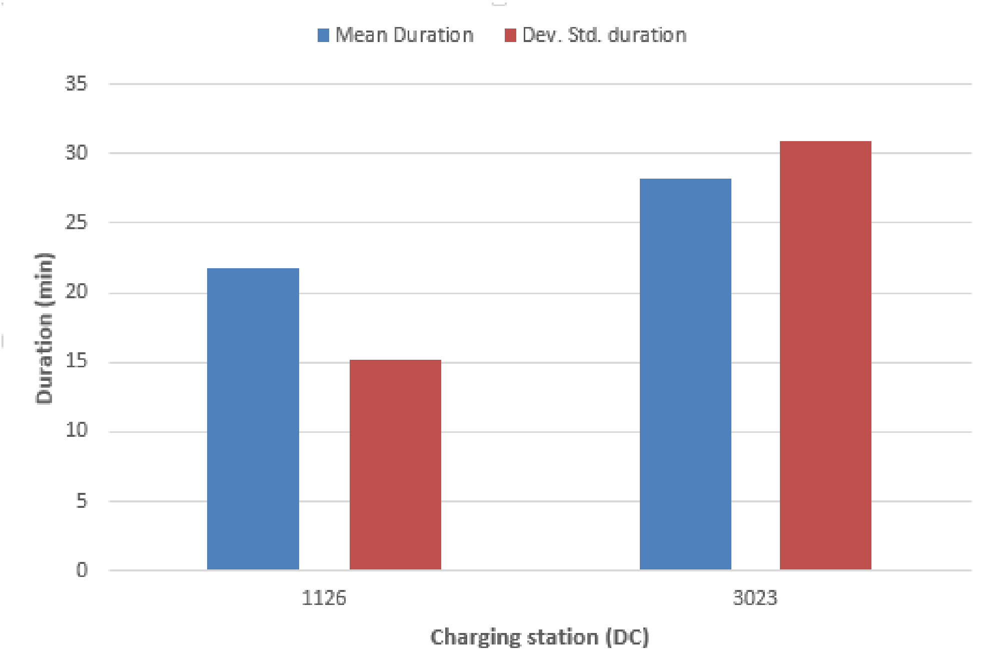

In the following, we analyse the distribution of charge during the day. Figure 22reports the hourly distribution of the starting time for the total number of charges over the year. As we can see, most charges started around 8 am, with a secondary peak at 12 am, followed by another local maximum around 4 pm.

Figure 22: Distribution of charges starting time during the day.

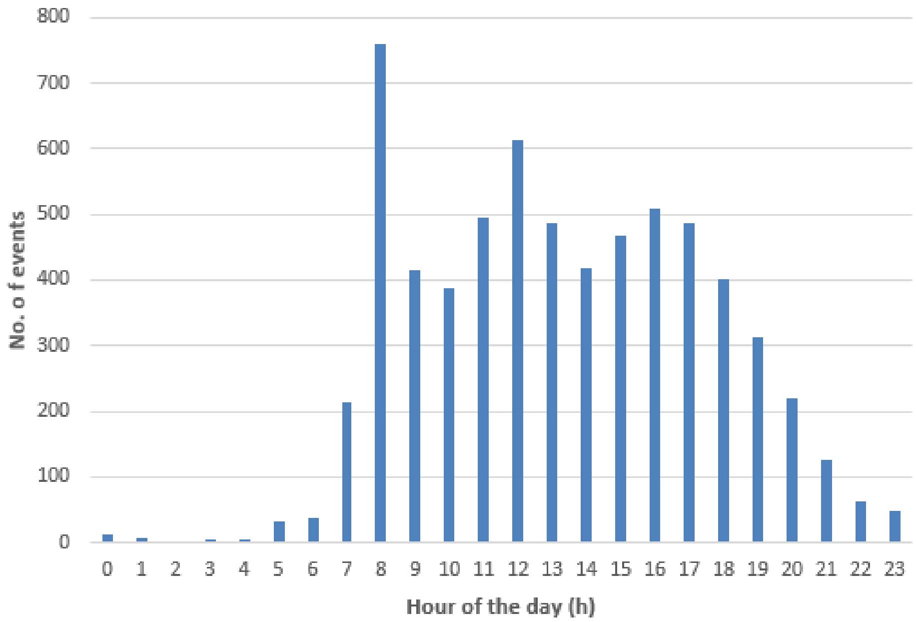

It is interesting to note the difference in the frequency distribution of charging starting hours during working days (Monday-Friday,) and weekends (Saturday and Sunday) reported in Figure 23 (a). The 8 am peak, present in the weekdays,disappears during the weekend.

As for the mean charge duration, Figure 23 (b), the longest charging sessions are in the afternoon during the weekends, while during working days there are three main charge starting peaks at 8 am, 12 am and 16 am, which roughly corresponds to the commuting hours.

Figure 23: Frequency distribution of charge starting hours (a) and charge durations (b) during working days and weekends.

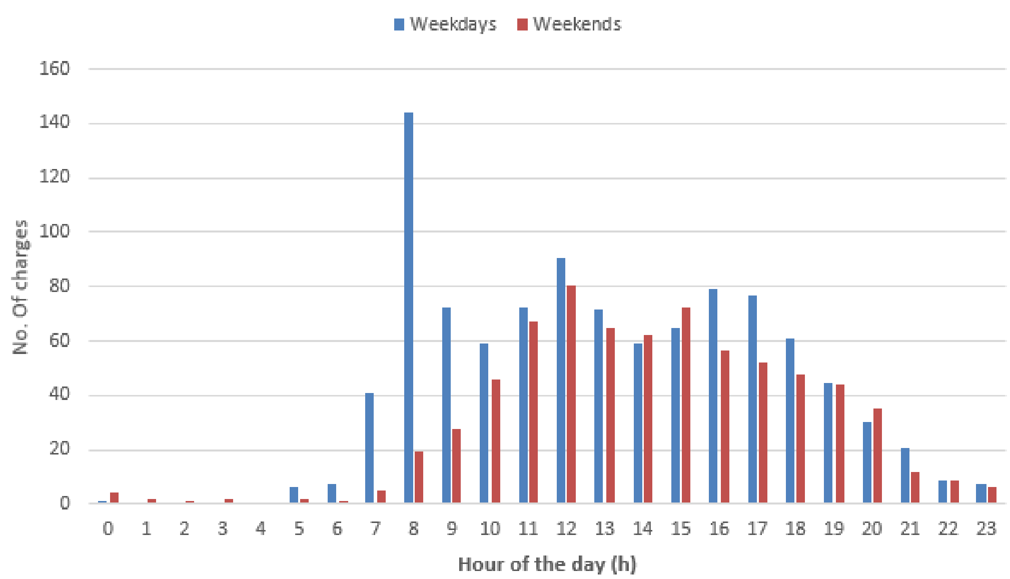

(a)

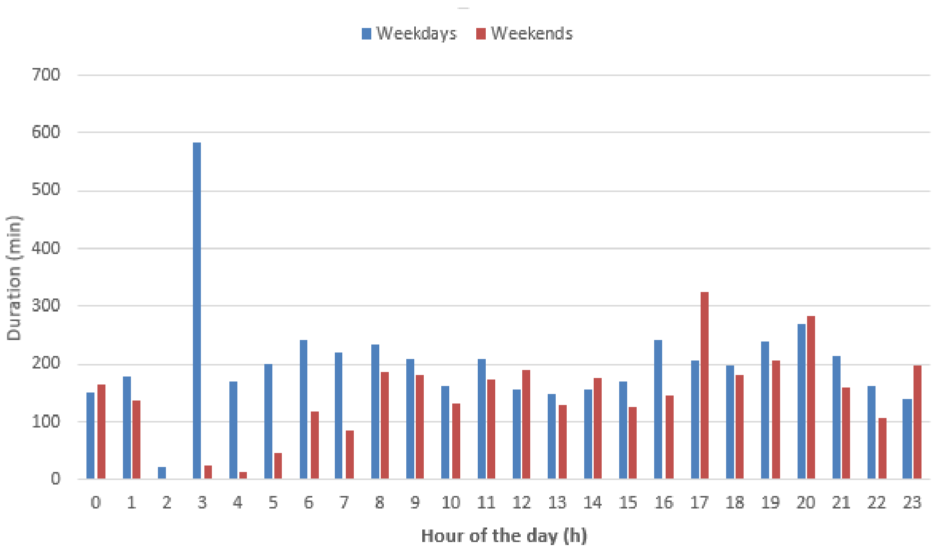

(b)

The differences between AC and DC of the charge duration distribution for working days and weekends are shown in Figure 24and Figure 25, along with the mean energy delivered. For AC, the energy delivered during the charge is similar for the weekdays and weekends dataset (Figure 24 (a)), except for the first hours of the day. However, there are few charges events in those hours (as can be seen from Figure 23 (b)), so the variability is high and no meaningful inference can be made. Also, the charge duration is comparable among weekdays and weekends events (Figure 24 (b)). However, the hourly distribution is different, as could be expected since the habit are usually different for working and non-working day.

Figure 24: Distribution of AC charge mean energy (a) and duration; (b) during working days and weekends.

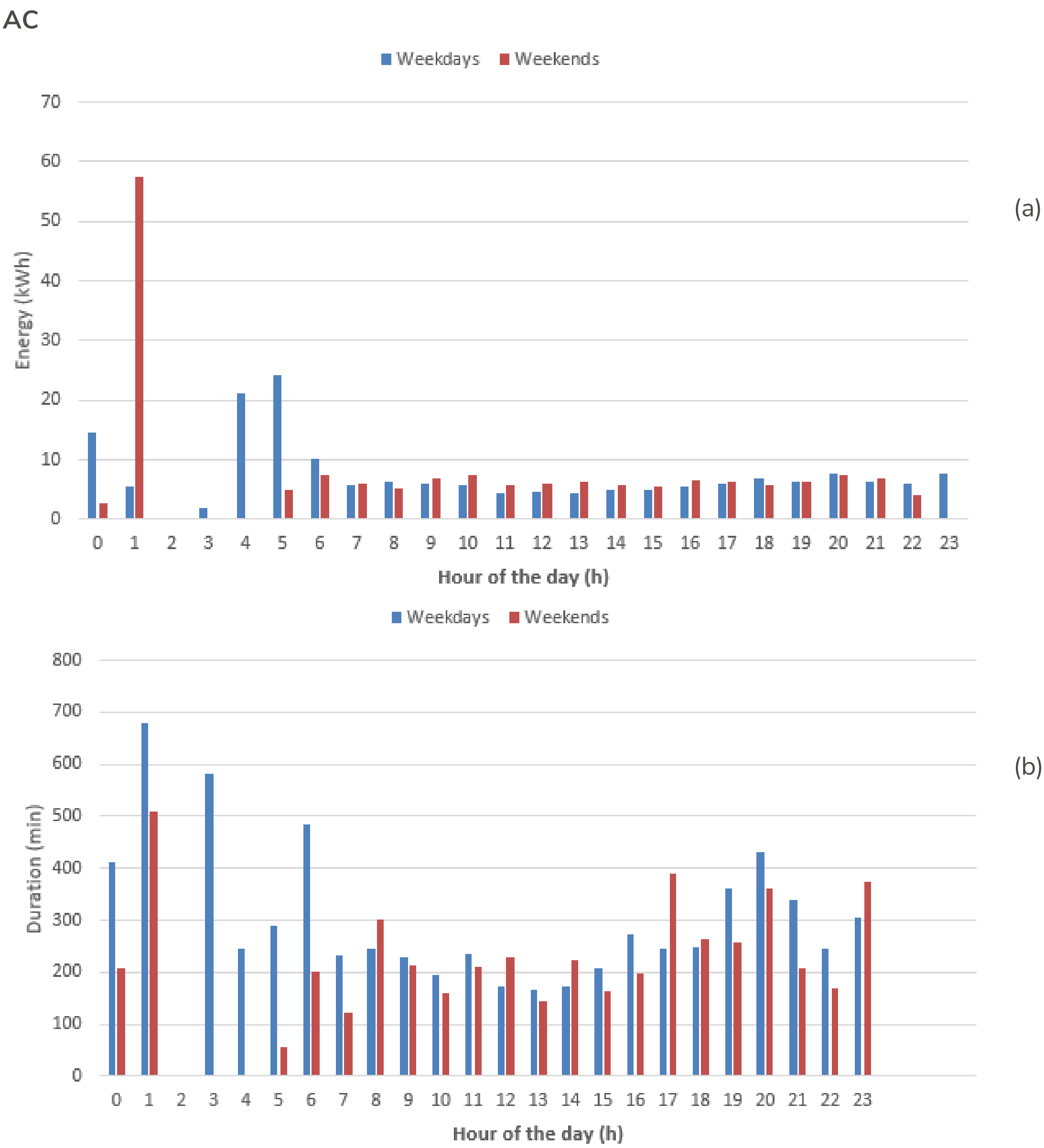

The DC dataset present a similar distribution for weekday and weekends both for the energy delivered during charges (Figure 25 (a)) and their duration (Figure 25 (b)). Also the time the charge events starts are very similar for the two datasets.

Figure 25: Distribution of DC charge mean energy (a) and duration (b) during working days and weekends.

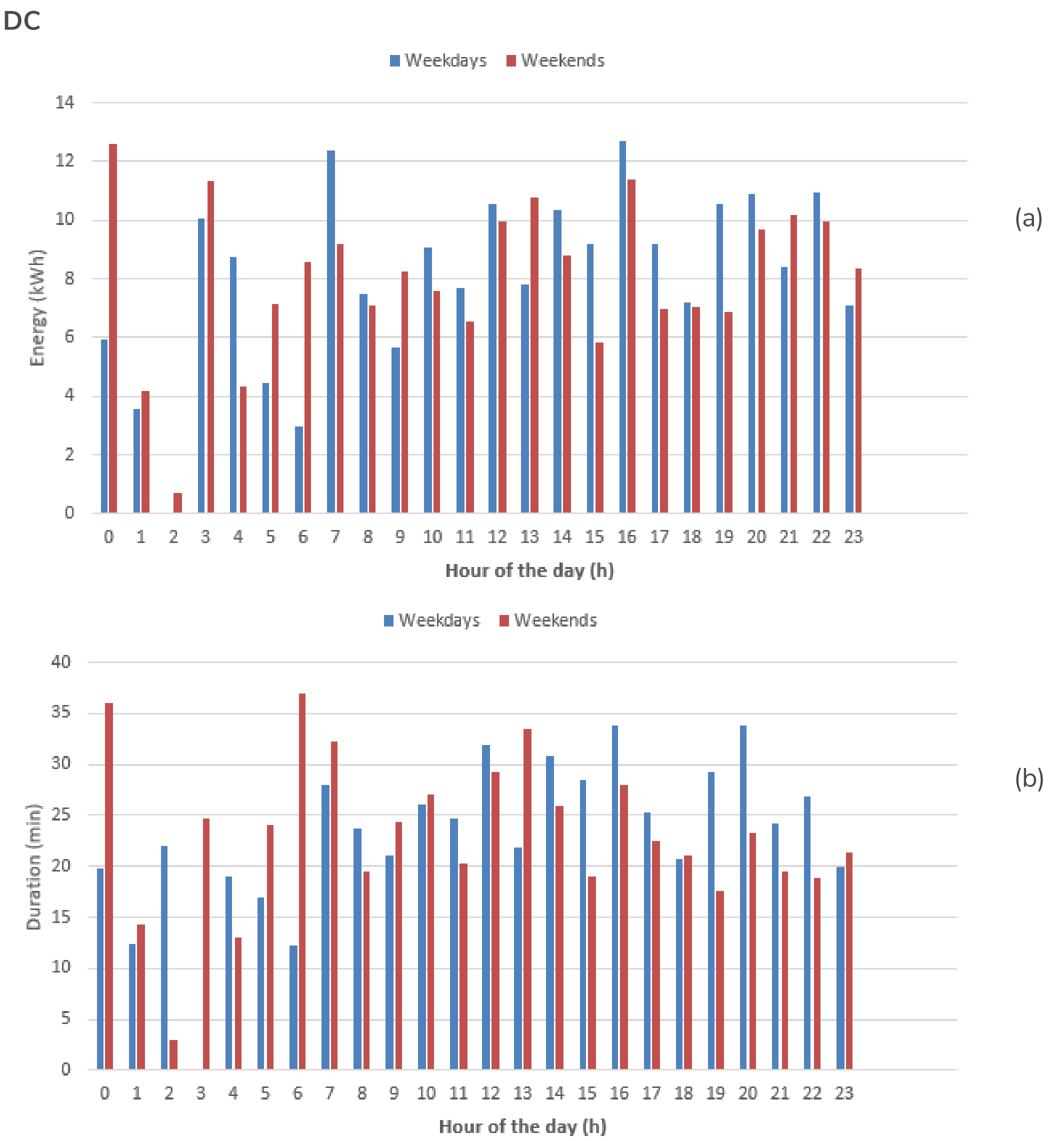

Charges during weekends tend to be shorter and deliver more energy than charges during working days (Table 8).

Table 8: Mean values of charge duration and energy exchange for working days and weekends.

Dataset	Mean duration Mon-Fri (min)	Mean duration Sat & Sun	Mean energy Mon-Fri (kWh)	Mean energy Sat & Sun (kWh)
Entire	199.98	178.72	6.21	6.67
AC	233.43	227.75	5.67	6.17
DC	26.36	23.69	9.02	8.27

DC charges tends to be used more often than AC chargers (Table 8), confirming what observed for AMB (Table 2).

Table 9: Average number of charges during the year and the day, for the AC, DC chargers.

Charge typology	No. charge/year	No. charge/day
AC	335.4	0.92
DC	584.5	1.6

Figure 26shows the seasonal influence on the charging behaviors. In this case, quick (DC) charge duration seems to be a little shorter during the summer, while the AC charge does not show this feature. In addition, the energy delivered is generally smaller, while it is higher during winter with longer charging session. Probably, this is because fast charges are quicker when the battery temperature is higher, while the battery consumption is higher in winter because of the use of auxiliary services such as heating.

Figure 26: Seasonal influence on charging parameters: (a) mean charge duration; (b) mean energy delivered during the charge, for 1: December, January and February; 2: March, April and May; 3: June, July and August; 4: September, October and November.

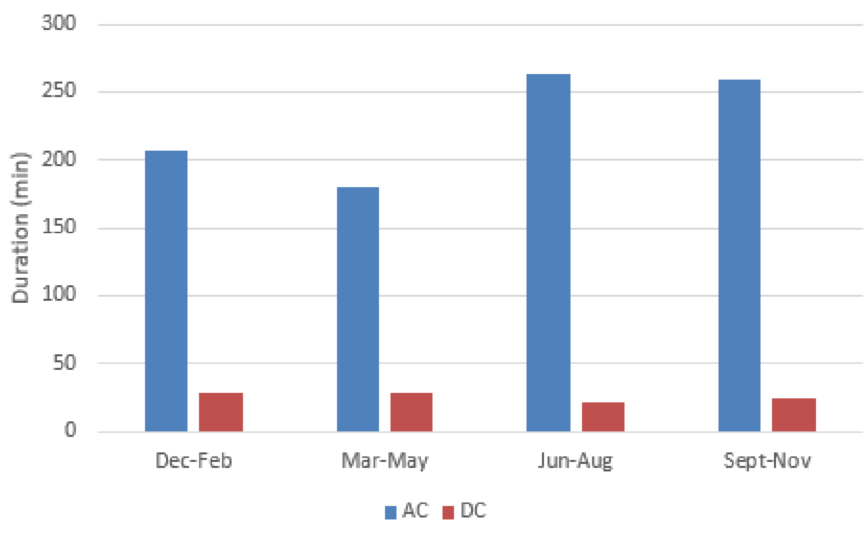

(a)

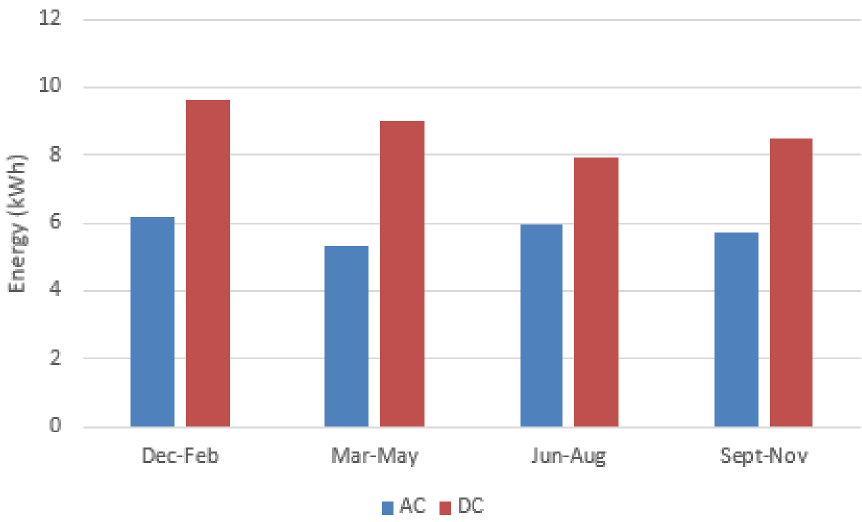

(b)

2.3 Rome

Rome dataset reports the daily number of charges and energy delivered for each charging point. The CPs are not classified as normal or quick type.

Number of:

1. Records: 56924;
2. Charging points: 514.

If null records are not considered (empty number of charges and/or energy delivered) the dataset reduces to 47083 records referred to 298 charging points. If we also exclude the records with zero energy, we obtain a further reduced dataset of 44947 records.

Table 10 shows that some relevant statistical parameters such as, the standard deviations for the daily number of events per CP and the energy delivered are quite large.

Table 10: Relevant statistical parameters for Rome dataset.

Rome	No. of events/CP/day	Energy delivered/CP/day (kWh)	Average energy/charges
Mean	2.66	19.36	7.28
Stdev	2.55	19.35	3.85
max	271	314.5	47.6
min	1	0.01	0.64

Figure 27 shows the average number of daily charge events for each month (starting from January). The values recorded for the month of January is the smallest ones. Indeed, the total number of charges during January is the smallest of the year (Figure 28). This is because of several reasons such as increasing number of EVs, new CP activated, etc. However, there are not enough elements in the dataset to clearly state any of the above hypothesis.

Figure 27: Average number of charging events by day for different month.

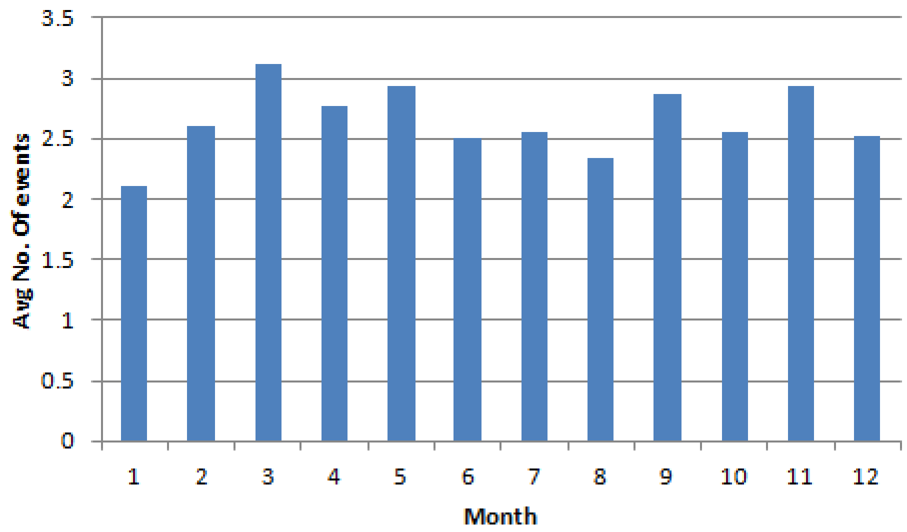

Figure 28: Total number of monthly charging events.

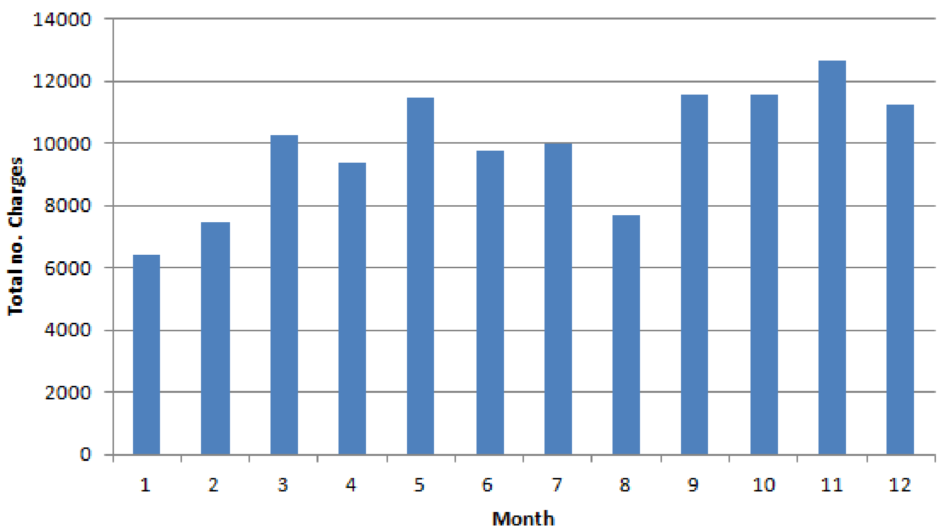

In the following we analyse the distribution of the average number of charges during weekdays. As shown in Figure 29, most charging events occur on Sunday (day 1) and Friday.

Figure 29: Average number of weekly charging events

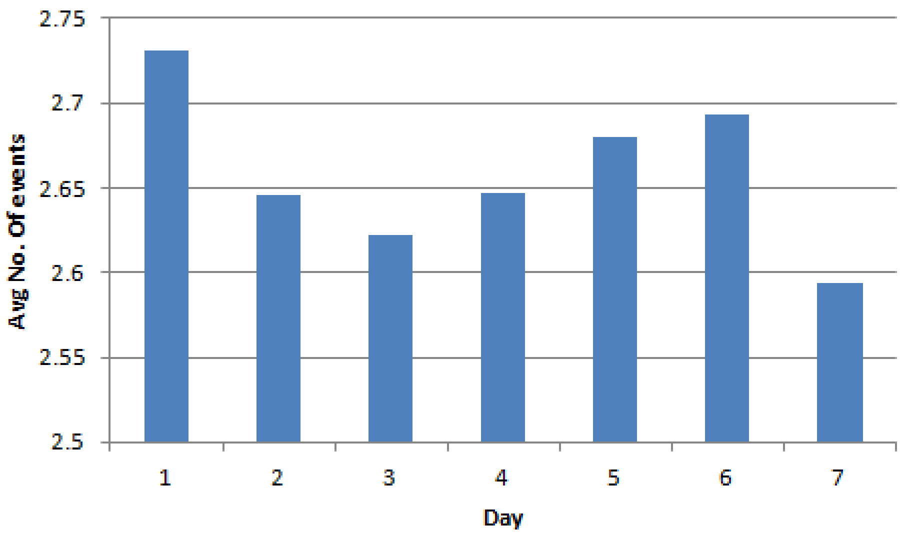

Figure 30 shows the averages values of energy delivered and the number of daily charging events during the quarters of the year. The energy delivered during winter and summer quarters are among the lowest recorded during the year. However, this is in contrast with what observed from the datasets of other cities for which the energy delivered during the winter quarter is the highest. Figure 31 shows the average number of charges and mean energy for each month. Again, we can observe different trends between the month of January and the two months of December and February. However, as before, we don't have enough information to investigate the reason for this behavior.

Figure 30: Average number of charges and mean energy for different quarters: (1) winter; (2) spring; (3) summer; (4) autumn.

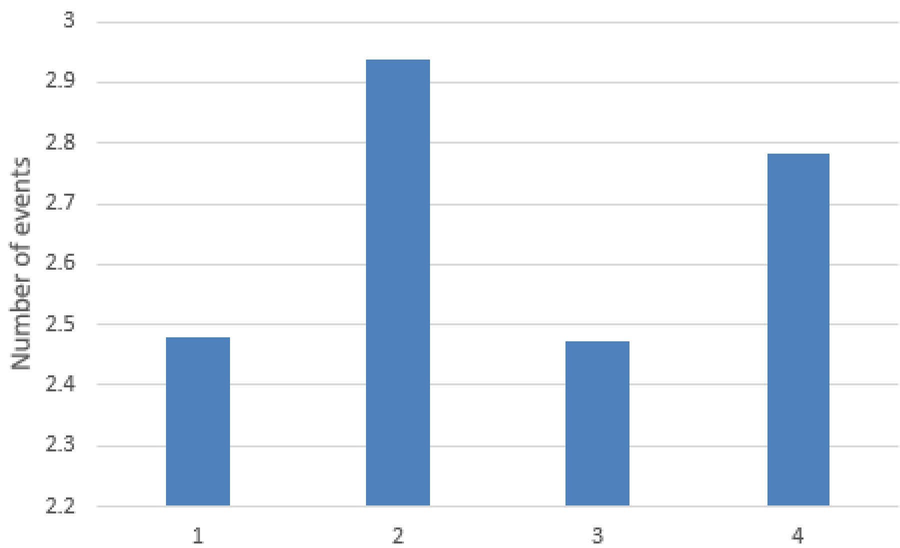

(a)

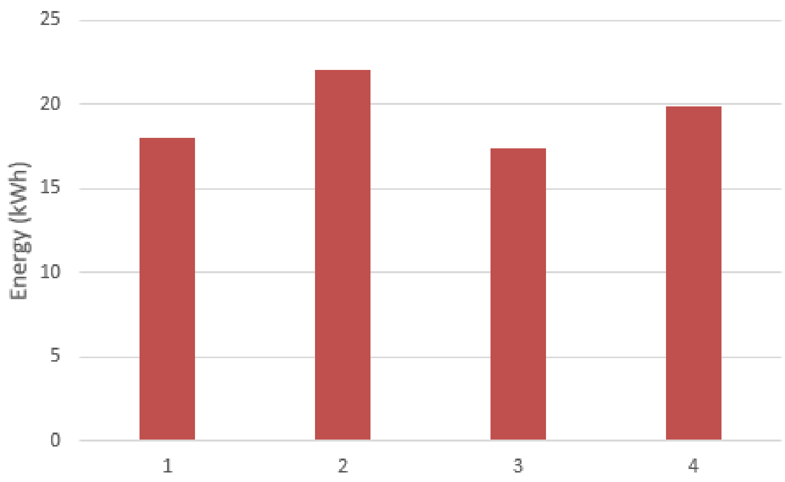

(b)

Figure 31: Details for the number of mean energies delivered per month.

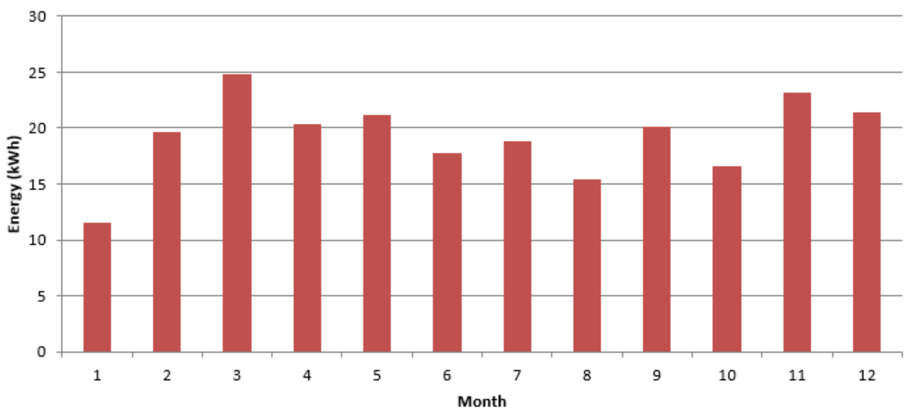

2.4 Simulations from data

When performing statistical analysis, we obtain a non-parametric distribution for the arrivals at the CP as a function of weekdays and weekends, based on the frequency of the events. At this stage, we disregard seasonal effects.

From the statistical analysis, we can generate several possible scenarios of charging demand to be used in Monte Carlo simulations to get information on several variables for CP management, such as energy demand, waiting time, etc. The workflow of the process is reported in Figure 32.

Figure 32: Workflow of the scenarios creation.

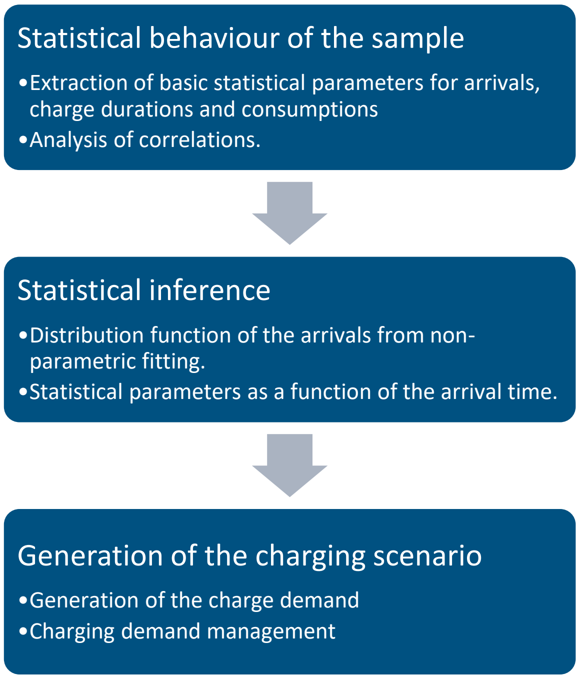

To determine the duration of the recharge and the energy required, the mean and the variance obtained from data within each time interval were considered for workdays and weekends.

With this data, and the a posteriori distribution of arrivals, a scenario of arrivals for a charging station can be determined, given an average number of daily arrivals. To increase the variability of the data, white noise was also introduced on the duration and energy values.

Once the hypothetical weekly request is generated, an algorithm executes the requests, simulating the recharge (in terms of duration and energy), managing the waiting queue and the possible loss of users due to long waiting times.

To simulate users' behavior, we used a Simevent-Simulink model integrated with a fuzzy model based on the waiting time, plus a random input variable to include the possibility of a user to decide waiting even if the waiting time exceed the threshold time of 10 minutes.

In the following we illustrate two examples extracted from AMB dataset for normal chargers. In the two examples the number of charging points is the same, as well as the average duration of the recharge of about three hours, and the average value of the recharged energy is about 5 kWh. However, the number of users almost doubles in the second case. As a consequence, the waiting time goes from zero to an average value of 15 minutes, with a maximum waiting time of 47 minutes.

Example 1: 123 users, 3 CPs in the station. In this scenario, the waiting time is always null, and there is no user-loss. The mean duration for the charge event is 185 mins and the mean energy delivered for charge is 4.9 kWh, which is in line with data reported in Table 1.

Figure 33 shows the CPs occupancy of the station during the week (starting with Monday), while Figure 34 reports the value of the energy delivered during the same time period. Since there is no information on the maximum power delivered during the charge, no further detail can be obtained for energy characterization.

In addition, since no meaningful correlation has been found among charge duration and energy delivered, the two quantities are uncorrelated also in the simulation.

Figure 33: Occupancy at the CPs for the week, example 1.

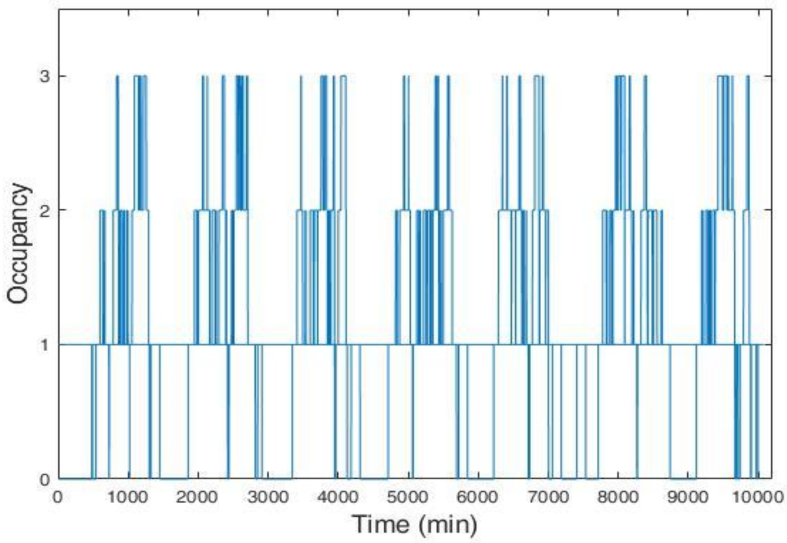

Figure 34: Energy delivered at the CPs for the week, example 1.

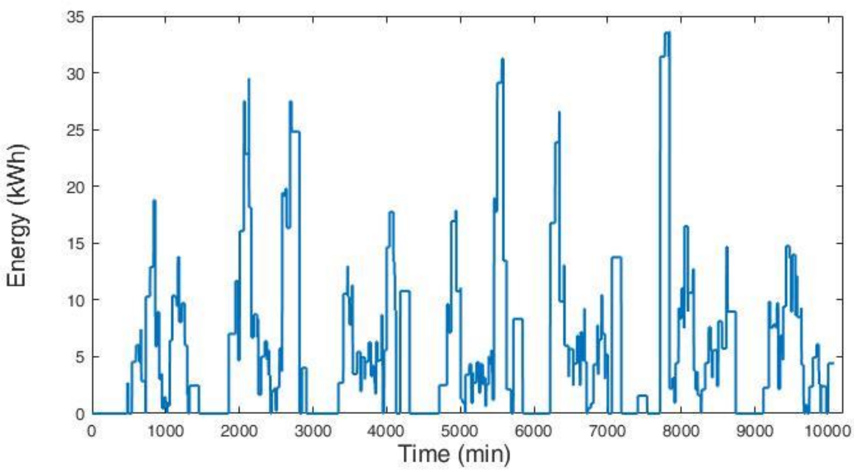

Example 2: 226 users, 3 CPs in the station. In this scenario, the maximum value for the waiting time is 47 minutes with an average waiting time of 15.5 minutes; the number of users lost is 26; the mean duration for the charge event is 185 mins, and the mean energy delivered for charge is 4.9 kWh, which is in line with data reported in Table 1. As shown in Figure 35, the occupancy is higher than in the previous case and the occupancy of the CPs is saturated almost all the time.

Figure 35: Occupancy at the CPs for the week, example 2.

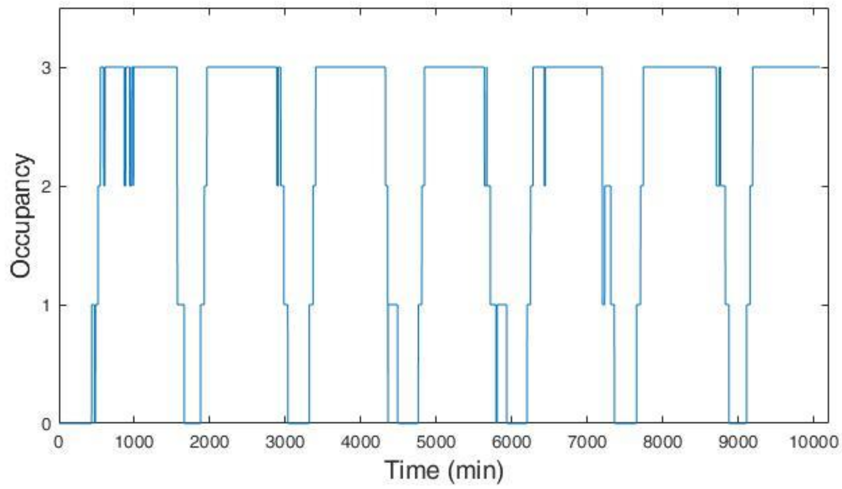

The energy delivered is also slightly higher than the previous case, as it is more probable that several charges occur at the same time (Figure 36).

Figure 36: Energy delivered at the CPs for the week, example 2.

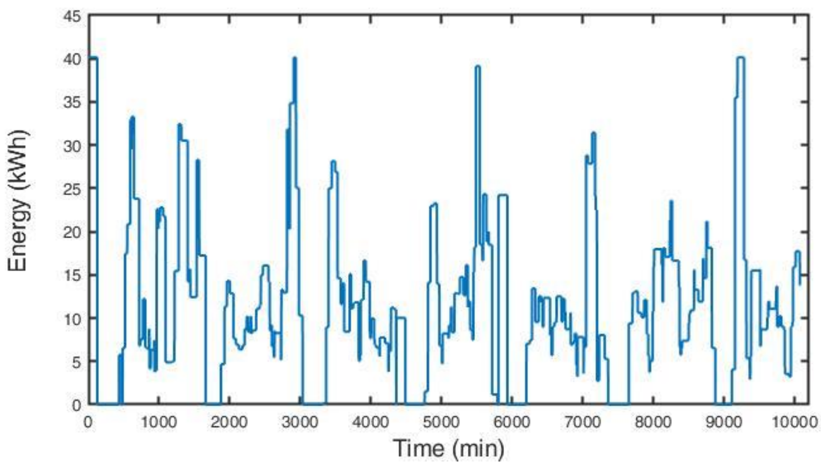

In this scenario, if the slow chargers were replaced with quick chargers, only 6 users would be lost.

These two examples show that the simulations of the load profiles can be used for the analysis of the scenario about penetration of electric vehicles and the diffusion of charging infrastructures of different types.

3. Battery modeling

A battery consists of one or more electrochemical cells connected in series or in parallel where electrochemical reactions happen. The conversion from electrical into chemical energy takes place during the charging phase, while the conversion from chemical energy into electrical energy takes places in the discharging phase. In general, each cell consists of an anode, a cathode, an electrolyte, and a separator. However, the specific composition of each cell can depend on the battery technology. Indeed, there are many different types of batteries (see Annex A – Electrochemical energy storage).

3.1 Electrochemical batteries

Electrochemical storages are characterized by various parameters such as capacity, voltage, specific energy and power, Coulombic efficiency, and operating life.

By comparing specific power and energy among the batteries commercially available, lithium-ion batteries are currently the best performing with specific energy up to 180 Wh/kg, power up to 10 kW/kg, and operating life of several thousand cycles (up to 5000). However, their costs per unit of storage capacity (€/kWh) are higher than lead-acid and nickel-cadmium batteries offering specific energies of the order of 40 and 80 Wh/kg, respectively and powers lower than kW/kg. Future developments for Li-ion are large format cells (>150Ah) with high energy density (> 400 Wh/kg and 800 Wh/L) by 2030[1].

On the other hand, flow batteries and sodium batteries offer high storage capacity (up to several MWh of stored energy) and are usually used at utility level. Sodium-sulfur (NaS) batteries and vanadium flow batteries are now commercially available, while sodium nickel chloride (Na / NiCl2) batteries and other types of flow batteries are not yet widely used in stationary storage. Sodium batteries have specific energy between 120 and 240 Wh/kg, specific power between 150 and 250 W / kg, excellent duration (2500-4000 cycles), and costs close to lithium batteries.[2]

Lithium-ion and sodium/sulfur batteries currently dominate the worldwide market of batteries for stationary use, although it is possible finding lead acid systems and flow batteries. In a short-medium term perspective (2020-2030) there is the possibility of a more massive penetration of lithium-ion batteries in the market and a significant increase in the production of flow batteries. In terms of cost, lead-acid batteries are between 30 and 170 €/kWh, lithium-ion batteries between 250 and 850 €/kWh and, nickel-cadmium batteries between 250 and 500 €/kWh. The gap in prices is due to the intrinsic characteristics of the batteries even though the cost of some innovative lead-acid batteries can reach 1400 $/kWh. Flow batteries cost between 400 and 1200 €/kWh, which however rapidly decreases as the size of the system increases. On the other hand, the cost of NaS and Na/NiCl2 batteries is between 300 and 500 $/kWh and 500-850 €/kWh, respectively. However, it should be pointed out that the real battery cost and the cost projections for stationary lithium-ion batteries are rapidly change for the automotive sector [2] [3].

The most promising technologies on the market today are lithium-ion batteries, high-temperature batteries (based on sodium-sulfur and sodium-metal chloride cells), and flow batteries. For these three categories, the installation costs are forecasted to be between 54 to 66 percent.[3]

3.2 Battery models

There are many studies about battery modeling in the literature. In general, battery models are classified according to the approach they use, although there no official classification exists, and approaches may be hybrid, or apply different mathematical methodologies. Some approaches are based on the physico-chemical phenomena occurring inside the battery and require a thorough knowledge of the materials that make up the battery and their interactions. In other approaches, the battery model can be seen as a black box based on a set of experimental data related to the input and output variables of the system. A black-box model is completely unrelated to the physics of the underling processes, such as the chemical reactions occurring inside the battery. For this reason, the black-box model is applied in cases where the elementary constitutive laws of the phenomenon are not easily identifiable, or when there is the need of reproducing highly complex phenomenon in a simple way. The accuracy of the model often depends from the quantity and quality of the available data.

For battery modeling, the most general inputs are the current (I), the state of charge (SOC) and the temperature (T). The output is the voltage (V), while the modelling parameters are the open-circuit voltage (E_0), the initial capacity (C_i), and the internal resistance (R_i), as reported in Figure 37.

Figure 37: Typical representation of a black box model for a battery.

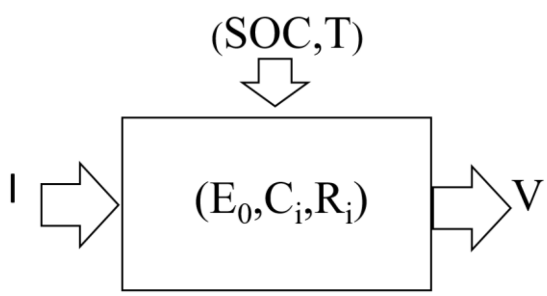

3.2.1 Electrochemical models

Among the most accurate battery models there are electrochemical models, often used to validate other types of models. Electrochemical models simulate the battery behavior by reproducing physical phenomena occurring inside the battery. In most cases, these models refer to the works of Doyle, Fuller, and Newman in which the charge-discharge phenomena [4] and the relaxation phenomena of the insertion processes of the lithium [5] are modeled using the theory of concentrated solutions.

Electrochemical models try representing phenomena occurring in the battery to describe the loss of active material due to the reaction of the solvents, the growth of the anode resistance, the diffusion phenomena, etc. Therefore, they are very complex and they are described by a system of coupled differential equations with a large number of parameters. For this reason it becomes crucial determining the values of microscopic variables starting from measurable macroscopic variables, often resorting to semi-empirical methods. Furthermore, simulations with these models allow accessing the values of the internal variables, which are difficult to measure in the laboratory under operating conditions. However, due to their complexity, these models can only be solved with powerful computational approaches. In order to reduce computation times and to make these models usable even in contexts where less accuracy is required, simplified hypotheses are often introduced, such as one-dimensional models or single-particle concentration. Electrochemical equations can also be coupled to other approaches, such as thermal models.

3.2.2 Analytical models

Analytical (or empirical) models show higher level of abstraction than previous approaches. In this model the battery is represented with a few equations that try to reproduce certain responses to given inputs. In particular, when it concerns battery aging, these models correlate the battery stresses with the trend of key variables such as capacity and internal resistance. Therefore, the estimation of aging parameters is based on experimental measurements. These models are often used for on-line battery prognostics (e.g., in electric vehicles). In addition, to monitor battery health, mathematical models should not be computationally expensive.

3.2.3 Stochastic or data-driven models

Compared to other models, stochastic models rely on experimental data to predict battery behavior. Therefore, stochastic models provide an abstract representation of the battery (cell or system) capable of reproducing its behavior with less computational effort than electrochemical models but with higher accuracy than other types of models. In particular, stochastic models are able to model sudden battery failure, charge recovery, capacity recovery and Peukert's law. On the other side, they need extensive laboratory tests to collect enough data.

3.2.4 Equivalent circuit models

Equivalent circuit models are among the most popular models since they show a satisfactory level of accuracy with lower complexity than electrochemical models and significantly shorter simulation times.

The simplest possible equivalent circuit consists of an ideal voltage source and a resistor. This simple system reproduces the main characteristics of a battery in a quasi-stationary condition, while its accuracy is very low when considering rapid dynamic conditions. Adding a capacitance-resistance (RC) branch, the model can reproduce the polarization effects of the battery and becomes more reliable. These types of equivalent circuits are called "Thevenin's models". By adding further RC networks to the equivalent circuit, it is possible to obtain models that are more realistic, with an increased resolution.

Most of the battery models require extensive datasets obtained with laboratory equipment to determine their parameters. However, it is possible to parametrize an equivalent circuit model using the information contained in a typical commercial Li-Ion cell manufacturer's datasheet. On the other hand, equivalent circuit models showed to perform better than some simplified electrochemical models in term of accuracy since they take into account relaxation phenomena.[8]

For this purpose, as shown in Figure 38, we use a model that can be represented by an equivalent electrical circuit. The model consists of a main reaction branch that takes into account the reversible process of charge and discharge, represented by the electromotive force (EMF) E_0, which corresponds to the open-circuit voltage (OCV). The EMF is in series with an equivalent series of resistance and a parallel resistance-capacity (RC) circuit accounting for relaxation phenomena. Other battery characteristics with faster dynamics can be described by adding more RC branches. The EMF, the resistances and the capacity are a function of the state of charge of the battery and of the temperature. However, the present model does not take into account the influence of temperature.

Figure 38: Equivalent circuit model

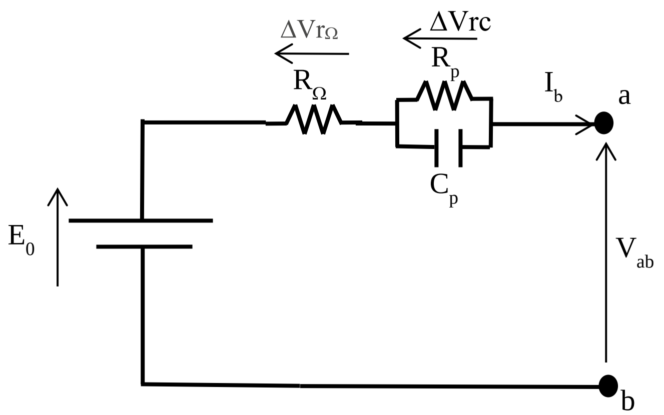

The SOC at a given time t is defined as the ratio between the charges accumulated in the battery at time t and the nominal capacity (eq. (1)). The charge stored in the battery is the integral of the current over the time with negative value for charging current and positive value for discharging current. Also, the so-called depth of discharge (DOD), defined as in equation (2) is defined:

$$SOC(t) = 1 - \frac{Q_e(t)}{C_{nom}} = \frac{1}{3600}\frac{\int_0^t i\,dt}{C_{nom}} \quad (1)$$

$$DOD = 1 - SOC \quad (2)$$

The battery capacity can be measured from a standard cycle, consisting in a complete charge/discharge/charge cycle, usually at a charge current C-rate[3] of 0.5C or 1C. A typical discharge-charge profile is reported in Figure 39, where the applied current profile and the measured voltage are shown.

Figure 39: Standard discharge-charge profile

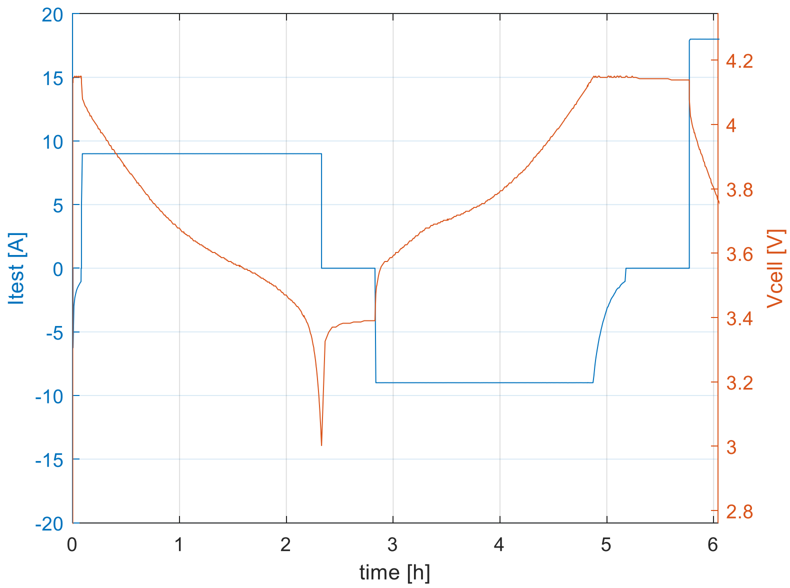

The capacity is then determined by the integral of the current over discharge time interval (eq. (3)).

$$C_{eff} = \frac{1}{3600} \int_{t_0}^{t_{dsc}} i \, dt \tag{3}$$

To determine the EMF E_0, a constant current is applied for a sufficiently long time to set the electric circuit to a steady state. At this point, the current is interrupted and the voltage response of the batteries to this current step is measured with E_0 corresponding to the asymptotic voltage value. The input current and the typical voltage response are shown in Figure 40(a) and (b) respectively.

[3] The C-rate is a conventional way to express the amount of current applied as a function of the battery capacity. C-rate = 1 is the amount of energy required to fully discharge (or recharge) the battery in 1 hour. C-rate = 2 refers to a current capable of discharging/charging the battery in half an hour. C-rate = 0.5 is a current capable of discharging/charging the battery in 2 hours, and so on. Different currents correspond to the same C-rate, depending on the size of the battery. A C-rate = 1C is equal, for example, to 10 A for a 10 Ah capacity battery, and 100 A for a 100 Ah capacity battery.

Figure 40: Determination of E0 with the current step method.

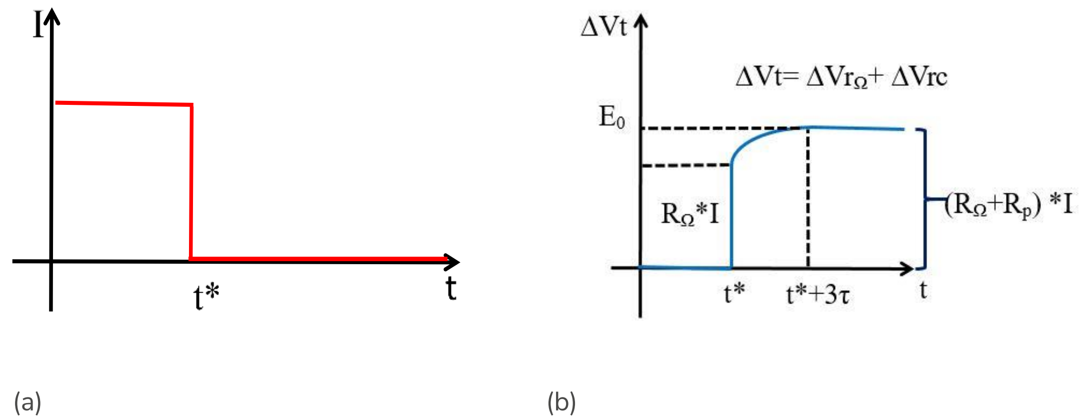

From the analysis of the voltage response to the current step, it is possible to extract the parameters of the equivalent circuit. The internal resistance is calculated as the ratio between the voltage drop and the amplitude of the current step. In the potential drop, two timescales can be identified. The first potential drop is due to the resistive part of the circuit R_{Ω}, while the second phase is due to the relaxation phenomena R_p. The capacitor value Cp is calculated from the relaxation time constant $\tau = R_pC_p$ assuming that the extinction time of the transient is approximately 3τ.

There are many methods to calculate the internal resistance of the battery as a function of SOC. [7] Internal resistance is usually calculated from multiple discharge/charge pulses at different SOC. In this way we obtain the SOC-dependent internal resistance. Depending how long the voltage is measured into the pulse, the gradient will represent a phenomenon between the pure Ohmic resistance R_{Ω} (milliseconds) and the cell's bulk total resistance (seconds) (R_{Ω}+ R_p). The test profile applied to a battery cell EIG 20 Ah is shown in Figure 41 and the results are used to calibrate the model.

Figure 41: Internal resistance test profile.

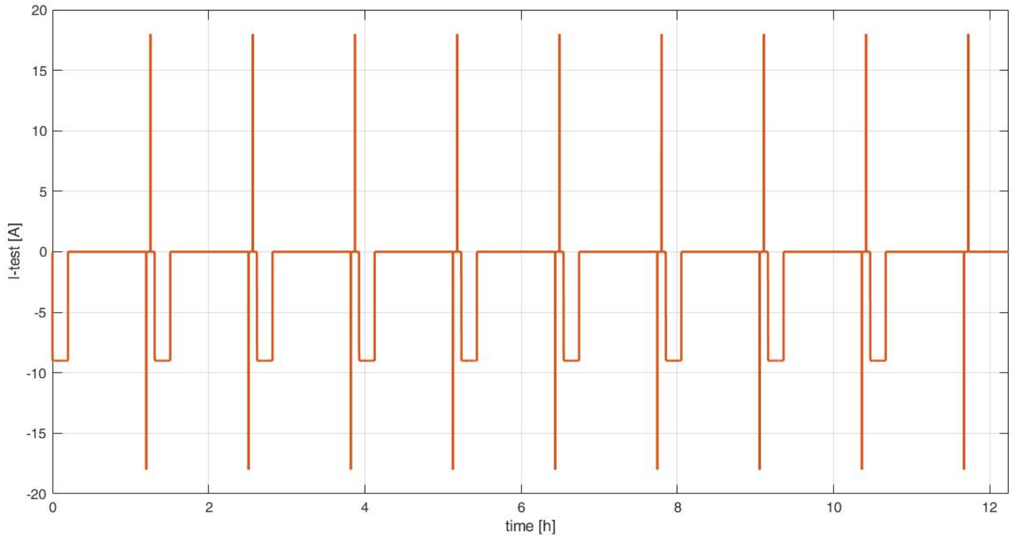

The two current pulses are used to calculate the ohmic and relaxation resistances during discharge and charge. On the other hand, the current step is used to discharge the battery by a 10% of the nominal capacity value and to calculate the rise in the voltage curve used to determine the value of open circuit voltage and of the capacitance Cp.

Figure 42 shows the open circuit voltage as a function of the depth of discharge E0 (DOD) calculated with the above method and using experimental data for an EIG 20Ah pouch cell.

Figure 42: E0 as a function of DOD for EIG 20Ah cell.

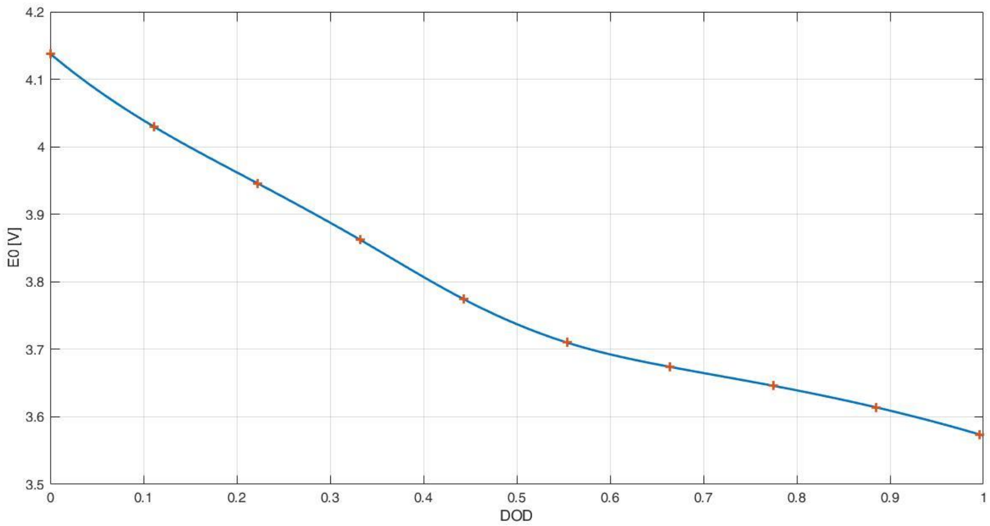

Figure 43 shows the Simulink complete model for a battery, while the battery subsystem is represented in an electric circuit equivalence, as reported in Figure 44.

Figure 43: Simulink model for the battery.

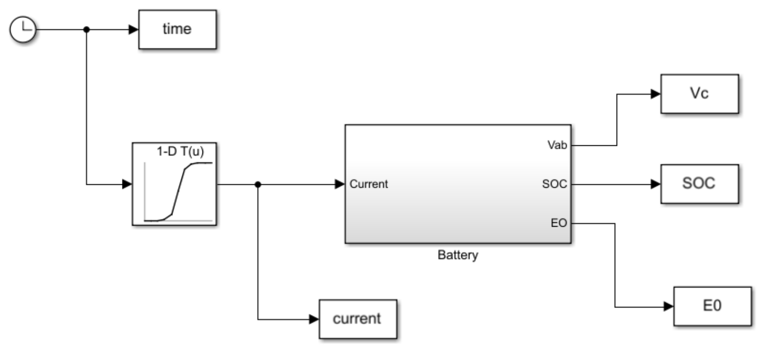

Figure 44: Details of the Simulink battery subsystem.

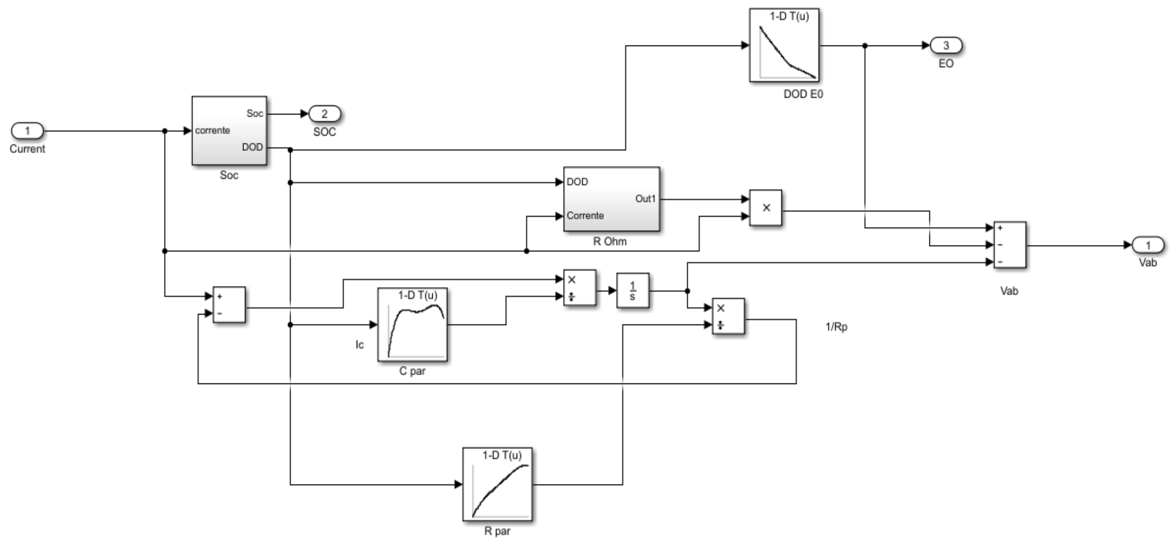

To verify the effectiveness of the model in reproducing the behaviour of the battery, we report the comparison between the measured voltage and the one obtained from the model using the calibration with pulses at DOD = 0.7 and a discharge to reach a DOD = 0.8 (Figure 45).

Figure 45: Comparison among the measured and the calculated voltage in the step between 0.7 and 0.8 DOD.

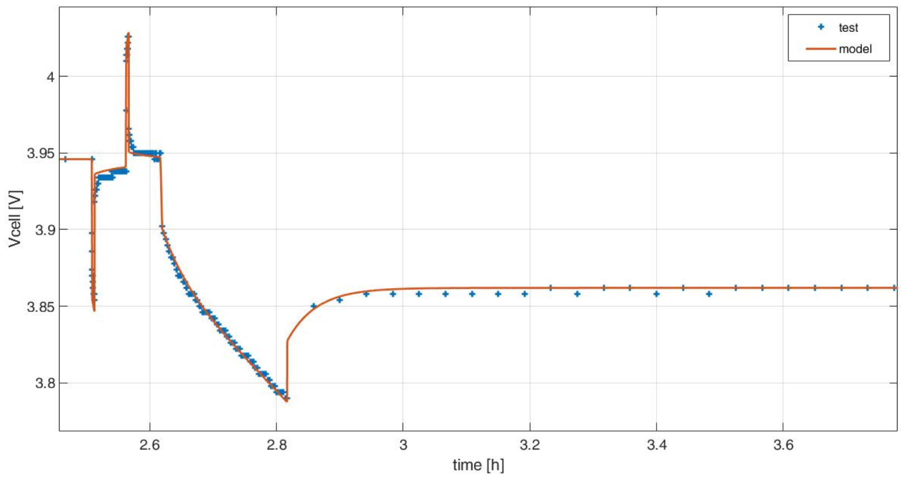

Figure 46 reports the comparison between the measured and calculated voltage response on standard discharge and recharge cycle.

Figure 46: Comparison on standard discharge and recharge cycle.

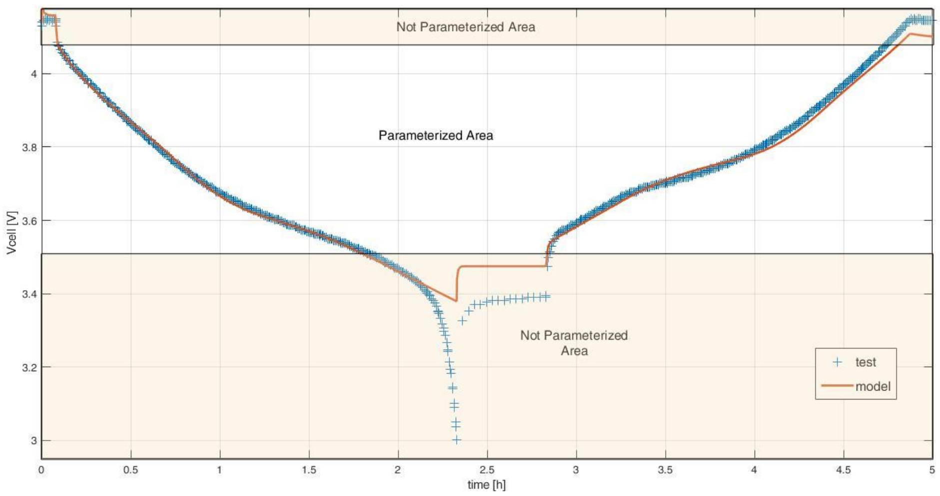

The curves shown in Figure 46 are very similar for almost all the length of the charge/discharge curve with the exception of the non-parameterized zone for DOD = 0 and DOD = 1, that is not calibrated in the model. However, in automotive applications, batteries rarely drop below 10% SOC.

In the following, the above model will be used in the simulation for the EV battery behavior.

3.3 Battery charging algorithm and profiles

Based on their power ratings EV battery chargers can be divided into level 1, level 2 and level 3 (Table 11).

Table 11: EV battery chargers characteristics.

Power level	Typical use	Typical power	Charging time
Level 1	Home	2 kW	4–11 h
Level 2	Public	20 kW	1–4 h
Level 3	DC Fast	100 kW	< 30 min

The chargers can be on-board or off-board, depending on the technology. Moreover, some chargers allow bidirectional power flow to implement vehicle-to-grid (V2G) interaction. This technology has met much interest due to its ability to supply power to the grid in the event of a peak load request, system failure, or other unexpected scenarios. For several purposes, V2G car batteries can be used as distributed energy storage systems that can improve energy quality, stability and operating cost of the distribution network, as well as power carriers to bring energy from one zone to another one.

Besides the charging technology, we also need considering the applied charging method. For Li-ion batteries, the most popular charging modes are constant current/constant voltage (CC/CV) and constant power/constant voltage (CP/CV) profiles. However, there are studies proposing different charging strategies aimed at improving charging times with the same power and mitigating the negative effects on the battery life.

3.3.1 Constant Current-Constant Voltage (CC–CV)

In this type of charge, an initial phase in which the current keeps constant and equal to the maximum value allowed by the type of considered charge is followed by a phase in which the current is progressively reduced to keep the voltage constant. The switch between the two modes occurs at a certain threshold voltage value that depends on the battery technology. Charging of the battery keeps going with a constant voltage equal to the cut-off value. Full charge stops when the current reaches a minimum value in between 3 and 5% of the rated current. Examples of charging curves are reported in Figure 47, where the CC-CV charge mode is shown for different charging power levels. These experimental curves have been recorder for a Nissan Leaf with 24 kWh battery pack with initial SOC of 20% at ENEA laboratory.

Figure 47: Charge profile for a Nissan Leaf (24 kWh battery) for different charging power.

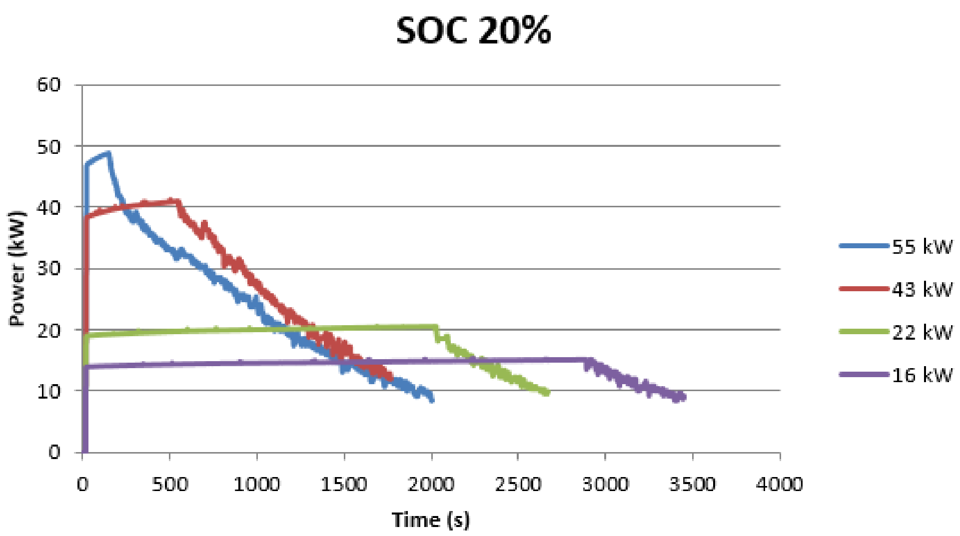

3.3.2 Constant Power – Constant Voltage

The other charging option available for EV chargers is Constant Power - Constant Voltage. The concept is similar to the one of the CC-CV charge, but in this method there is a first phase at constant power (CP) until the maximum cell voltage is reached. Considering the voltage increases with the SOC, the current must be adjusted ensuring a constant charging power. At this stage, a constant voltage recharge takes place in the same way as illustrated in the previous case.

3.3.3 Advanced charging pattern

In literature, it is possible to find many charging algorithms that are tailored to improve the charge speed and/or the battery life and safety.

The Five-Step Charging Pattern is a multistage constant-current (CC) charging method starting with the charge stage at the highest current until the pre-set limit voltage is reached. In the following, in order to induce a voltage drop, the current is switched to the next constant value, which is smaller than the previous one. These steps repeat to obtain five CC stages. [19] Even if the algorithm can shorten the charging time, finding the correct values of the currents for the five stages can be difficult and time-costly making this method cumbersome for real-world applications.

The pulse charging method suggests charging the battery with a sequence of pulses. During the rest periods between two pulses, the ions can diffuse and neutralize. In that case, the charging phase can continue at high rate with the following pulse avoiding harmful phenomena in the battery. Different strategies exist to control the width or the peak value of the pulses. As for the five-step, this charging algorithm is not currently used in any commercial solution.

Other strategies rely on the battery physical-based models which take into account the side reaction occurring in the battery and the aging process to design a tailored charge profile minimizing the charging time while preserving, the battery lifetime [12]. However, these models are strictly dependent on battery chemistry and technology.

3.4 Charging strategies

An electric car being charged represents an additional load for the electricity grid. While there are industry standards, such as IEC1000-3-2, requiring low distortion on the side of the charger to minimise the impact on power quality, they do not take into account the aggregate effect of many simultaneous charges. These can cause problems such as deterioration of energy quality; the instability of the electricity grid and the degradation of operational efficiency [13]. To ensure stability in the grid, energy demand and supply must be matched. However, this is difficult to achieve because of the unpredictability of the charge events and of the large variations they present over the time. The situation is further complicated by the introduction of renewable energy sources. To address this problem, suitable charging schemes can be introduced. There are many possible approaches whose characteristic are reported in Figure 48

Figure 48: Charging scheme classification (adapted from [13]).

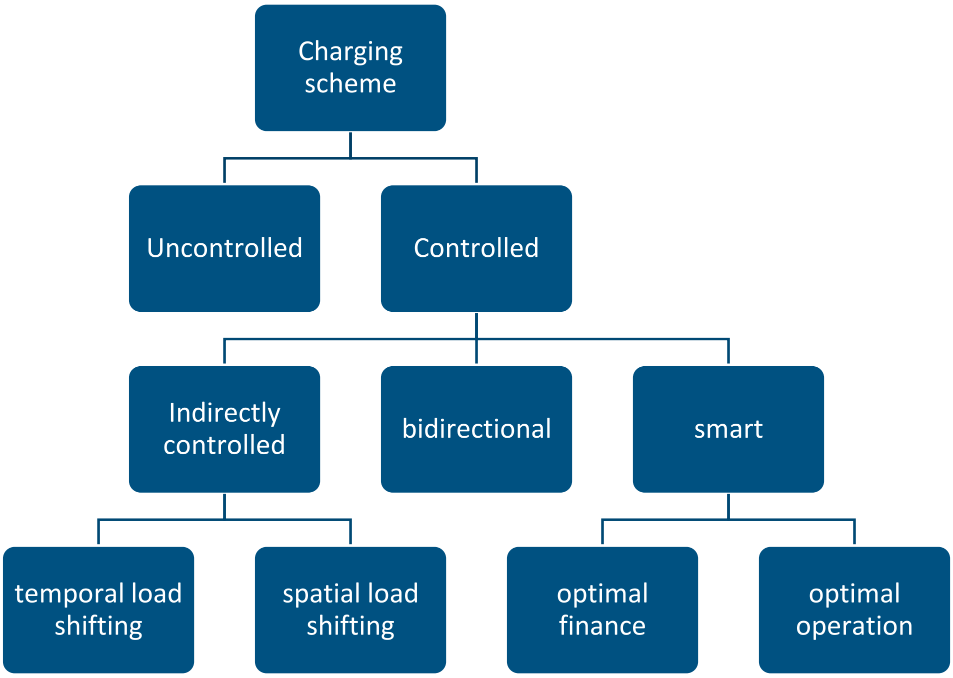

Uncontrolled charging applies when the controller (i.e., the grid operator) doesn't have information to control the charging profile. Therefore, the batteries start charging immediately when they are plugged-in, or after a user-specified delay.

In controlled charging schemes, different strategies can be applied. In indirectly controlled charging, the schemes do not directly control the charging parameters. However, external variables can indirectly influence the charging operation. For example, the price of energy can influence the decision recharging and thus help avoiding grid overload. The smart charging schemes directly control the charging parameters, such as the output of the electrical sockets or the set-point of the chargers so that the power delivered can be varied. Therefore, the charging time does not necessarily coincide with the time of connecting the vehicle to the socket. Smart charging schemes implement a series of actions in order to achieve monetary (optimal finance) or operational (optimal operation) performance goals. Bidirectional charging scheme acts as a smart charging scheme which includes the possibility of bidirectional power flux, i.e. vehicle to grid (V2G).

The charging control strategies can be centralized when information from many charging infrastructures are collected and coordinated by a single/central entity or even distributed, if the computation load for the optimization strategy is performed by several entities [14].

Offline strategies provide for the calculation of charging profiles based on the expected operation of the system and therefore, assume that all electric vehicles are available for negotiation of their tariff plans since the beginning.. However, in a more realistic context, neither the arrival times of electric vehicles nor the state of the electricity distribution network is known a priori. In contrast, online strategies are able to handle numerous uncertainties, including the mobility of electric vehicles [14].

To test a possible charging strategy, we consider data on real charging events. The data refers to the charging event in a given day at different charging sites, but as a hypothesis, we will assume that all the sites, and thus the charging events, refer to the same charging infrastructure. The chart in Figure 49 represents the arrival time at the charging sites and the charging durations.

Figure 49: Arrival time and charge duration for the charging events selected.

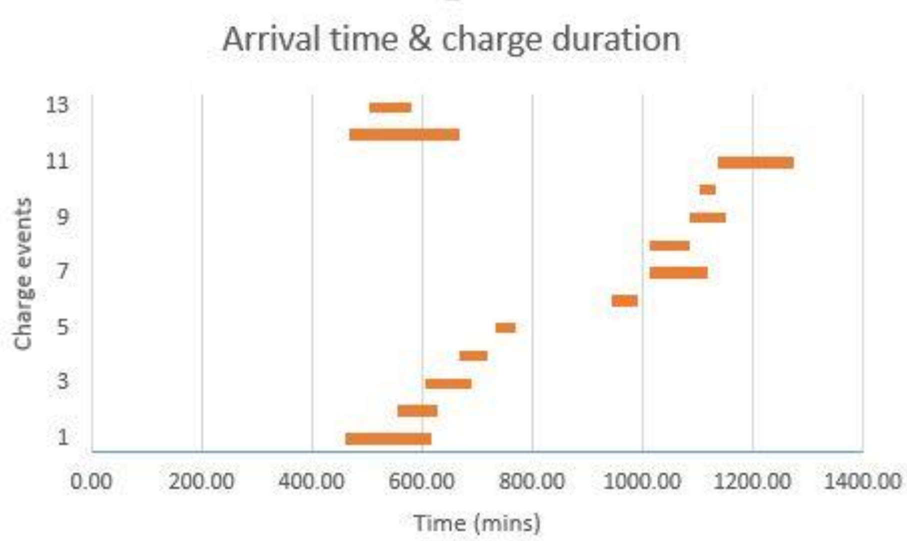

The corresponding load power profile at the hypothetical charging infrastructure is presented in Figure 50. The bold line represents the total power load at the station, while the light lines refers to the single charge events load profile. As shown in the figure, the total request of power varies amply with time and can be quite high for some periods of time.

Figure 50: Load power profile for the charging events.

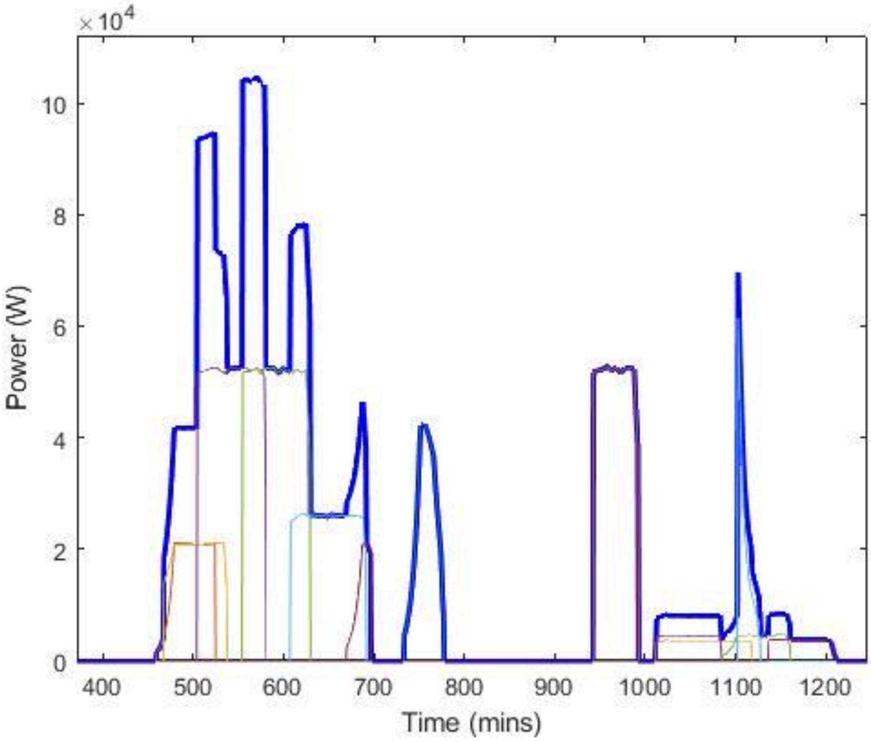

If, for any reasons, the power at the station should be limited, it is necessary to put in place some charging strategies to cope with the power demand and the limitations. We will apply a local (decentralised) charging strategy, where the charging infrastructure operator limits the power available for the charges on the basis of an external constraints on power level. For this purpose, we implemented the time-load shift. This consists in the possibility of having a variable rate charging. In this way, the power used to charge can be varied in time within a range between zero and the maximum charging power compatible with EV battery SOC and technology.

We propose an on-line algorithm that does not need any forecast data on EV arrivals. We assume that information on energy required and parking time is available on EV arrival. Different charging sockets of different charging power are also available. Based on this information, we can derive the amount of energy to be delivered before departure at any time. Our approach is based on a fuzzy model that, using the available information as an input, it gives the value of the power at a given time for each charging event. We compare two fuzzy models having different inputs and we show that more data can give better results complying with the objectives.

The model can handle time-variable limit, but for simplicity we suppose the charging station should limit the absorbed power to 60 kW.

For each time, we calculate the energy to be charged and the time left before departure for every EV in charge. Since we don't have information on battery SOC and size, we must rely on the experimental charging profile to infer the behavior when the input power is changed. This is especially important in the last part of the charge, when the battery can enter the CV charging phase, thus limiting the input power. Moreover, we set three profiles for the user:

- Long parking time: these are the more prone to be included in the power modulation;
- Medium parking time: these stay a little more time than required and can participate to the power modulation;
- Short parking time: the park and charging times coincide and they won't participate to the power modulation.

When the total load request at the charging station exceeds the power limit, for each EV we calculate for the ratio between the remaining energy to be charged and the time left before departure. This "average power" is compared to the maximum power accepted by the EV (taken from experimental data) and the result is the input for the first fuzzy model (M1).

The graphical representation for M1 is reported in Figure 51.

Figure 51: Graphical representation of M1 fuzzy model.

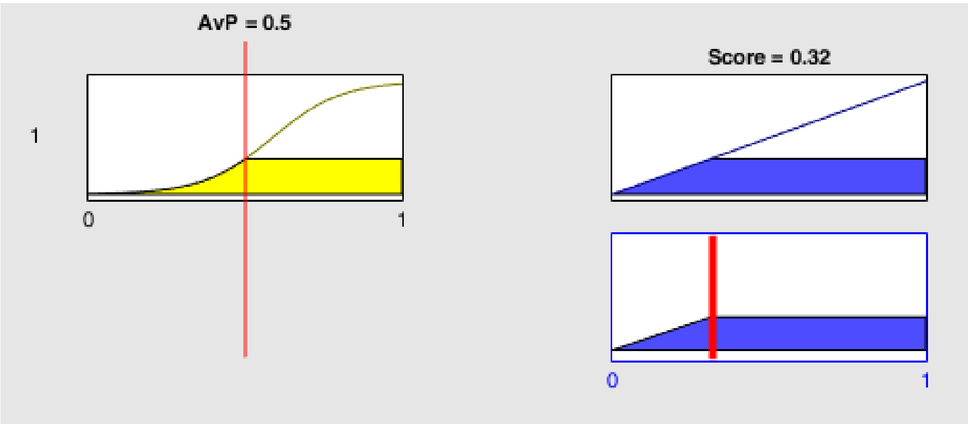

The score is close to zero if the remaining recharge can be completed in much shorter times than the available one or with much lower power levels of than required. Conversely, the score is close to one if the recharge requires times close to the available one and power levels are close to the maximum ones. It follows that, the lower the score, the lower will be the priority to finish charging with a greater the flexibility in modifying the power supplied.

The other fuzzy model, M2, takes into account the "average power" and the time left before departure ("deltaT"). Therefore, the score is calculated taking into account both inputs (Figure 52).

Figure 52: Graphical representation of M2 fuzzy model.

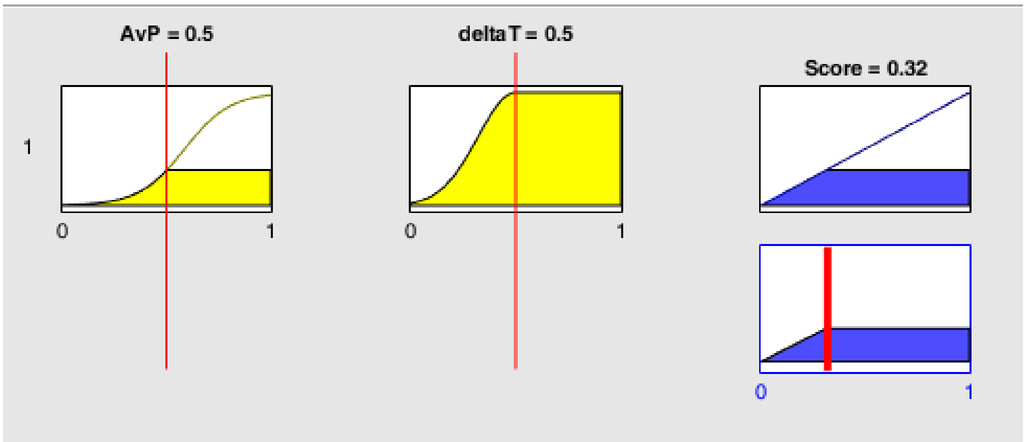

The score obtained for the model M2 has the same interpretation of model M1.

In Figure 53 we compare the results for the two model, along with the load profile for the original data. As it can be seen, both model reduces the power load. However, M1 still show some peaks, while M2 manage to contain the power load in the required limit.

Figure 53: Comparison among different charging control algorithms.

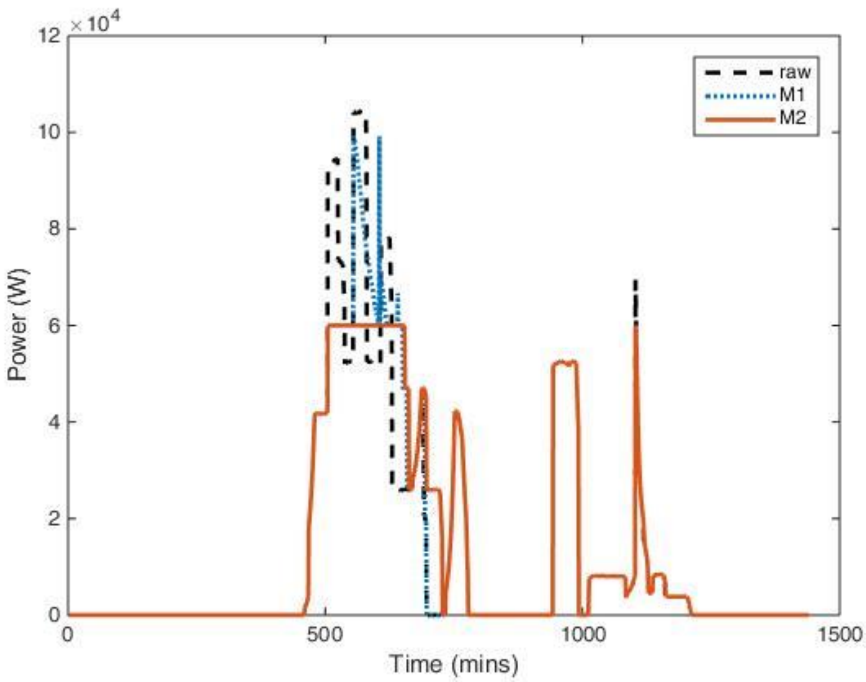

To understand the different results, we can investigate the single charging profile. As shown in Figure 54, both M1 and M2 profiles are longer that the original one. However, M2 model acts more on the initial part of the charge profile (see profile (b)) than M1: this has a major impact on the total power profile.

Figure 54: Single charge profiles for different charging algorithms.

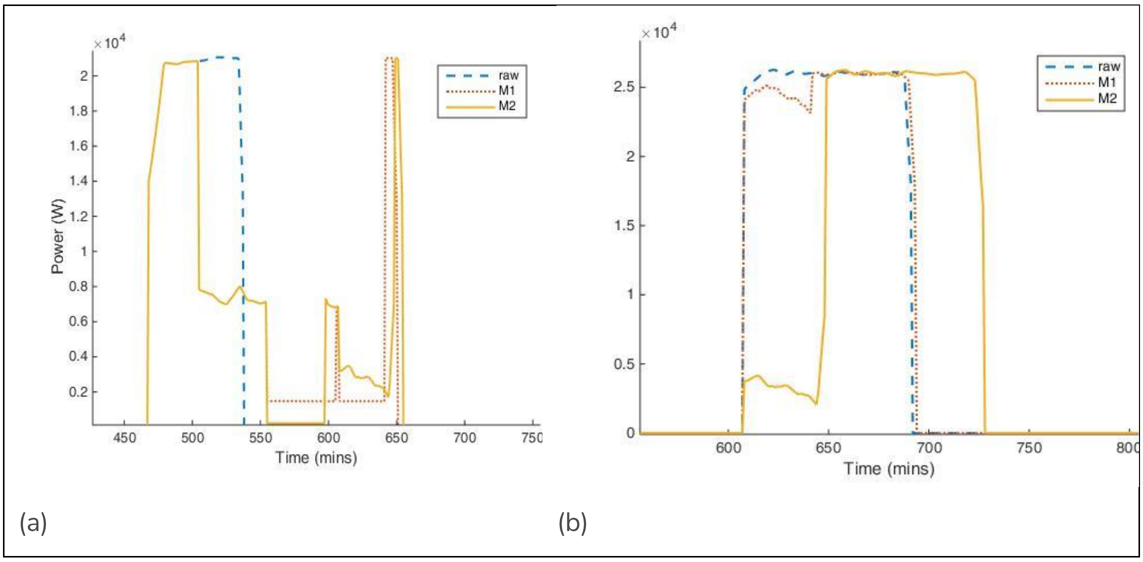

The fuzzy approach can be further extended to include other input variables, as the SOC, or model V2G. In order to show the effect of V2G, we lower the overall CI limit to 50 kW. This is possible because the 60 kW limit can be managed with the charge shift. It is important to stress out that in our model we are dealing with unscheduled arrivals. However, as long as the occupation frequency of the CPs remains low as in the analyzed sample, even in the case of scheduled arrivals, only a small part of the energy available from the V2V could be used. This drawback could be overcome by using a stationary storage system. However, this solution would be detrimental to the overall energy efficiency of the system, as an effect of the finite efficiencies of the various components (batteries, converters, etc.).

In Figure 55 we show the load profile at the CI with and without V2G that, in this specific case, is a vehicle-to-vehicle (V2V) application. Only two cars were allowed to get bidirectional power flux: one in the time slot between 450 and 700 minutes, and the other one in the time slot between 800 and1000 minutes. We have increased the availability period of the vehicles compared to the original data allowing them to be used in V2V. In Figure 56, the power profiles with or without V2G for the first of the two EV is shown. The two discharge events contribute to lower the peaks observed in Figure 55.

Figure 55: Overall load at the CI with and without V2G.

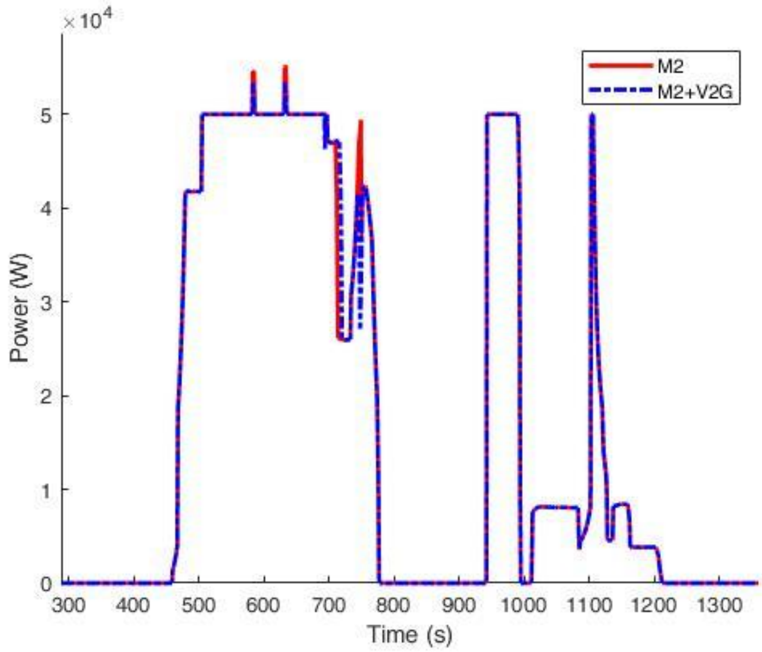

Figure 56: Power profile for the EV with and without V2G.

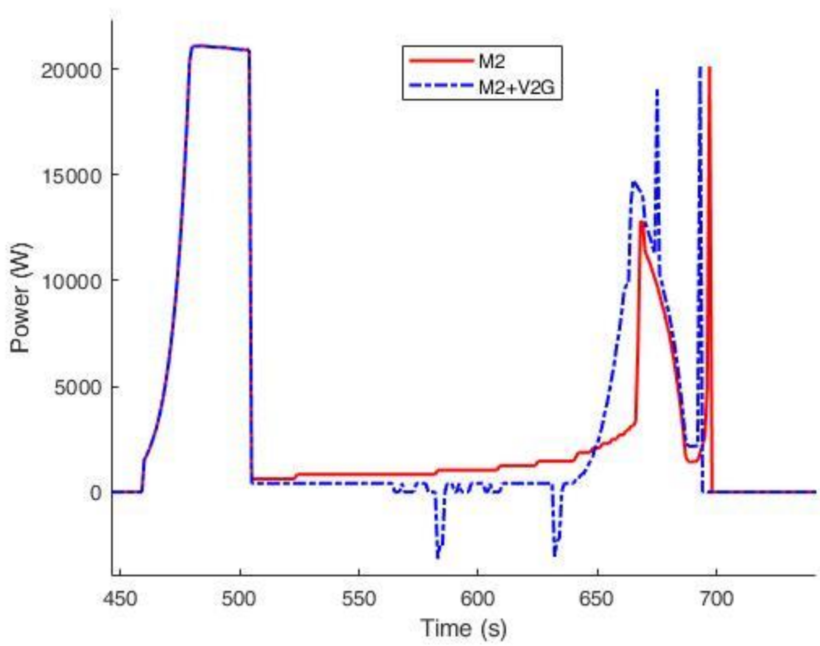

The fuzzy model is very sensitive to its design and can produce different profiles, depending on the objectives of the designer, and on the model parameters. For example, to smooth the peaks in the final part of the reload profile, it is possible to reshape the membership function of the time variable. The comparison between the profiles for the same vehicle and two different membership function is shown in Figure 57.

Figure 57: Comparison between profiles with different membership function.

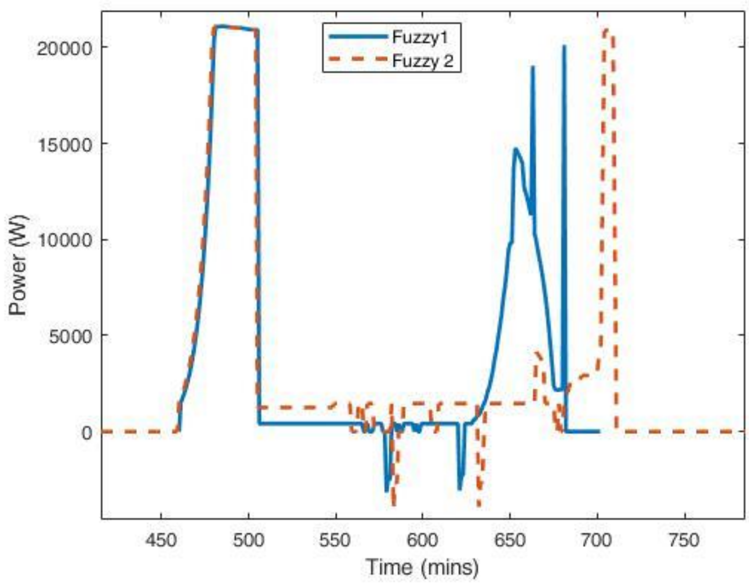

3.5 Battery simulations

In this section we illustrate the response of the battery model presented in the previous paragraph 3.2.4. The parameters used in the calibration are the ones obtained from tests made on battery cells EIG 20 Ah with a nickel-manganese-cobalt compound at the cathode and graphite at the anode.

We compare the results of our model with the Battery block implemented in the SimEscape tool of MatLab. According to MatLab documentation, “the Battery block implements a generic dynamic model representing most popular types of rechargeable batteries.” [15]. The underling model of the battery block represents a simplification with respect to the one we proposed because its equivalent circuit neglects the RC network, thus neglecting the diffusion dynamics. The equivalent circuit for the battery block is reported in Figure 58.

Figure 58: Simplified battery model used in MatLab battery block

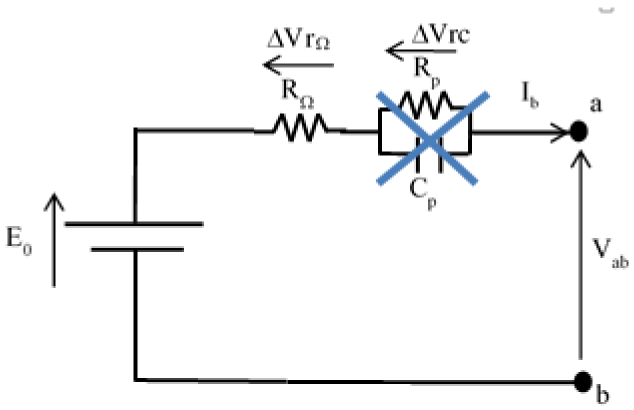

Notwithstanding its simplicity, the model can reproduce the charge-discharge characteristic of a battery, and its behavior is characterized by the parameters set in the circuit. The maximum error of the model dynamics with respect to experimental data is 5% in the SOC range 10%-100% and for charge currents between 0 and 2 C, and discharge currents from 0 to 5 C. [16]

In the model, some simplifying assumptions are made. Among those, the most relevant for Li-ion batteries are the following:

- Constant internal resistance during the charge and discharge cycles and independent from current amplitude.
- The discharging and charging characteristics are assumed to be the same.
- The capacity of the battery does not change with the amplitude of the current.

Even with the above limitation, the model has been proven to effectively simulate the demand charging profile of an EV battery.[39]

The open circuit voltage for the Matlab battery block id reported in Figure 59. It shows there is a different trend compared to the one observed for the EIG battery cell (reported in Figure 42). This will influence the voltage outputs of the two models.

Figure 59: E0 curve for the MatLab battery block

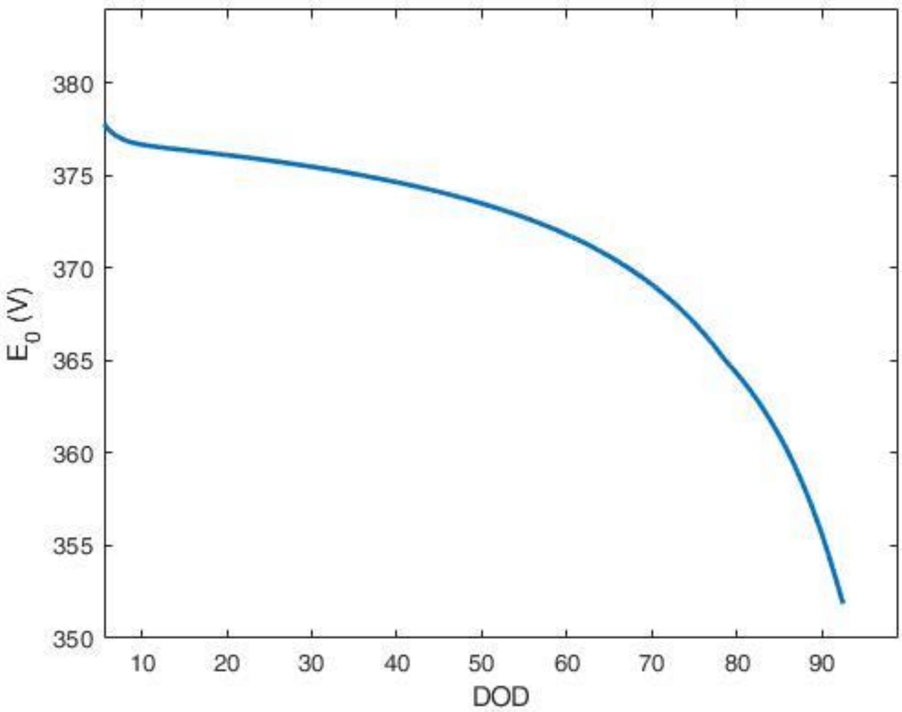

For the battery data, we used voltage and energy capacity values similar to those of the Chrevolet Bolt-EV (350V and 60 kWh),[40] and the ones of the first-generation Nissan Leaf (350V and 24 kWh) [41]. Since the Simulation models accepts the values of nominal voltage and battery capacity in Ampere-hour as input, the previous values have been approximated, and are shown in Table 12.

Table 12: EV batteries main characteristics

Battery	Nominal Voltage (V)	Capacity (Ah)	Energy (kWh)
A	350	68	23.8
B	350	170	59.5

The model for the battery pack was created by putting in parallel elementary battery modules placed in series. Since the elementary batteries have a nominal voltage of 3.7 V and an effective capacity of about 17 Ah, 97 modules consisting of 4 elementary cells in series were put in parallel for battery A, while for battery B 97 modules consisting of 10 cells in series were put in parallel.

In the following, we compare SOC, voltage and input current for the two battery models, and for both EV batteries characteristic set. Indeed, the input current C for the battery is a function of the applied power P and the battery voltage V, C=P/V.

Firstly, we analyze the response to the original charge power profile and the one generated by the fuzzy model M2. The left part of Figure 60 shows the results for the battery A. On the other hand, the right part of Figure 60 shows the results for battery B. Solid blue lines represent the outputs of the model for the EIG battery cells, while red dashed lines refer to the simplified circuit of the MatLab battery block.

The two models perform almost identically for the SOC value. It can be noted that the two profiles bring the battery the same amount of charge, even though in a different way. Since battery B is bigger than A, the final SOC for the first is smaller. On the other hand, differences are evident in the battery voltage behavior. As mentioned above, this is due to the difference in the open circuit voltage behavior as a function of DOD and reflects the difference among different battery chemistry. The voltage of battery B values remain always well below the voltage values of battery A. This is one of the reasons why bigger batteries are less prone to deteriorate if fast charged. As we can see, the proposed model shows a wider range of voltage values for battery A than the Simulink model. In particular, higher peak value is reached, which is lower than the maximum battery voltage for both profiles. The Model 2 profile achieves a slightly higher value for peak voltage. The same behavior is found for battery B, although in this case the voltage variation amplitude is lower than that for battery A. For battery B, the Simulink model gives higher and more similar voltage values to those obtained for battery A. This may depend on the fact that the proposed model represents the car battery pack as a network of cells in series and parallel, while the Simulink model represents the battery pack with a single circuit.

Figure 60: Comparison of the battery main output characteristics for different sizes and models.

Battery A	Battery B

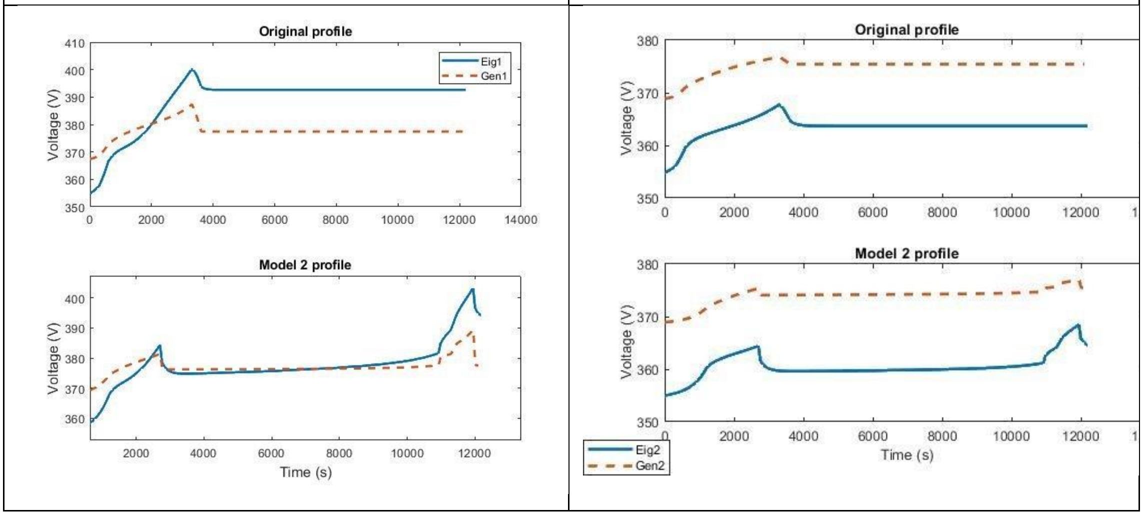

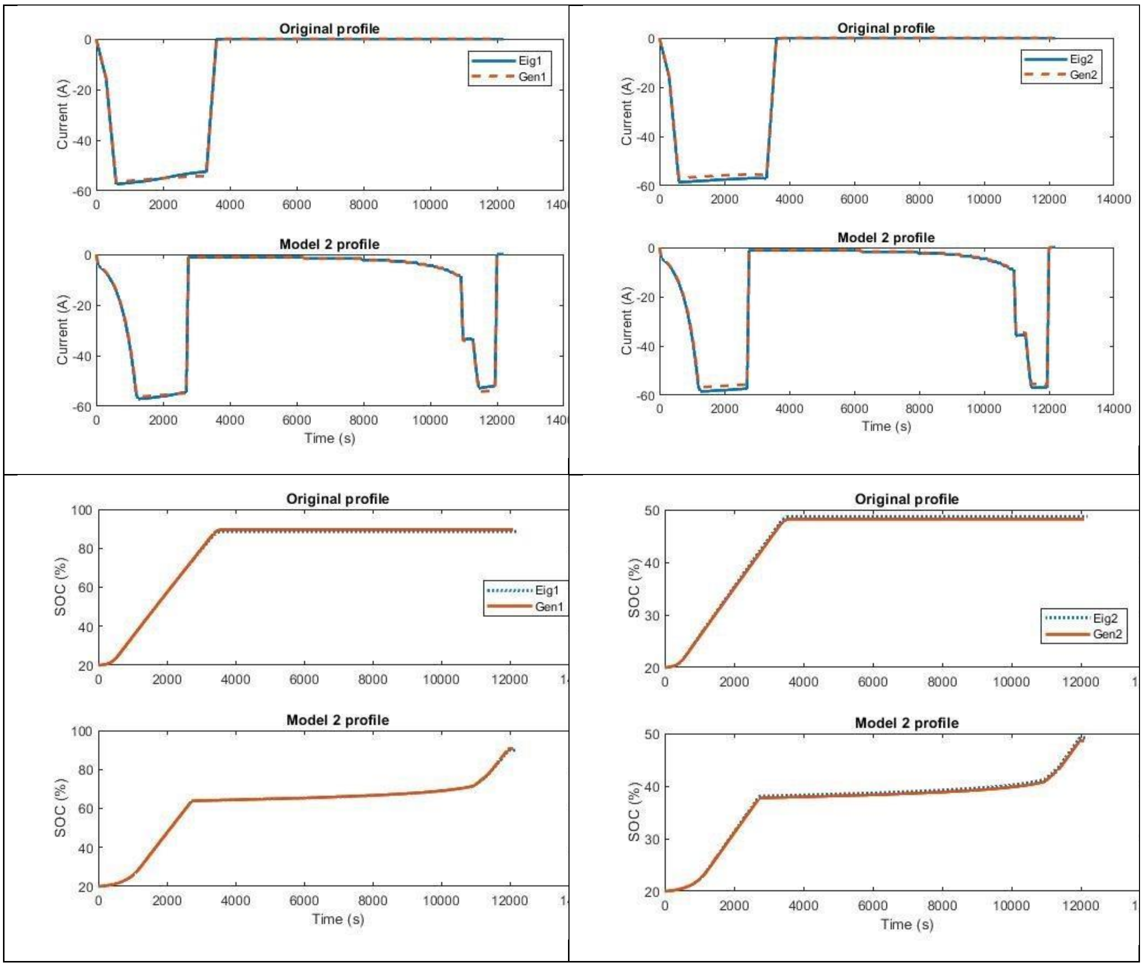

In the following, the outputs of the model when the battery A is selected and the V2V is present have been analyzed and compared to the case with no V2V. The input power profiles are the one reported in in Figure 56. The outputs are reported in Figure 61. The dynamic of the battery when V2V is applied is quite straightforward in the lower panel of Figure 61(a), where the voltage is reported. However, the peaks are quite small, therefore we don't expect detrimental effects of V2V on the battery.

Figure 61: Outputs for the battery profile with and without V2V: (a) Voltage; (b) Current; (c) SOC.

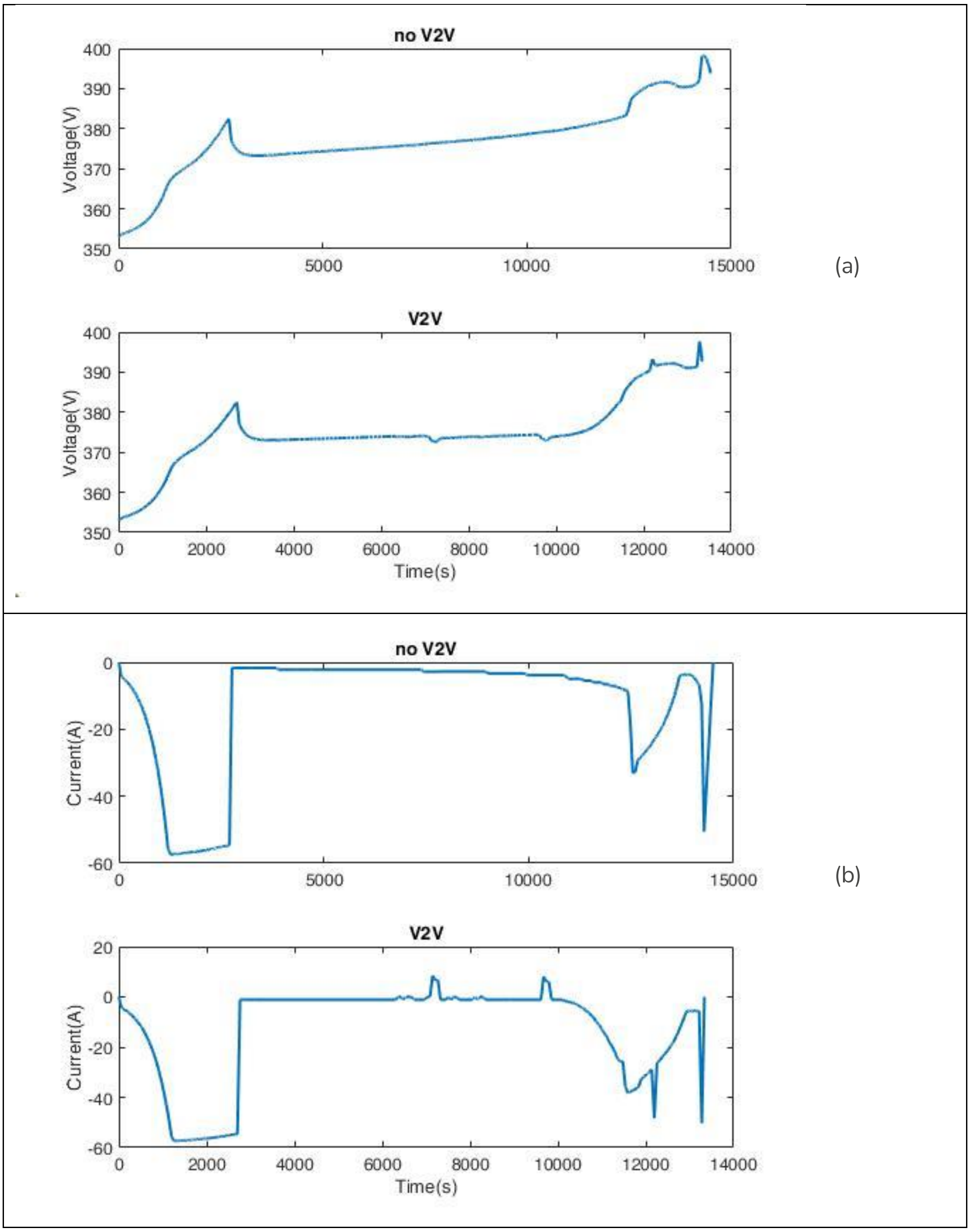

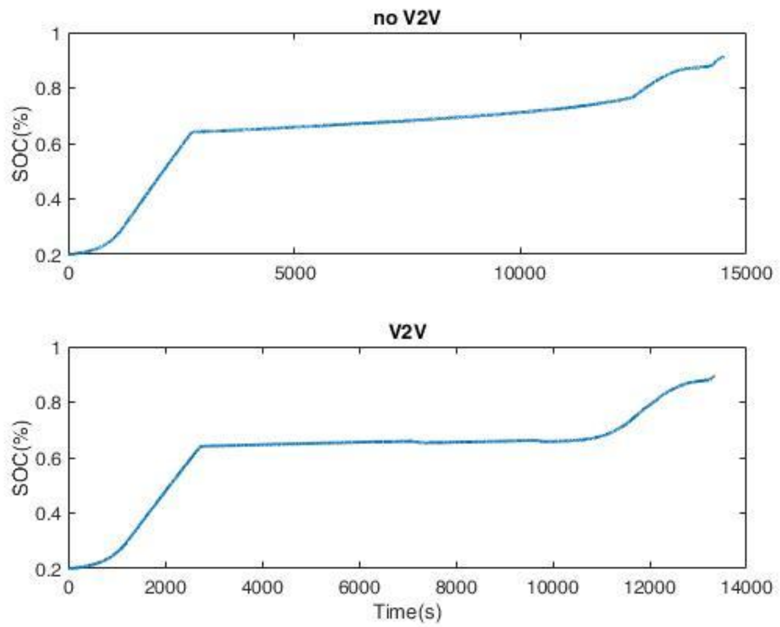

(c)

3.5.1 Ageing effects

In order to simulate ageing effect on the battery, we consider the battery at the begin and at the end of its life (EOL). The latter one is usually reached when the effective capacity reaches the 80% of the nominal capacity and/or its internal resistance doubles.[18]

We use the Simulink battery to model the aging effects, as we can directly change the capacity and internal resistance values. Even if this is a simplified model, it can give a first idea of what happens with battery aging. We applied the profile obtained for the V2V (Figure 56) to the battery A with an initial SOC of 20%. Figure 62 shows the response of the Simulink model for battery A when its nominal capacity is reduced by 20% and its internal resistance is doubled. As shown in panel (a) of Figure 62, the charging process is shorter and the voltage rises faster compared to the battery at the beginning of its life due to higher internal resistance. In addition, the quantity of charges delivered to the battery is smaller because its effective capacity is reduced.

Figure 62: Effect of aging on the battery response (Simulink model).

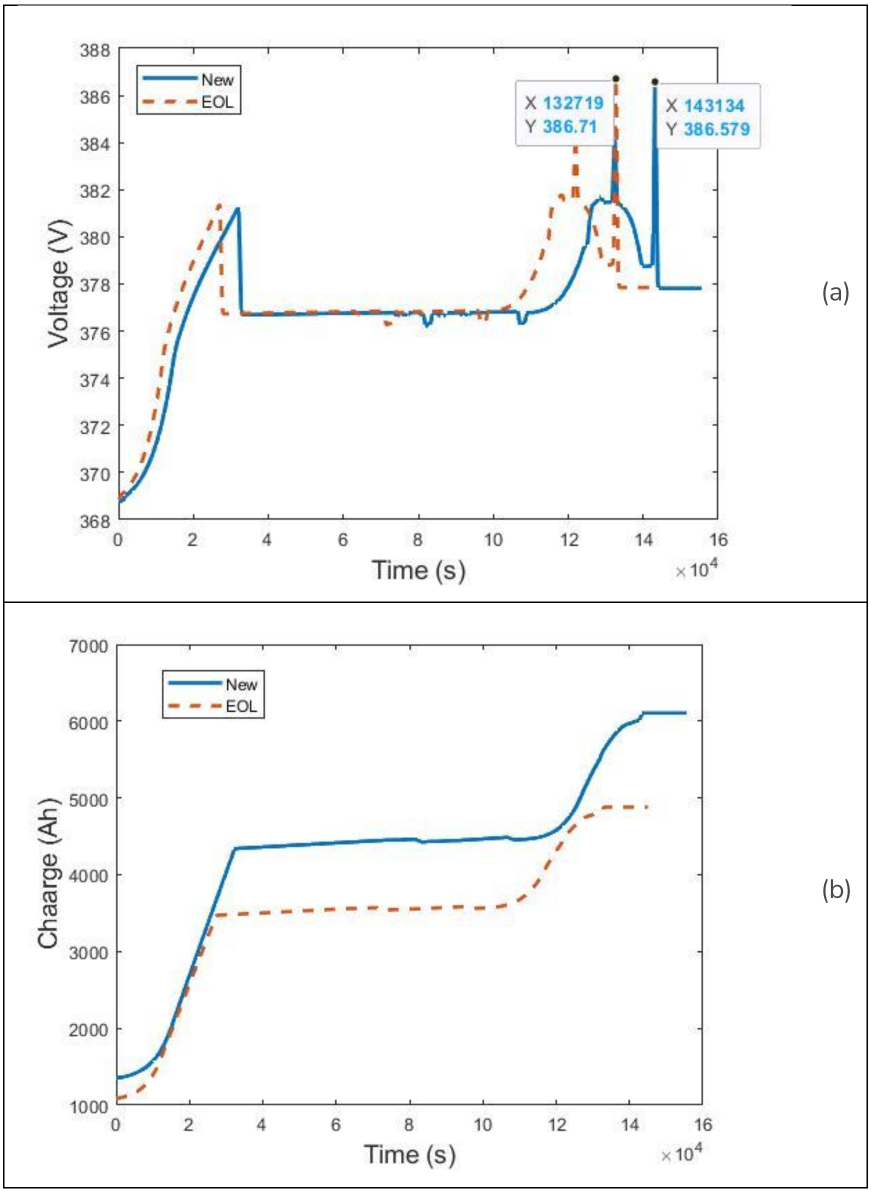

The outputs shown in Figure 62 simulate ageing for a single cell. However, the behaviour of the battery pack is slightly different because the pack is managed by a Battery Management System (BMS) communicating with the charger and preventing the battery from exceeding the operational limits. Since the increase of internal resistance results in a higher voltage cell, the net results is an increase of charging time because the BMS limits the charging power or current to maintain the voltage inside the limits. Differences in battery response due to aging can also lead to faster battery deterioration especially if the BMS fails to correctly identify the health of the battery.

3.6 Conclusions

In this section, we have proposed an equivalent circuit battery model, whose parameters have been extracted from experimental tests. The model has been validated against experimental data and it has been used to simulate the response of a battery to different charging profiles: a simple constant-power, a modulated-power and a modulated-power plus V2V, which are the output of a fuzzy model that controls the power level in a charging station. The response of the battery model demonstrates the feasibility of complex charging strategies, including bi-directional ones, even for mid-range car batteries.

4. Planning a charging infrastructure integrated with a PV-battery system

In the present section, we present an approach for the optimal sizing of a renewable energy source (RES) and an energy storage for a charging station in an urban area. In particular, the considered RES is a photovoltaic (PV) system, since it is the most suitable for an urban environment. The analysis is based on real data on charging events from two the demo cities, Turku and Barcelona.

4.1 Method

The basic hypothesis of the study is the following:

- PV system: it consists of a finite number of identical solar panels, with inverters and balance-of-system (BoS). The space available to install the subsystem can be constrained or not.
- Battery system: it consists of a finite number of identical battery units of common technology integrated with a BoS.
- Balance-of-system BoS: generally, it consists of power conditioning devices, inverters, wiring, and installation hardware. The specifics of a BoS system depend on the location of the installation. In our model, we treat the BoS cost as a fixed cost. Usually, it does not affect too much the project costs [10].

In general, PV sizing depends on the following constraints:

- The available surface (physical constraint);
- The load and solar irradiation (power constraint);
- The energy storage (size and characteristic);
- The grid (availability, net metering, energy price, etc.).

Battery size should be determined by:

- PV size;

- Load demand;
- Battery price;
- Grid availability.

Moreover, the battery size depends on its characteristics: in particular, the power is one key parameter in the size determination. However, batteries performances are generally expressed in terms of different parameters, such as the maximum charge and discharge currents (that usually vary with temperature and ageing), maximum, minimum and operating voltage (this last is a function of the SOC), and capacity (expressed in Ah). Power (P) is related to voltage (V) and current (I) by the simple relation: P=V*I (for direct current, DC), where V is the voltage at the battery terminal.

Since voltage is not a linear function of SOC, also current intensity, temperature, and power are not a linear function of SOC, which makes difficult implementing a simple algorithm for size optimization. This problem is partially overcome by the fact that the curve (representing the relation between voltage and SOC) can be approximated by a straight line within the SOC range of 20-80%.

4.2 BESS and PV cost

Different models for the estimation of battery energy storage systems (BESS) are available for both behind and in-front meter applications. In this study, we limited to the study of the behind-the-meter (BTM) case that is used for commercial and residential applications where capacity ranges from 0.01 to 0.25 MWh [11]. Usually, the battery technologies used in “behind the meter” (BTM) applications are based on li-ion and lead-acid.

An analysis from Lazard, the financial advisory and asset management firm, shows the behind-the-meter system costs are substantially higher than the in-front-of-the-meter system due to higher unit costs. Moreover, initial cost of lead-acid batteries is outweighed by higher operating costs when compared with li-ion [20].

To compare different BESS, the leveled cost of storage (LCOS) metric has been introduced, that is the analogous of the leveled cost of energy for energy sources. The LCOS has been introduced by Belderbos, et al.[21] and has been defined as “the fictitious average electricity price during discharging needed over the lifetime of the storage plant to break even the full costs for the investor”. This value takes into account many parameters, such as that capex, cycles and discount rate.

Without entering into detailed calculations, Table 1summarizes the founding from LCOS reported by different sources for BTM applications.

Table 13: LCOS for different battery systems

Source	Battery type	Capex [USD/kW]	Opex [USD/kW]	LCOS [USD/kWh]
Apricum [22]	Li-ion	500	10	0.53
Lazard	Li-ion	576-1289	0	0.89-1.27
Lazard	Lead-acid	445-835	0	1.06-1.24
SolarPro[4] [25]	Li-ion	1406	0	0.56
World Energy Council [25]	Li-ion	300-3700	7-74	0.15-0.7
World Energy Council	Lead-acid	500-1700	10-34	0.1-0.4

A study of the International Renewable Energy Agency (IRENA) [27], reports the CAPEX will decrease for all technologies by the year 2030, estimating a drop of about 60% for li-ion system capital costs, and of 50% for lead-acid systems. Instead OPEX are assumed remaining unchanged, as the maintenance costs are already very low compared to capital costs.

According to a study presented by Fortum [29], the average battery pack price in 2020 was around 200 €/kWh for residential-commercial use. However, battery system CAPEX can be as high as 500-400 €/kWh, although it is supposed to halves by 2025. The OPEX for a utility-scale system is around 1.5% of the CAPEX.

The photovoltaic market has a higher degree of maturity. According to European Energy Innovation, the cost of a PV residential system without tax is about EUR 1210/kWp. Adding a surcharge of EUR 140/kWp for fees, permits, insurance, etc., an installed PV system can cost around EUR 1350/kWp without financing and VAT. [9] The price for modules is constantly decreasing, as shown in the graph taken from pvXchange.com and reported in Figure 63.

[4] Residential case: 6.4 kWh installed.

Figure 63: Trend for EU module prices by technology. Source: pvXchange

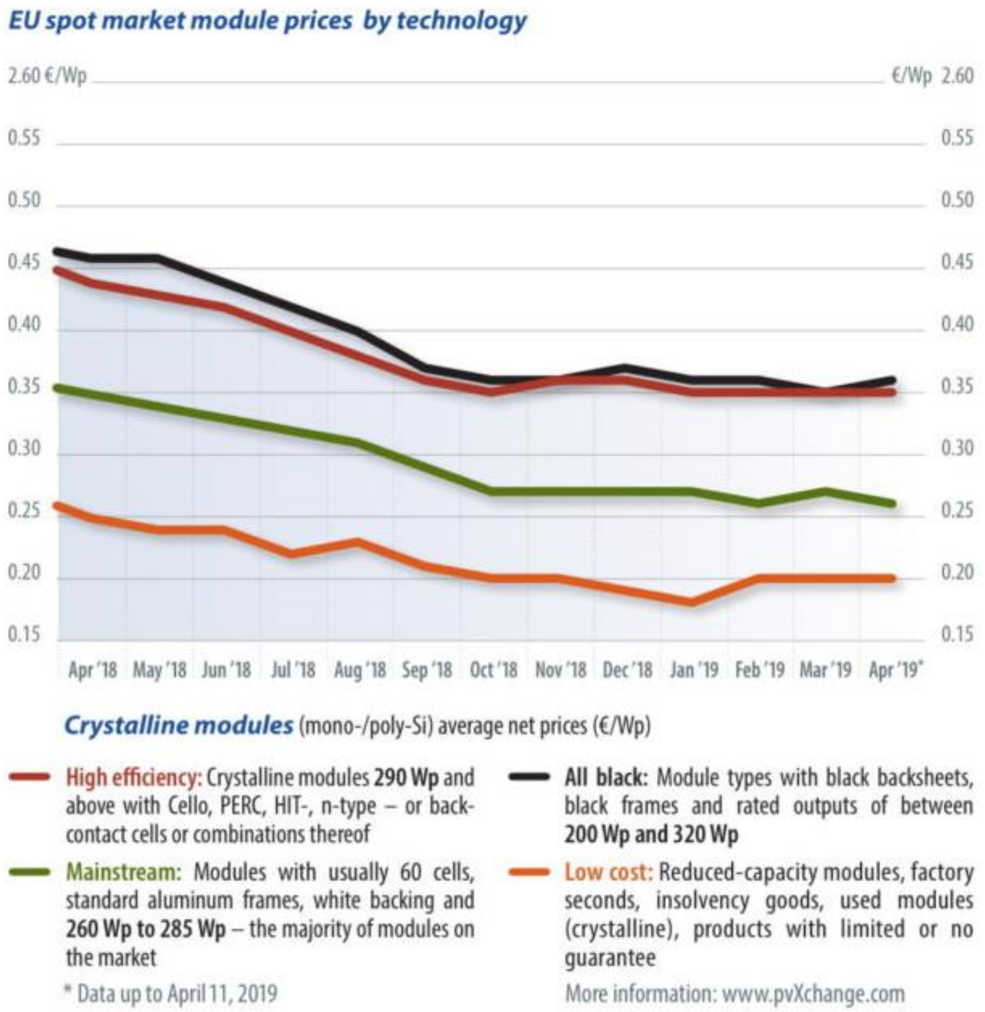

The European Technology and Innovation Platform for Photovoltaics estimates that the cost for a 50MWp utility system is about 65% of the residential one; for a 1MWp system it is 80% and for a 50kWp (commercial) system it is 90% of the residential cost [1][30]. On 2014, since the cost of a turnkey photovoltaic utility scale was 955 €/kWp, in front of a reduction to 823 and 724 in 2020 and 2025 respectively [31], we can deduce the PV price in 2020 for residential is around 1200 €/kWp, while for commercial is around 1000 €/kWp. In this estimation, we did not include any analysis of Covid-19 influence on PV system price. Thereafter, Capex for PV system is estimated at 1200 €/kW.

4.3 Charging infrastructure and energy fluxes

A number of studies have been carried out on the planning and operation schedules of renewable energy sources and storage systems. There are several issues and technologies to take into account the correct design of charging infrastructures for electric road vehicles. In fact, these could be integrated into smart grids, as well as with different types of renewable energy sources and stationary electrical storage systems [23]. It is also necessary taking into account different charging devices and their architectures as well as the configuration of the charging station which can be in DC or AC. Particular attention is also paid to rapid charge of electric vehicles and related issues.[24]

Fast charging of EVs is an attractive way to restore energy of depleted batteries in short time. Fast charging (FC) is generally operated according the IEC 61851 rule mode 4 DC current. AC grid power is interfaced with EV using an AC/DC converter placed on ground in order to decrease the vehicle weight. Different types of standards were developed in the past few years: CHAdeMO (Charging de Move) was the first solutions presented on the market by Japanese EVs manufacturers. This was followed by CCS (Combined Charging System) in Europe, Tesla Supercharger and Chinese GB/T.

First series of CHAdeMO fast charging stations were able to supply 50 kW DC power at 400 V and 125 A having a maximum charging time of half hour with a 24 kWh battery size (i.e. old " Nissan Leaf"). The increasing demand in EV power has led to double or triple the battery size growing up to 70 kWh and over. Developments in fast charging station brought the charging power available at 120 kW for Tesla Supercharger, 150 kW for CHAdeMO/CCS and 125 kW for the Chinese GB/T. The competition to achieve higher charging power (XFC Extreme Fast Charger) is currently ongoing and 350 kW is now offered by some manufacturers of charging station (ABB, Ionity, Tritium, etc.). Relevant characteristics of some fast charge standards are reported in Table 14.

Table 14: Characteristic of different fast charge standards.

	 CHAdeMO	 CCS	 GB/T	 Tesla
Max power	400 kW	350 kW	185	
Max Current (A)	400	400	250	
Max Voltage (V)	1000	900	750	
Market Power	150 kW	350	125	120

Further development in the CHAdeMO protocol was announced in 2020 presenting a new version (3.0) harmonized with the Chinese GB/T protocol under the ChaoJi project. It brings a new design of the plug with the introduction of a cooling liquid and more higher operating power at 500 kW and 600 A, but with a target of 900 kW (600 A, 1500 V).

Usually, EVs battery voltage of are limited around 400 V and each increase in charging power is mirrored in higher charging current. Luxury cars, such as Porsche Taycan and Lucid Air, represent some limited exceptions (Table 15).

Table 15: EV cars that accept ultrafast charge.

Model	Battery capacity (kWh)	Voltage (V)
Porsche Taycan	96	800
Lucid Air	113	900

High level of current requires an appropriate plug-cable design to decrease the contact resistance and thermal losses by using cooling liquid for the cable and the plug.

Nowadays, high batteries voltage up to 1000 V are presented as solution to increase on-board energy storage and to limit at 500 A the charging current in fast charging applications. Electric heavy-duty vehicles and electric buses benefit from higher battery voltage that implies higher potential charging speeds. However, these batteries have less weight limitations which gives the opportunity increasing battery size in order to raise their operative range.

High charging power is attractive because it decreases charging time but it involves some issues on battery management and lifespan. Figure 64 reports the charging time as function of charging power of four battery size: 24, 40, 60 and 100 kW. The charging time is evaluated in ideal condition with an applied constant power and a SOC span from 10% to 80% in order to maintain safety condition during fast charging. The dashed lines identify the current (expressed in C-rates[5]) as a function of the size of the battery as the charge power increases. Figure 64 also shows charging currents as a function of the charging power for each battery size.

[5] The C-rate is a conventional way to express the amount of current applied as a function of the battery capacity. C-rate = 1 is the amount of energy required to fully discharge (or recharge) the battery in 1 hour. C-rate = 2 refers to a current capable of discharging/charging the battery in half an hour. C-rate = 0.5 is a current capable of discharging/charging the battery in 2 hours, and so on. Different currents correspond to the same C-rate, depending on the size of the battery. A C-rate = 1C is equal, for example, to 10 A for a 10 Ah capacity battery, and 100 A for a 100 Ah capacity battery.

Figure 64: Charging time vs. charging power (ideal case 10-80% SOC) for different battery size (24, 40, 60, and 100 kWh). Measurements and elaborations made at the ENEA laboratory.

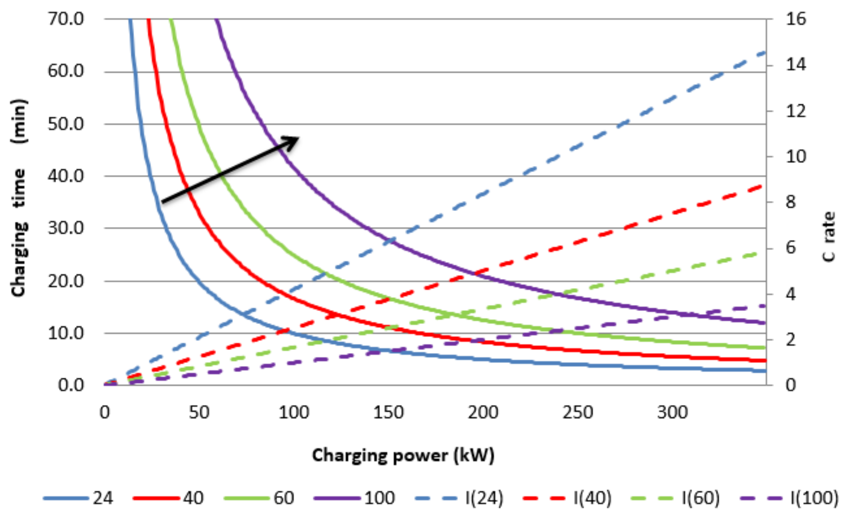

From Figure 64 it is possible to observe that charging time decreases when power increases independently from battery size, but with a different rate: bigger battery sizes require more time due the lower charging current C-rate.

4.4 Model

A proposed system for charging infrastructure with renewable energy source is shown in Figure 64. The DC bus connects the different energy sources: the grid, the photovoltaic system (PV) with the electric storage system (ESS) and the charging infrastructure (CI), while the inverters guarantee the voltage stability. This configuration allows optimization of the power flows from each source to minimize the impact of electric vehicle recharges on the network. In particular, the storage system allows storing the energy from the photovoltaic system and/or from the grid, when the electricity cost is low. The energy stored in the ESS is then used to recharge electric vehicles when the photovoltaic source is absent and/or the cost of energy from the grid is high.

In the design of this system, the main problem is to establish the size of the renewable sources and of the storage system that makes the whole system suitable from a technical-economic point of view, according to the operating conditions. Therefore, it is necessary to determine a series of information form the basis of the preliminary design of the system in order to set the optimum daily power flows of the overall system:

- Solar irradiance of the area;
- Storage system technology;
- Load demand;
- Other constraints (policies and regulations, space constraints, etc.)

As discussed above, for BTM applications, the EES is represented by battery systems (BESS).

Figure 65: Proposed system for charging infrastructure with renewable energy source

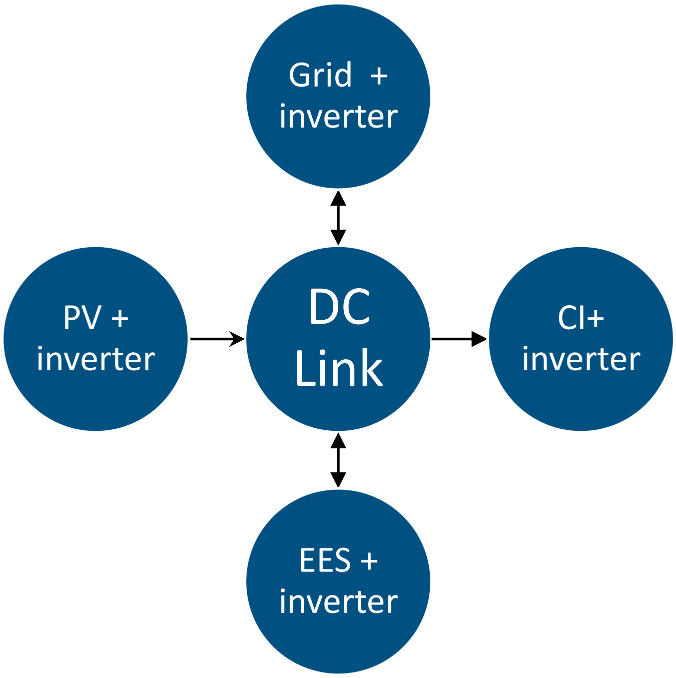

Based on the technical-economic constraints, a numerical platform determines the optimal configuration of the system according to the operating conditions and plant costs. The sizing of each component of the system (auxiliary sources, storage) is carried out according to the charging profiles, energy costs, device costs, operating costs, and by analyzing the optimal power flows as a function of the period of the day/year. Through the economic criterion of the Net Present Value (NPV), by projecting the analysis over the entire depreciation period of the infrastructure, it is possible to determine the optimal system solution and identify the basic information for the preliminary design of the plant.

The numerical platform performs the monthly averages of the following hourly input data:

- The market price of electricity;
- Productivity and cost of the photovoltaic system;
- Costs of the storage system;
- Charging power profiles.

In the following, the platform determines the sizes of different components. The algorithm uses the sizes of the auxiliary energy sources and determines the optimal operation of the proposed system for each day. This minimizes the operating cost while ensuring the power required by the charging infrastructures.

In the monthly analysis, a representative day of the average monthly production of photovoltaics and the average monthly cost of electricity purchased from the grid is considered. The 15-year NPV is used as a basis for comparison of the different investment projects, which is a tradeoff between the duration of a PV system (20-30 years) and a CI and BESS (10-15 years).

The power flows coming from the sources through the conversion systems are summed up in the common DC bus. In particular, it is possible to write the balance of the input powers coming to the DC bus:

$$P_{grid}\eta_{grid} + P_{PV}\eta_{PV} + P_{B,D}\eta_{B,D} - \frac{P_{B,C}}{\eta_{B,C}} = \frac{P_L}{\eta_L} \quad (4)$$

Where:

P_{grid}: Power withdrawn from the grid;

P_{PV}: Power supplied by the photovoltaic system;

$P_{B,D}$: Discharge power of the battery pack;

$P_{B,C}$: Charge power of the battery pack;

P_L: Power required by the load;

η_{grid}: Efficiency of the network converter;

η_{PV}: Efficiency of the photovoltaic system converter;

$\eta_{B,D}$: Efficiency of the bidirectional converter of the battery pack, discharge mode;

$\eta_{B,C}$: Efficiency of the bidirectional converter of the battery pack, charge mode;

η_L: Efficiency of the output converter.

The optimization problem aims minimizing the objective function represented by the daily operating cost of the charging infrastructure (Ce) consisting of two components: the cost of the energy supplied by the grid and the cost of the degradation of the storage system. In particular, the optimization problem was expressed as follow:

$$\min C_e = \min \sum_{h=1}^{24} (C_r(h)\, P_{grid}(h)\Delta t + C_{deg}(h)) \quad (5)$$

Where:

$C_r(h)$ is the price of the energy at time h [€/kWh];

$P_{grid}(h)$ is the power withdrawn from the grid at time h [W];

Δt is the sample time (1 hour);

$C_{deg}(h)$ is the degradation cost for the EES [€].

The model of the system must respect a series of constraints listed below:

$$P_{grid}(h)\eta_{grid} + P_{PV}(h)\eta_{PV} + P_{B,D}(h)\eta_{B,D} - \frac{P_{B,C}(h)}{\eta_{B,C}} = \frac{P_{L(h)}}{\eta_L} \quad (6)$$

$$P_{grid}^{min} \leq P_{grid}(h) \leq P_{grid}^{Max} \quad (7)$$

$$P_{PV}^{min} \leq P_{PV}(h) \leq P_{PV}^{Max} \quad (8)$$

$$P_{B,D}^{min} \leq x_{B,D}(h)P_{B,D}(h) \leq P_{B,D}^{Max} \quad (9)$$

$$P_{B,C}^{min} \leq x_{B,C}(h)P_{B,C}(h) \leq P_{B,C}^{Max} \quad (10)$$

$$x_{B,D}(h) + x_{B,C}(h) \leq 1 \quad (11)$$

$$P_{PV}(h) \leq P_{mppt}(h) \quad (12)$$

$$SOC(h) = SC(h-1) + \left(\eta_{B,C}\frac{P_{B,C}(h)\Delta t}{E_B} + \frac{P_{B,C}(h)\Delta t}{\eta_{B,D}E_B}\right) 100\% \quad (13)$$

$$SOC^{min} \leq SOC(h) \leq SOC^{Max} \quad (14)$$

$$SOC(0) = SOC(24) = SOC_{in} \quad (15)$$

Equation (6) represents the power balance of the system taking into account the efficiencies to ensure the charging power required by the load at the h-th hour. Equations (7)-(10) define the operating limits of the system based on the minimum and maximum power of the sources. The battery is characterized by a minimum and maximum discharge with a charge power linked to the nominal characteristics of the battery pack and to a design sets to reach the maximum charge/discharge current. $X_{B,D}$ and $x_{B,C}$ constraints (11) are binary variables necessary preventing the battery pack from being simultaneously charged and discharged.

Equation (12) limits the power that can be drawn from the photovoltaic system to the maximum extractable power P_{mppt} in the h-th hour.

The constraint (13) links the state of charge at the h-th hour (SOC (h)) to that one of the previous hour (SOC (h-1)) as a function of the charge/discharge power used, the nominal energy stored by the battery pack and the charge and discharge efficiency of the storage system.

According to the constraint (14), the SOC must be within a minimum (SOC^{min}) and a maximum (SOC^{Max}) to limit the depth of discharge and therefore, the cost of degradation. The values for these limits depend on battery technology.

The stability of the state of charge between one cycle and another one is imposed by equation (15). This constraint ensures the energy stored in the battery pack at the beginning of the observation period is the same of that one at the end of the observation

The optimization problem has been applied to the case study of two demo cities: Barcelona and Turku.

To define the sizes and the optimal technical solutions for the various components of the charging infrastructure, the following input have been used:

- Price of electricity: for the city of Barcelona, the data has been deonloaded from the Comisión Nacional de los Mercados y la Competencia (CNMC) website (https://www.cnmc.es), while for Turku the data have been extracted from the Nord Pool site (https://www.nordpoolgroup.com). Data for the 2019 have been used in both cases;
- Cost of the photovoltaic and storage system: for both cities we used the following values: 1.2 €/Wp and 0.019 €/Wp, for the CAPEX and OPEX for PV system, respectively [30]; for BESS systems, we used the data taken from [32]. By the time of this this report,

the lithium-ion technology has a system cost lower than the lead-acid one, therefore we considered only the first one. The system price is calculated as a media of the 2018 and 2025 costs (0.35 €/Wh). We did not consider OPEX costs, since they are negligible compared to the CAPEX costs. We did however consider degradation costs;

- Productivity of the PV system: data are taken from the “Performance of grid-connected PV” tool of the Photovoltaic Geographical Information System (PVGIS) [33]. The data contains the monthly production for installed peak PV power of 1 kWp and system loss of 14% (mounting configuration: slope 35º, azimuth 0º) from the PVGIS-SARAH data base for the selected locations.
- Efficiencies of the conversion systems: some new solutions show efficiencies higher than 0.9 [34]. However, efficiency values of 0.9 have been used for all systems, except BESS for which the value has been set to 0.8;
- Required charging power profiles: these have been extracted from historical charging events provided by the cities. For each month of the year, it has been created a synthetic daily load profile representative of all monthly load profiles. The number of charges per day and the duration of the charges are taken from the database statistics. Details on the calculation of the charging profiles are given in Section 2.4.

Example of synthetic load profiles for a typical day of some months are reported in Figure 66 for the metropolitan area of Barcelona, and in Figure 67 for the city of Turku. The graphs represent the power charge request for a typical day of January, April, July and October. These power charge loads for representative day of every month is used as an input to the evaluation process for the economic feasibility of the investment.

Figure 66: Synthetic load profiles for Barcelona

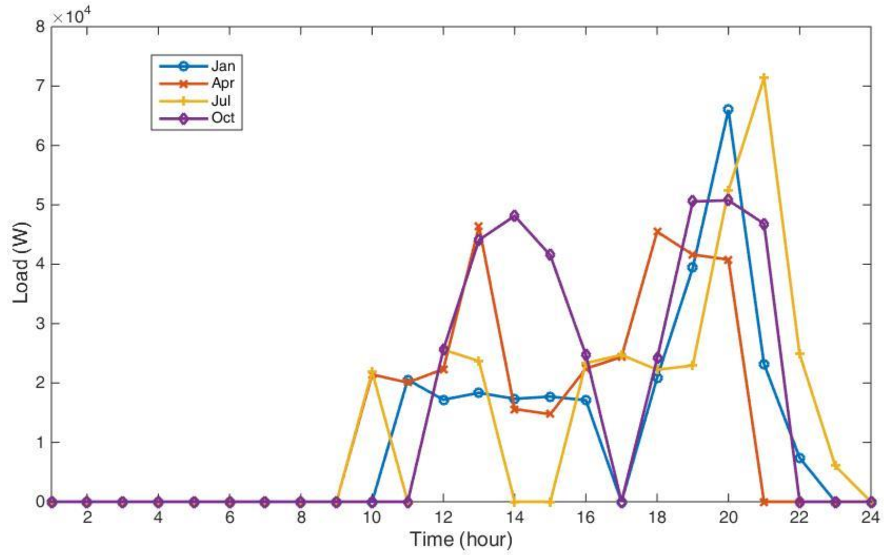

Figure 67: Synthetic load profiles for Turku

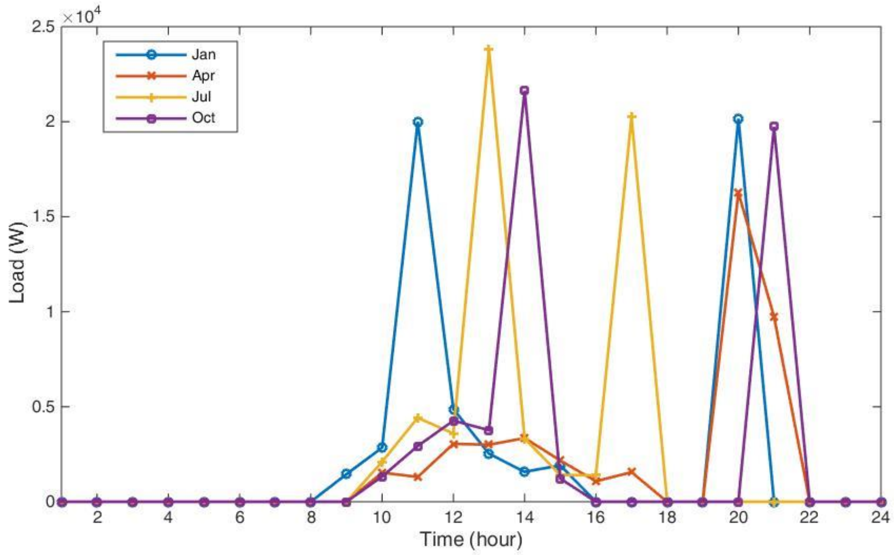

The PV system degradation rate is fixed to an average value of 0.5% per year [35].

Battery degradation has been characterized by two parameters, the calendar life and the life cycle.: For the calendar life, the duration has been fixed to 15 years, while life cycle has been fixed to N_{life} =5000 cycles at 70% of depth of discharge (DOD). To determine the degradation cost, we use a very simple model based on the counting cycles (similar to the rain-flow counting).

This simple model was adopted to use simple linear integral equations while a more realistic model would make it non-linear. However, in the preliminary phase, this simple model is sufficient to take into account the costs deriving from the battery usage.

Assuming a cost per watt-hour of the battery degradation the price for the battery pack C_B = 0.15 €/Wh [30], we can obtain the cost for a cycle with DOD=70% is: $C_C = C_B * E_B / N_{life}$, where E_B is the battery size (in Wh).

Therefore, the degradation cost for a generic cycle "i" with DOD= DOD_i, is given by: $C_i = C_C * DOD_i / 70\%$.

4.4.1 Space limitation for PV

On average, to install a PV system of 1 kW (about 4 panels) on a pitched roof you need a surface of 6-7 square meters. On a flat roof, the space required is 9-10 square meters because of the supports to tilt the panels [16]. Therefore, we will also consider space limitation in the analysis.

4.4.2 Growth in demand

In the current analysis, we also took into account the projections for the growth of the electric car market.

The share of electric vehicles is growing quite fast. According to the European Automobile Manufacturers' Association (ACEA), the market share of electric cars in 2019 was 3.0%, which is one percentage point more than in 2018 [37]. On the other hand, the International Energy Agency estimated that electric cars accounted for 2.6% of the global car sale and for about 1% of global car stock in 2019, with a 40% increase in registered cars. Because of the continuous increase in sales, EVs are expected accounting for about 7% of the global vehicle fleet by 2030 [38]. In the current analysis we will include a growing rate of 1%, 5% and 10%. .

4.5 Application to the demo-cities cases

In the following, we report the results of the optimization problem for the city of Barcelona and Turku. The optimization problem has been modeled with the MatLab software to solve a linear programming problem defined by an optimization problem. Even if Eq. (2) with constraints (3)-(12) represent a mixed-integer linear programming problem, it can be reduced to a linear programming problem since the constraint (8) is implicitly satisfied when minimizing battery degradation costs.

4.5.1 Technical-economic evaluation criterion

The Net Present Value (NPV) is a method used to determine the current value of all future cash flows (positive and negative) generated by a project over its lifetime, discounted to the present. Including the initial capital investment, it is a criterion for selecting among different investment projects. In particular, this parameter makes possible evaluating the feasibility of an investment.

An investment is advantageous when the NPV is positive, that is when the project frees flows of sufficient size to repay the initial outlay by providing a net gain. The NPV is assessed over a time horizon of N years and it is a function of the cash flows related to the investment made, including the interest rate (*k*). Therefore, the investment can be expressed as follows:

$$NPV = \sum_{t=1}^{N} \frac{F_t}{(1+k)^t} - I$$

Where:

N is the time horizon of the investment in years, fixed in 15 years;

F_t is the cash flows in the t-th year, calculated as the difference among cash flow with and without the PV+BESS system;

I is the initial investment calculated as the sum of the PV and BESS CAPEX;

K is interest rate fixed in 3%.

A sensitivity analysis for the interest rate was conducted on one case study. By doubling the value of an interest rate of 6%, the NPV becomes negative for all the analyzed system configurations. If the interest rate halves by 1.5%, the NPV increases with a shift of the maximum towards larger PV size values. In the first instance, the size of the BESS is linked to the size of the PV, therefore, it reflects less the variability of the interest rate.

In the following, the results for the optimization procedure and NPV calculation for the city of Barcelona and Turku are presented. Beside data on charging events, we also asked the partners to give us some information that could be useful in the analysis. We received feedbacks from questionnaires to AMB, Turku and Munich, and the answers are reported in Annex C – Questionnaire. The answers reveal a quite inhomogeneous situation both for the charger's typology choice and the incentives policies in force in different Countries. In particular, for AMB, the local administrations promote the installation of CI in the streets. In this case, the municipalities act as CPO. The regional and the national governments subsidies this infrastructure. In Turku, there are governmental incentive for the housing when installing new charging points up to 45% of the price and 90k€; in Munich, only governmental grants apply, which could arrive up to 40% of the hardware cost. For PV systems, in Finland different government incentive policies apply: subsidies cover 40%, 25% and 40% of the costs for private housing, companies and farms, respectively. In AMB, the Consorci Metropolità de l'Habitatge has subsidies programs oriented to the PV panels for housing. However, all the cities agree there are space limitation in downtown to install PV systems.
It is especially interesting to compare the existing incentive policies with the ones that arise as favorable from our analysis, and that are shown in the next sections for AMB and Turku.

4.5.2 AMB

The charging infrastructure (CI) is composed of 3 fast charging points (2 CPs for 43kW + 1CP for 55 kW) and two slow CPs (2 CPs for 3kW). This is the standard configuration for metropolitan area (estimated dimension of the roof: 5x2x5=50 m2 ~ 8 PV modules of 1kW).

4.5.2.1 No BEES

As a first step, a PV system without BESS is considered. Without incentives on the investment costs, the renewable source is not convenient. However, applying 20% incentives on the PV investment cost, the NPV become positive and the optimal size for the PV system, that is the one giving the highest NPV, is around 23 kWp for the ideal case (the efficiency of all converters is equal to 1). In a more realistic scenario of efficiencies lower than 1, the optimal size is around 25.3 kWp. If the degradation of the PV system is included, the optimal size is 27.25 kWp (see Figure 68). In the following, only non-ideal system will be considered, unless explicitly stated.

Figure 68: Optimal PV size without BESS.

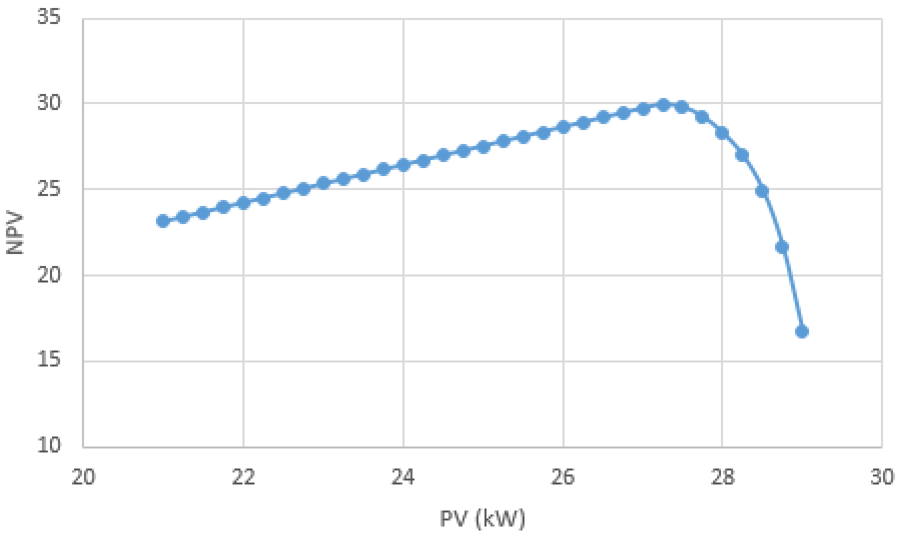

As shown in Figure 69, if we include a demand growth with different rate, we obtain an increase of the PV size with the growing rate, as well as an increase in the NPV.

Figure 69: Optimal PV sizing with no BESS for the metropolitan area of Barcelona (left) and NPV (right).

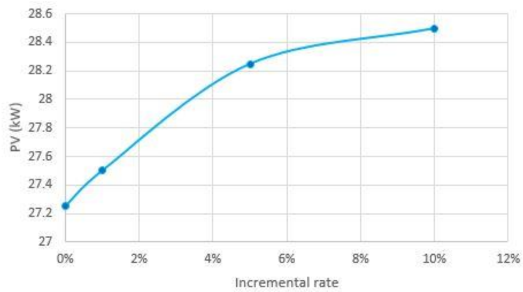

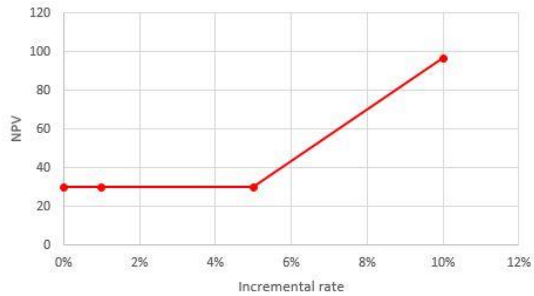

On the other hand, as shown in Figure 70, the increment of the NPV can be correlated to the increase of the self-consumption of the PV energy when the load demand increases.

Figure 70: Self-consumption at different load incremental rates.

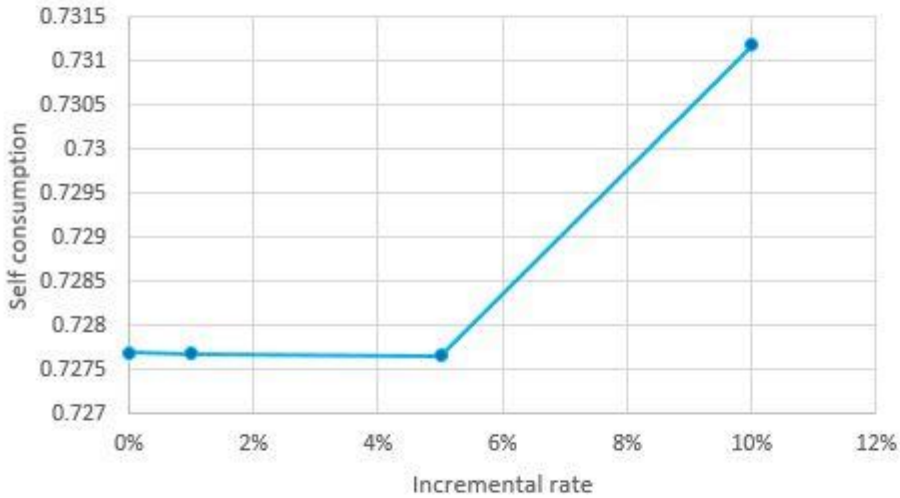

4.5.2.1.1 BESS

To evaluate the size of the system when there is also a storage system, we initially consider a zero-investment cost for the BEES plant. We obtain that the investment is feasible if the incentives on PV costs are preserved. The optimal value for the PV increases to 39.5 kW with a BEES of 98 kWh. This value of the BEES is the one for which all the energy produced by the PV is entirely consumed by the CI (Figure 71).

Figure 71: Self-consumption for different BEES size when no CAPEX cost is considered

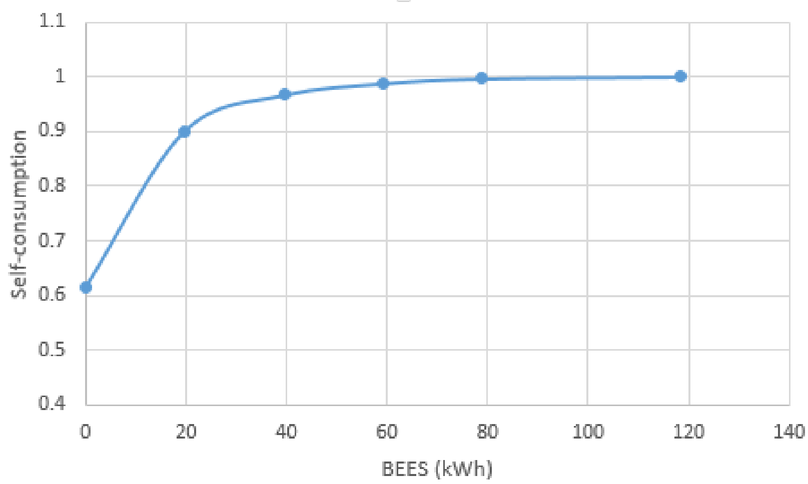

However, when the investment cost for the BESS is considered, there is no convenience in designing the BESS to obtain the total self-consumption of the PV energy. In particular, if the BESS CAPEX is equal to or greater than 0.35 €/Wh, to obtain a positive NPV, the incentives of 20% should be extended to the total system investment cost.

We have analyzed the possible BESS solution doing a sensitivity analysis on the BESS CAPEX, using three values: 0.35 €/Wh, 0.2 €/Wh, 0.15 €/Wh. For all these values of the BESS CAPEX we obtain positive NPVs for the PV+BESS system, at least until a limit size of the BESS that depends on the CAPEX price is reached. As an example, Figure 72 (a) shows the results for the optimal BEES size as a function of its CAPEX for different incremental rates, while in Figure 72 (b) the variable is plotted as a function of the incremental rate for different CAPEX.

Figure 72: Optimal BEES size as a function of BESS CAPEX costs and incremental rate.

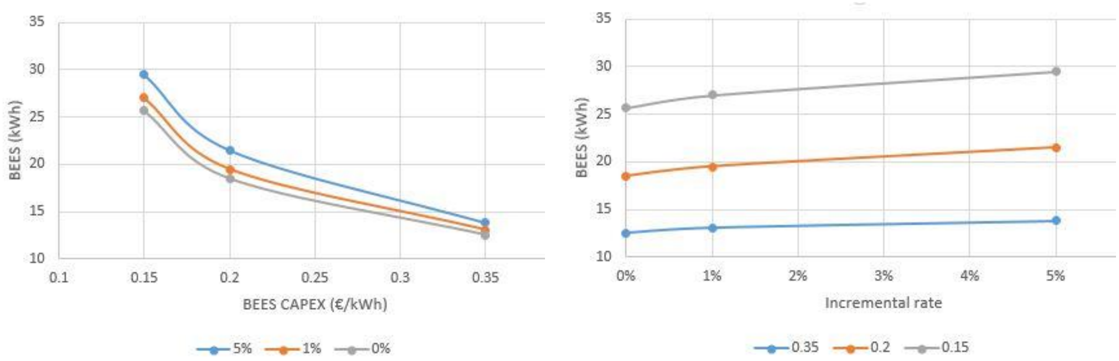

(a) (b)

Figure 73 shows the trend of the NPV for different BESS size when associated to the optimal size of PV in three scenarios: with a 5%, 1% and 0% growth rate per year of the load demand for a BESS CAPEX equal to 0.35 €/Wh. As said above, in this case, the 20% incentives are calculated on the total investment cost of the system PV+BESS. The optimal size for the PV in the three cases is around 37 kW, 35 kW and 33.5 kW, respectively. It can be seen that the BESS optimal size increases as the load increases. This remains valid for all the scenarios investigated, independently from the values of CAPEX BESS and the incentives put in place.

Figure 73: NPV trend for different scenarios.

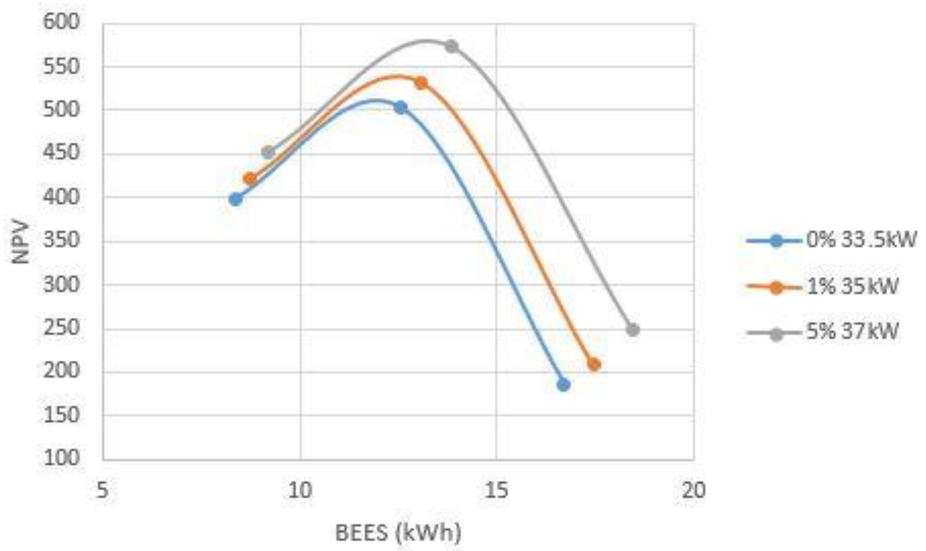

The optimal PV size as a function of the incremental rate is reported in Figure 74 (a), and as a function of the BEES CAPEX in Figure 74 (b). As we can see, the trend is almost linear in this case.

Figure 74: Optimal PV size for different scenarios.

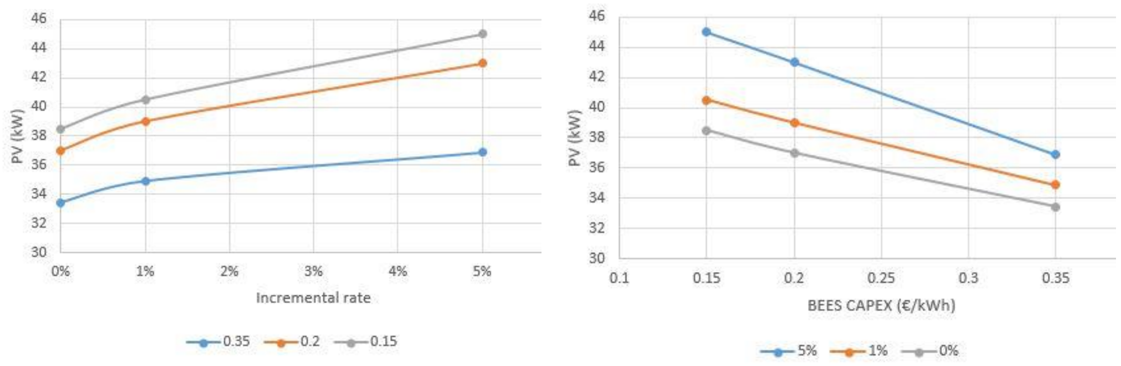

(a) (b)

It is important to remark that the ratio between the optimal BESS size and the optimal PV size is constant compared to the incremental rate at a given BESS CAPEX value. The dependence of the ratio from the BESS CAPEX is reported in Figure 75.

Figure 75: BEES to PV ratio as a function of the BEES CAPEX.

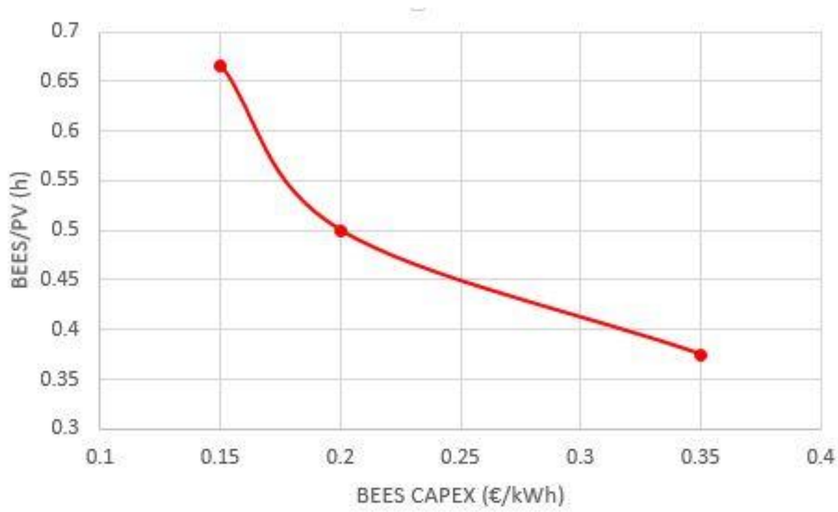

4.5.2.1.2 Space restrictions

We also perform an analysis for the case of space restrictions when installing the PV system, namely considering the roof to the CI. In this case, the PV would be around 8 kW, which is much smaller than the estimated optimal size. However, the BESS remains favorable if the appropriate incentives are put in place and the best ratio BESS/PV is chosen according to Figure 75. An example of optimal size for 0.35€/Wh CAPEX and zero growth rate is shown in Figure 76.

Figure 76: NPV for BEES and 8kW PV

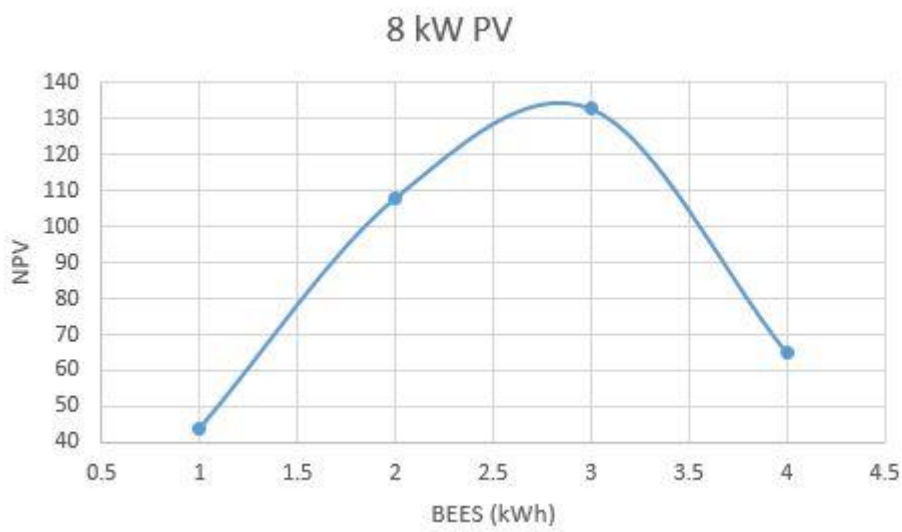

We can conclude that for the Barcelona scenario, the use of BEES with PV can lead to positive VNP values, if some incentive policies are put in place.

4.5.3 Turku

The CI analyzed for the city of Turku is composed of 2 fast charging points of 22kW and one of 43kW. In the analysis, the non-ideal system (i.e., system component efficiencies lower than 1)

4.5.3.1 No BESS

For the city of Turku, the average daily load for CI is about 1/2 of the one observed in Barcelona. Furthermore, the insolation in Turku is very different than in Barcelona, concentrated in the summer months due to the much greater latitude. This translates into much lower values, of an order of magnitude smaller, for the dimensioning of the photovoltaic field. The analysis shows the use of a PV for a station sized as above is not economically feasible with the actual usage. To obtain a positive NPV there should be an average of 16 users per day. However, if the user influx at the charging station doubles, a small PV system can become profitable if it is possible to access to incentives of 40% on the installing costs for the PV system, as shown in Table 16. In this cost evaluation, a PV degradation rate of 0.5% over a year with no increment in the load has been considered.

Table 16: PV sizing with no BESS for the city of Turku.

PV size (kWp)	NPV	NPV + 25% incentive	NPV + 40% incentive
2.35	-1122.39	-558.39	5.61
2.4	-1146.3	-570.29	5.70
2.45	-1170.32	-582.32	5.68

The optimal size in this case is around 2.4 kW, as shown in Figure 77.

Figure 77: NVP value for different PV size when no BESS is present.

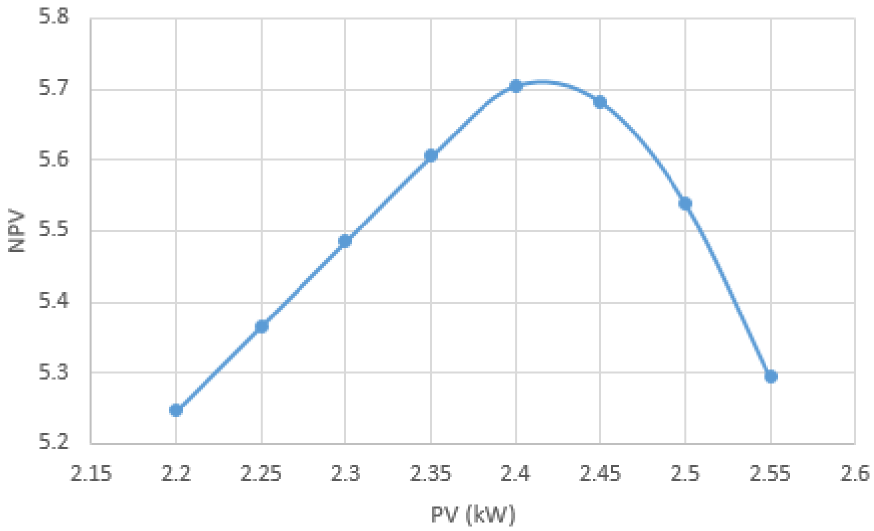

If an increment in the yearly demand load is included for the given CI, the optimal size of the PV changes. The result for the case including 40% incentives with a demand growth of 0%, 1%, 5% and 10%, is shown in Figure 78:

Figure 78: PV sizing with no BESS for different electric market grown rate- incentives at 40%.

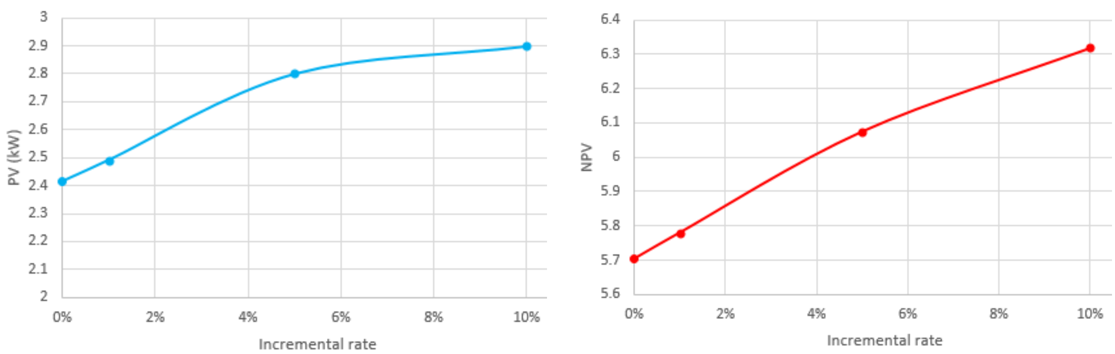

The increase in the demand makes more convenient moving forward a bigger PV size and increasing the NPV of the investment. However, we need to point out that the increase in PV size seems saturating at high incremental rate. This could indicate that, currently, the CI has been probably overestimated compared to the real demand.

4.5.3.2 BESS

As shown in Table 17, the presence of the BESS improves the self-consumption.

Table 17: Annual average self-consumption for different BESS size.

PV (Kw)	No BESS	65 Wh	325 Wh	813 Wh
3.25	0.887	0.892	0.912	0.967

However, from an economic point of view, The BESS does not improve the investment revenues, unless the incentives of 40% if the installation costs are applied to the entire PV + BESS system (and not just the PV), and the cost of the CAPEX for the BESS drops below 2 €/Wh.

The effects of BEES CAPEX is illustrated in Figure 79. This shows the trends of the NPV for the entire system for three different BESS CAPEX values: 0.35 €/W, 0.2 €/W and 0.15 €/W. The analysis is made using the optimal PV size for each BESS CAPEX (2.75 kW, 3 kW and 3.5 kW, respectively) and for a demand growth of 5%.

Figure 79: NPV for different values of BEES CAPEX.

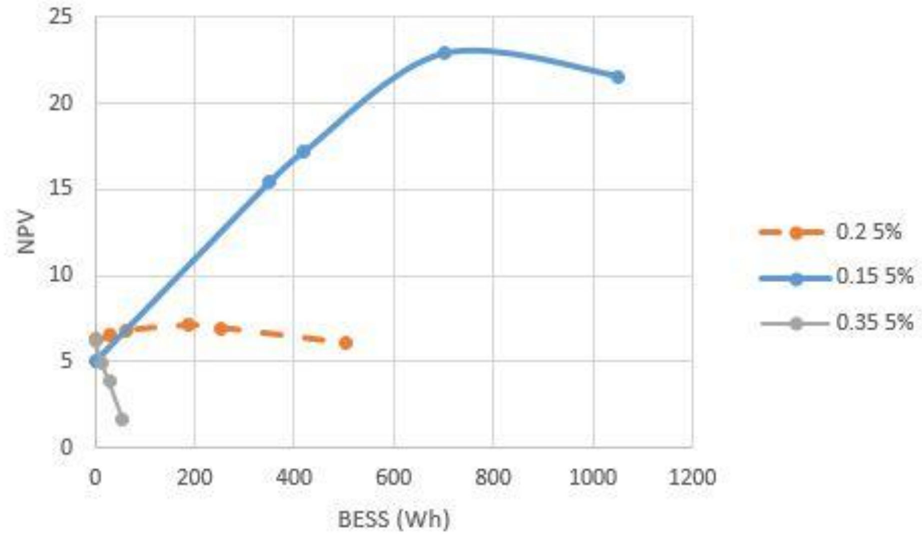

Figure 79 shows that, for the current CAPEX cost of 0.35 €/W, the best investment is the system with only PV, even though the NPV is positive for small values of BESS. However, both the BESS optimal size and the NPV increase strongly with decreasing CAPEX cost.

On the other hand, also the PV size depends on the BESS CAPEX, as well as on the load incremental rate. As expected, the PV size increases with the increasing demand. However, as shown in Figure 80 (a), the ratio between these two values changes with the BESS CAPEX values. In Figure 80 (b) it is evident the change in the curve slopes with different BESS CAPEX values

Figure 80: PV optimal size at different BEES CAPEX

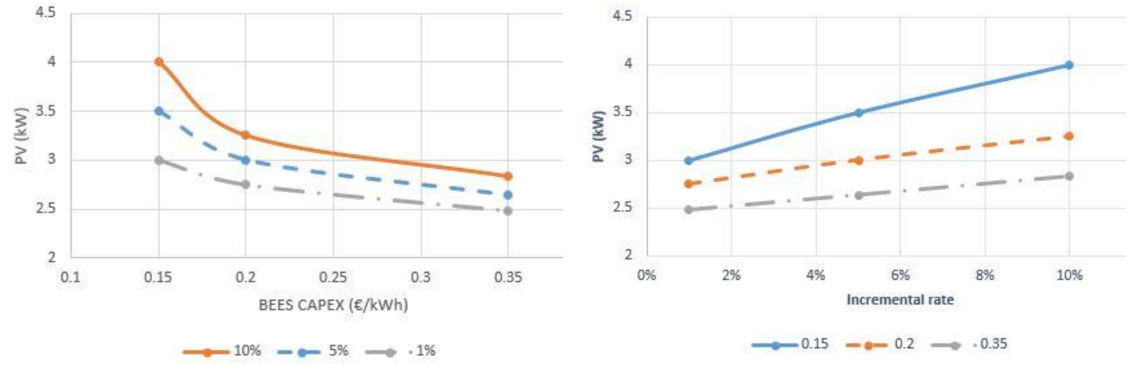

(a) (b)

We want to point out the ratio between the optimal BESS size in kWh and the PV size in kW is a function of the BESS CAPEX alone, and the ratio dependence is shown in Figure 81.

Figure 81: BEES/PV ratio for different CAPEX and incremental rate.

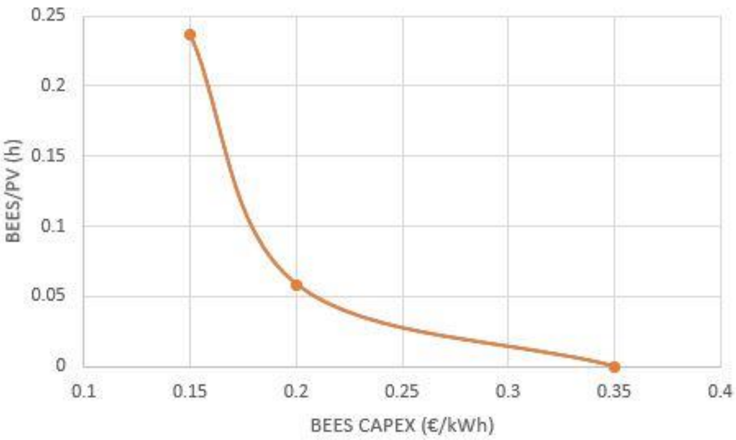

Figure 82 shows the trend of the NPV in the absence of BESS (solid blue line) together with the trends for the complete system PV+BESS when the incentives are applied to the entire system (Incentive policy 1, red dashed line) or only to the PV system (Incentive policy 2, green line). The BESS CAPEX is 1.5 €/Wh and the growth rate for the load demand is 5%. However, the results can be generalized to all the considered scenarios. We can see that Incentive policy 1 brings to higher NPV compared to the other two solutions, and it is usually obtained for a slightly higher value of the PV size, compared with the other two cases. The incentive policy 2 is not sufficient for outperforming the NPV in the case of no BESS. The best sizing for policy 1 is a PV of about 3.5 kW and BESS of about 840 Wh.

Figure 82: NPV for a 5% growth rate with two different incentive policies compared to the case with no BEES.

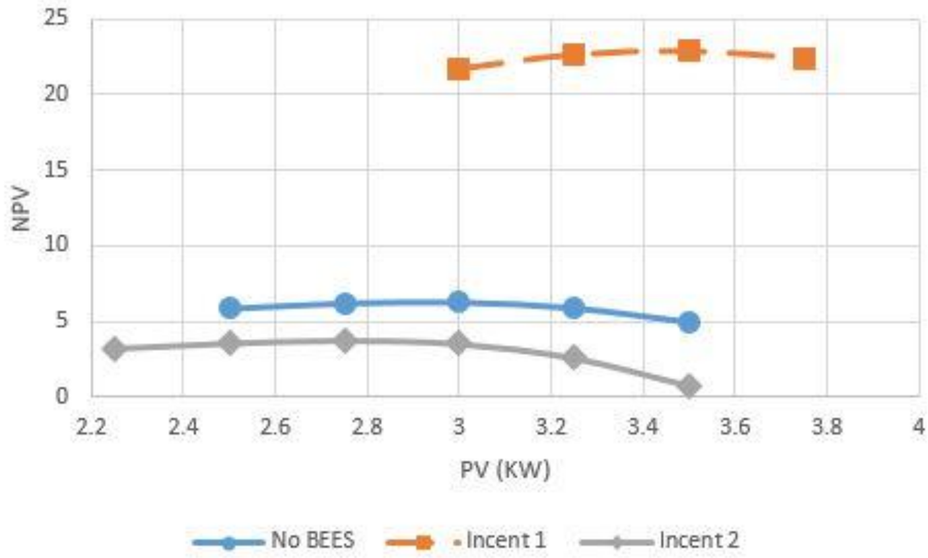

At this time, for Turku it is not convenient installing a PV system because the charging station are not fully exploited. However, if the user influx would at least double, a PV system could become profitable. On the other hand, in the analyzed scenario, the installation of a PV system could lead to a positive NPV with appropriate incentive policies.

As for the BESS system, it could be profitable in a near future if its cost keeps falling and the use of the CI increases.

4.5.4 Discussion

From the analysis for the investment costs we can observe a criticality regarding the BESS. A possible solution can be found in the adoption of second-life battery packs as stationary storage. Indeed, second-life batteries are an opportunity to maximize the battery market, since they can be used for stationary energy storage applications requiring infrequent and shallow battery cycles. In 2025, second-life batteries could be 30 to 70 percent less expensive than new ones in these applications, using significantly less capital per cycle. [42] It is reported a cost of 50 $/kWh, which is much less than the cost of a pristine battery.[43] However, the second-life battery market is still limited and the large-scale implementation is hampered by some problems related to regulatory issues and lack of data on the second-life battery's performance. At present, logistic issues related to the transportation of used or damaged batteries and the lack of safety and environmental regulations for used battery make the cost of second-life battery projects unsustainable and limit the number of possible applications.

There is also a lack of data on the performance of batteries in the second-life, concerning different chemistry and technologies. Even the assessment of the health status of the individual cells making up the battery remains a complex task. This is also due to the lack of development for detailed cell monitoring of the first generation of BMSs, and the lack in providing technical data on the previous use of the battery.

Taking into account the previous legal and technical obstacles, it is difficult to estimate when it will be possible to use second-life batteries in public or private contexts open to the public.

4.6 Charging infrastructure operations

To determine the optimal operation of the charging station, we used a probabilistic approach. This because some inputs of the system, such as the production of the photovoltaic generator, the power required by the vehicles in the charging processes and the presence of vehicles connected and available for the V2G mode, are affected by intrinsically random temporal variations. The approach adopted to take into account the uncertainty of these inputs is numerical, and it is based on the Monte Carlo method. This method is used for stochastic simulations, where the input data are obtained in a pseudo-random way starting from the probability density functions (PDF) of the random variables of interest. An example of randomly-generated inputs are shown in Figure 83 for the solar irradiation that hits the PV panels, and in Figure 84 for its load. These profiles are generated from the PDF previously discussed (see Section 2.4). Samples of inputs thus obtained are used in the deterministic model to create datasets the outputs of interest, which can then be used for statistical analysis. Through the stochastic solution of the optimization problem, the time intervals of the storage system usage of the infrastructure and vehicles for the V2G are most likely identified. In the same way, the initial value of the SOC of the integrated storage system, to achieve optimal operation of the infrastructure is also identified. Starting from the initial SOC, and the average distribution of photovoltaic energy of the load and in the presence of vehicles in V2G, the platform determines the optimal activity scheduled for the following day.

The system illustrated so far shall be integrated with another real-time control system consisting of a numerical platform to tune the control system of the entire system according to the differences between model output and the actual operating conditions of the system. Starting from a forecasting exercise set for a generic day, the management and control system optimizes the power flows in the charging infrastructure in real time, defining the new power values to be drawn from different sources according to the variations occurring during the operation of the infrastructure. This algorithm can be implemented with several approaches including an expansion of the fuzzy model already presented above. However, the study of this algorithm goes beyond purpose of this work.

Figure 83: Randomly generated profiles of the power produced by PV in January.

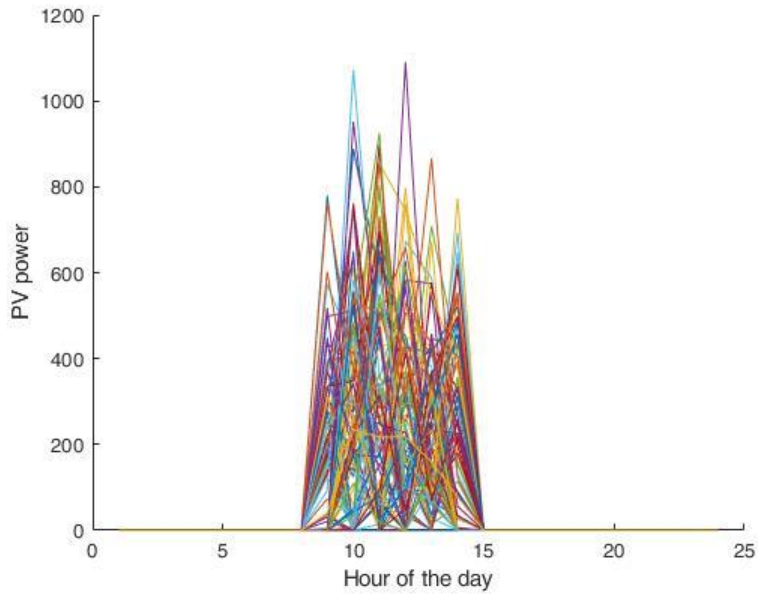

Figure 84: Randomly generated power load profiles for Turku in January.

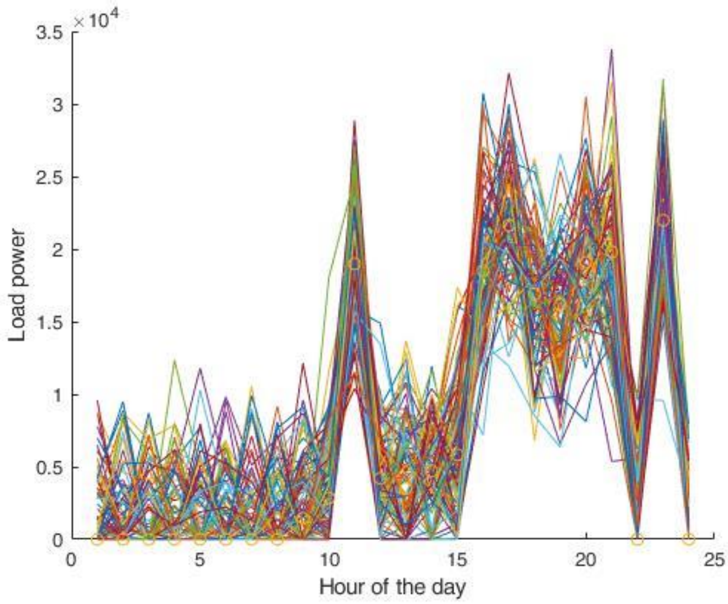

4.6.1 No BEES

We start the analysis considering the charging infrastructure with only a PV system as a renewable energy source. We will consider efficiency lower than one for all the system components.

For AMB, the technical-economic evaluation gave an optimal size of 27.5 kW for the PV system without BEES. In Figure 85 we reported the stacked histogram representing the contribution of different power sources to supply the loading demand in a typical day of January (a) and June (b). The bar of each color represents a definite contribution: the red bars are the grid contribution, the blue ones are for the PV contribution, while the yellow ones represent the amount of PV power in excess and available to be sold to the grid.

Figure 85: Power fluxes and optimal operation of a CI with a 27 kW PV during a day of (a) January, (b) June for AMB

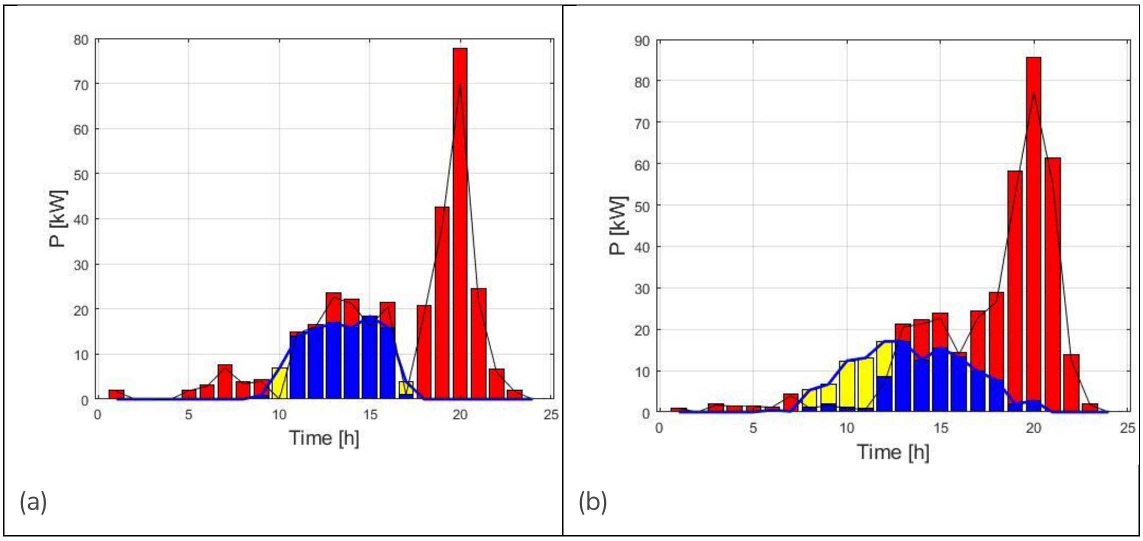

The PV energy is almost completely used for the load demand in January, while in June almost half of the energy produced cannot be used for the load, and could be sold to the grid, if and when possible. For comparison, we analyzed the results in the case of a PV of 35 KW system, roughly corresponding to the optimal size when a BEES is present. Figure 86 reports the result for the power flux.

Figure 86: Power fluxes and optimal operation of a CI with a 35 kW PV during a day of (a) January, (b) June for AMB.

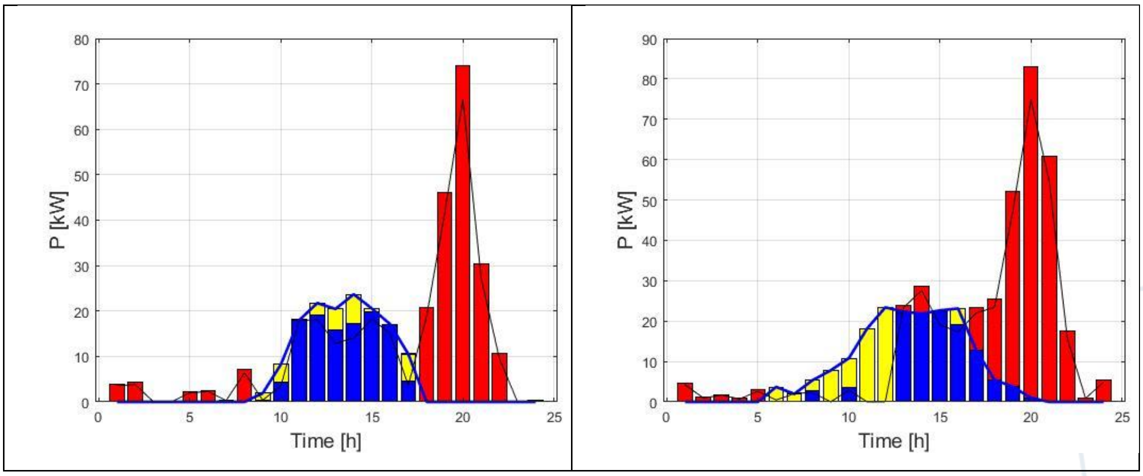

(a)	(b)

As for the PV power consumption, in a typical day of June we have a situation similar that one observed for the 27 kW PV, in the case of energy distribution among used and available for sale PV power. In January, the typical daily consumption shows higher percentage of PV energy not directly used for the demanding load.

From the results obtained in the planning phase for Turku (2.4 kW for optimal PV size with no BEES), it is clear that the energy demand is almost entirely supplied by the electricity system, as shown in Figure 87 that reports the power distribution for a representative day in the months of January and June. In Figure 87, the blue bar is the PV power used while the red bar is the grid power used, with the black line representing the power load, the blue line the PV production.

Figure 87: Power fluxes and optimal operation of a CI with a 2.4 kW PV (a) January, (b) June for the city of Turku.

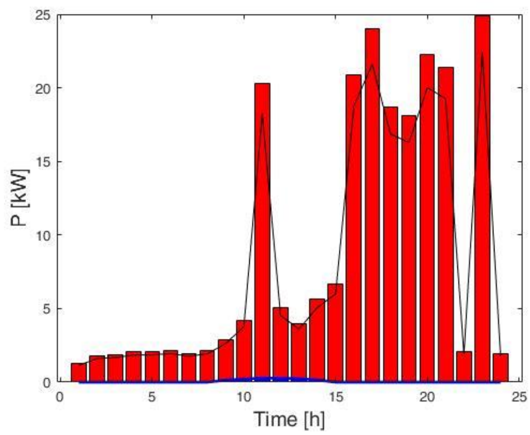 (a)	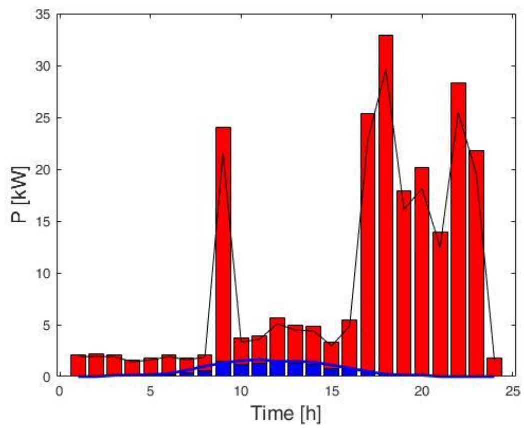 (b)

The discrepancy between the grid and photovoltaic power values compared to the load and solar production values is due to the conversion efficiency of the individual systems. This means the effective power supplied by the photovoltaic system is lower than the ideal one, just as the effective energy supplied by the grid is greater than that used due to the conversion losses.

With a size of 2.4kWp, the savings calculated as the difference between the operating costs without and with the PV system are about 120 euros per year, while for the PV 15 kWp the average annual saving is about 490 euros. Although revenues are higher for larger PV sizes, the fact the NPV is negative means that they are not enough significant to pay back the initial investment. For comparison, the breakdown of energy sources to meet demand in the case of PV 15 kWp shows that, in June, some of the energy produced by photovoltaics is not consumed for the load (yellow bar, Figure 88).

Figure 88: Power fluxes and optimal operation of a CI with a 15 kW PV for Turku: (a) January, (b) June.

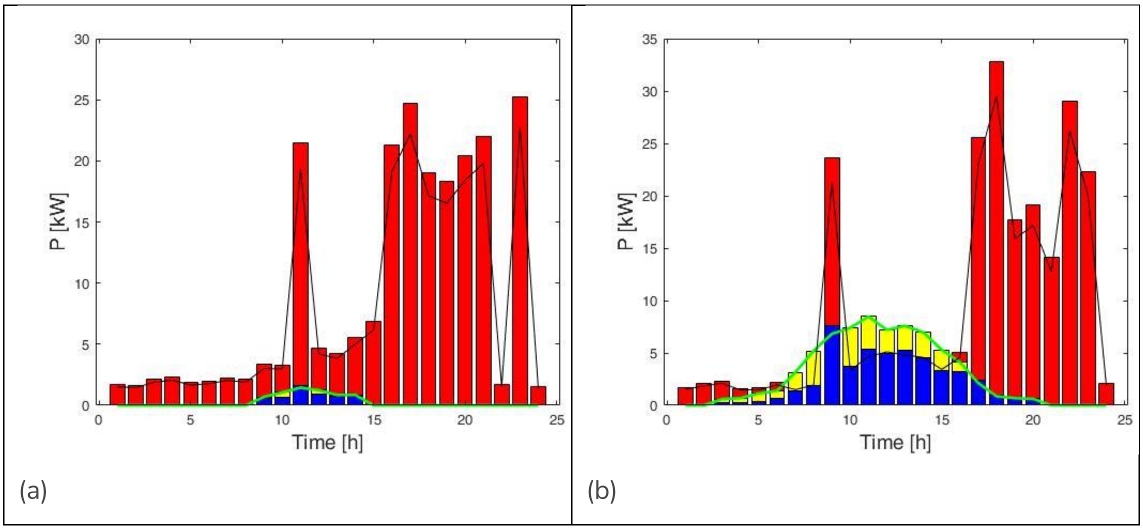

The extra power produced by the PV can be sell to the network to improve the investment revenues, but the actual profit depends on the purchase price and therefore, cannot be quantified without additional information.

4.6.2 PV and BEES

When the PV system is coupled with a BEES, the power fluxes modify. In the simulation, the degradation of the battery has been included. Indeed, at every charge/discharge operation, it is associated a cost calculated in the CI planning (see BESS and PV cost). In this analysis, we allowed the SOC varying between 20% and 100%. Moreover, it is allowed to use the BESS for power-shifting from the load.

In the following, we illustrate two simulation for AMB. For both runs, we use the optimal value for the PV found in the section 4.5.2.1.1 “BESS”, and two different values for the BEES. In the first one, the BEES is 15 kWh and the results are reported in Figure 89. The top stacked histogram chart represents the contribution of the different energy sources to the power demand of the load. In particular, the red bar is the grid contribution, the blue bar is the PV contribution, and the cyan is the BEES contribution. The yellow bar represents the PV power exceeding the load demand and that can be sold to the grid, while the magenta is the power withdrawn from the grid to charge the battery. The bottom chart represents the SOC of the battery during the day.

Figure 89: Power fluxes and optimal operation of a CI with a 35 kW PV system and a 15 kWh BEES for AMB: (a) January, (b) June.

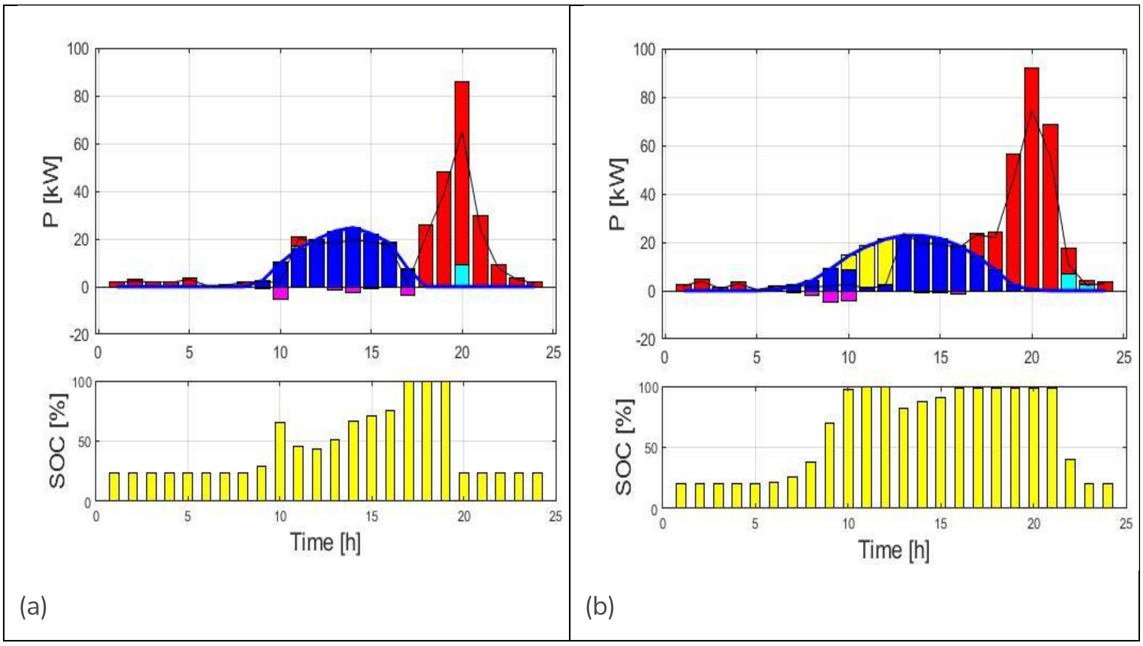

Briefly, the battery takes part to the power flux exchange helping the self-consumption. In fact, the surplus of PV power is used to charge the battery (the part of the bleu bar exceeding the black line), as it can be seen at 10 am, 1-2pm and 5pm during the day of January (Figure 89 (a)). From Figure 89 (b) it can be seen that a part of the PV energy produced is not absorbed by the BEES (yellow bar), since the battery SOC has already reached 100% value (10 am).

In the following, we consider a BEES size of 35 kWh for a typical day of January and June (Figure 90). The contribution of the BEES is similar to the previous simulations but with a larger energy delivered. On the other hand, in a typical day of January (Figure 90 (a)), the SOC variations are slightly less than in the previous simulations. However, since the BESS size is bigger, the total energy exchanged with the BEES is greater than the previous case.

Figure 90: Power fluxes and optimal operation of a CI with a 35 kW PV system and a 35 kWh BEES for AMB: (a) January, (b) June.

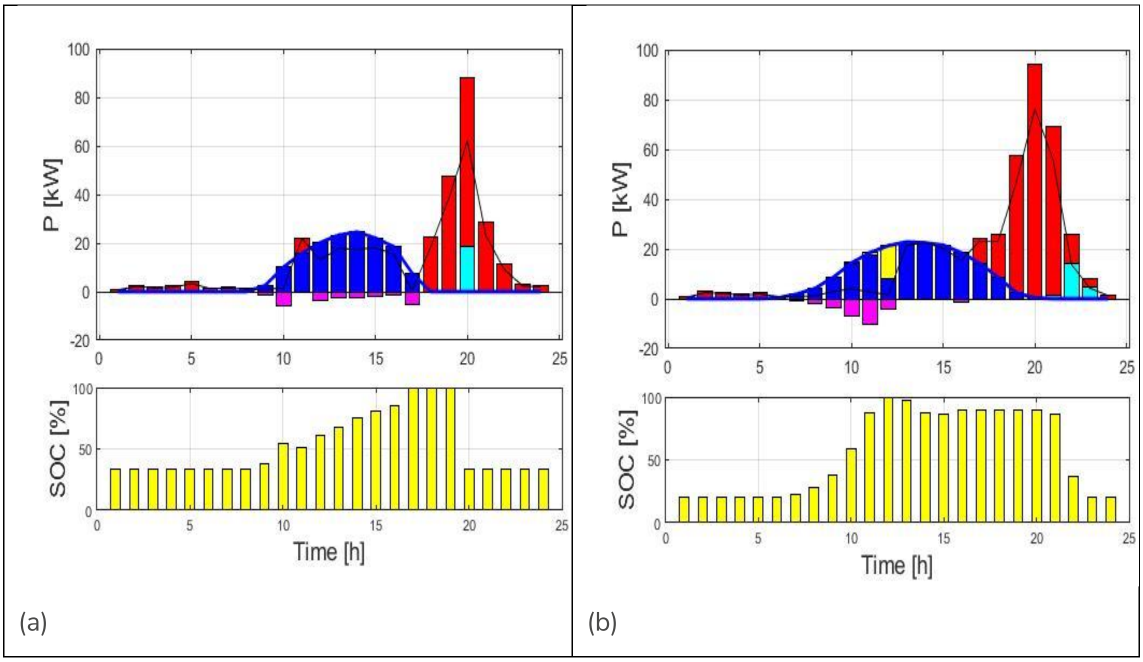

For the city of Turku we consider a 15kW system to simulate the possible roles of the BEES, since for a PV of 2.4 kW the energy is almost used up to its production therefore, the involvement of the BEES is minimal. In Figure 91, we show the results for the optimal usage of a 15 kW PV system and a 5 kWh BEES in a representative day of January (a) and July (b). As observed before, the top stacked histogram represents the contribution of the different energy sources to the power demand of the load, while the bottom histogram represents the SOC of the battery during the day.

Figure 91: Power fluxes and optimal operation of a CI with a 15 kW PV system and a 5 kWh BEES for the city of Turku: (a) January, (b) June.

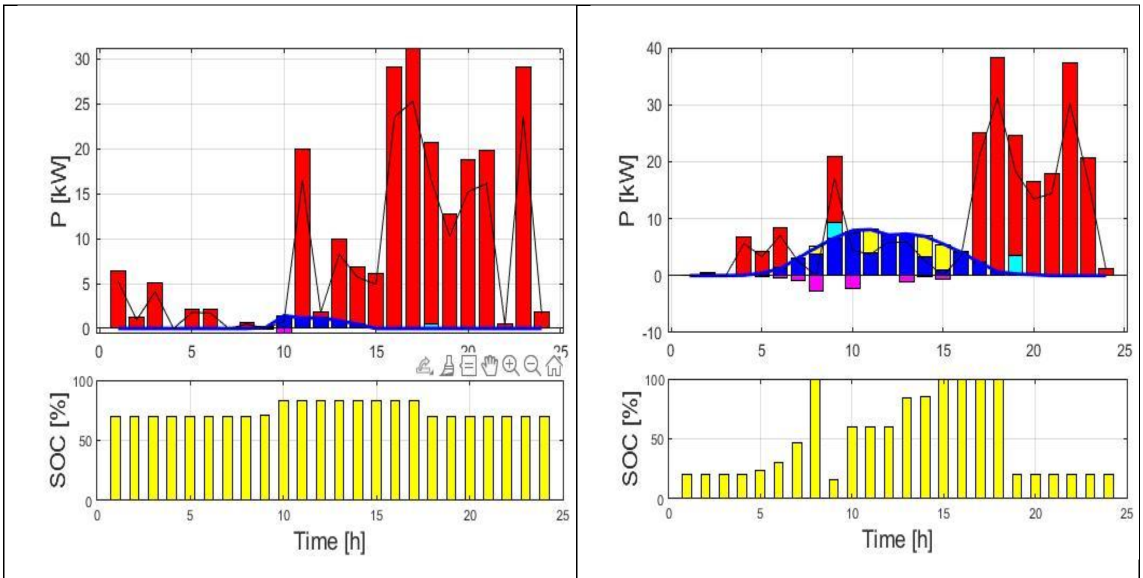

(a) (b)

Form Figure 91 we can see the BEES usage is less pronounced in January when the SOC varies between 70% and 83%, than in June when the SOC varies between 20% and 100%. In January, the BEES is only charged from the grid, while in June it is charged also from the PV. It can be seen that some of the PV production of June cannot be absorbed by the BESS (yellow bar in the upper chart in Figure 91(b)) because the amount of energy produced exceed the battery capacity.

In the following, we simulate the case of a 15 kWh BEES. The results are reported in Figure 92 where we used the same color convention to describe the outputs.

Figure 92: Power fluxes and optimal operation of a CI with a 15 kW PV system and a 15 kWh BEES for the city of Turku: (a) January, (b) June.

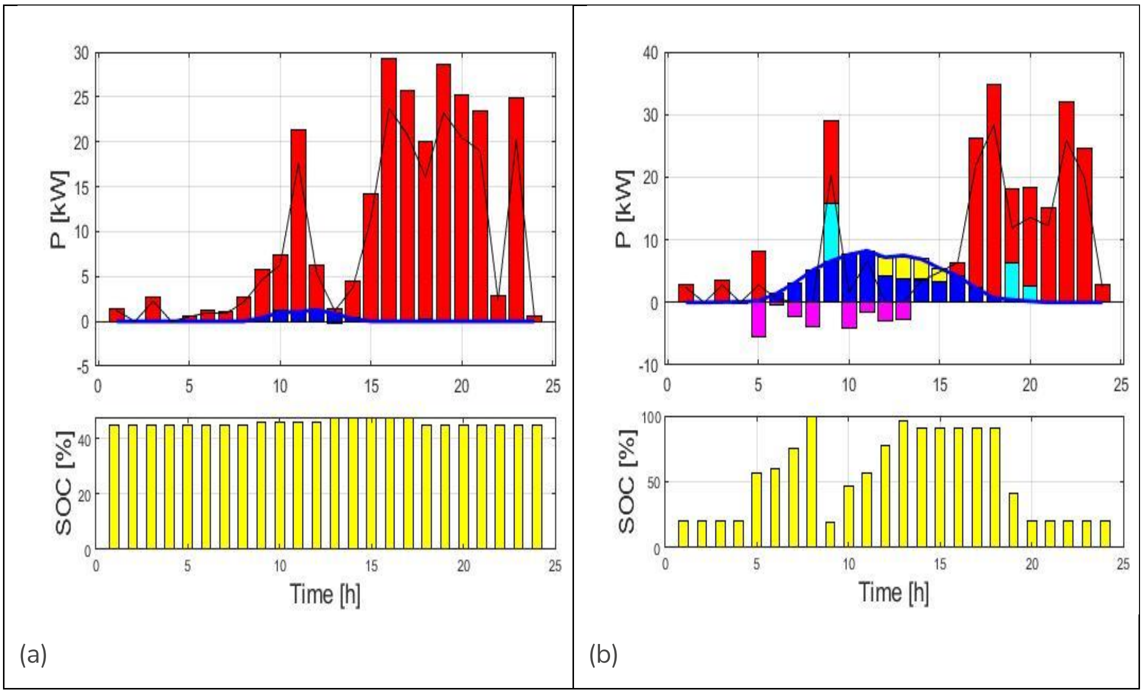

For this BEES size, the battery usage is similar to the case above illustrated. Indeed, during the day of January the SOC ranges between 45% and 48%, which is a very shallow percentage variation. However, during the day of June, the usage of the battery intensifies, and the SOC varies between 20% and 100%, so the use of the BESS is profitable during the summer time. Hoverer, a percentage of PV production in June remains unused (yellow bar in the upper chart) also in this case.

It can be concluded that, for the operation of the charging infrastructure with PV, the presence of the BEES is beneficial. Because of that, there is a decrease in the energy withdrawer from the grid and an increase in the exploitation of the PV production. Note that the use of BESS is very different in the AMB case study and the Turku case study. While in AMB case the storage is exploited both during the summer and winter months, in the case of Turku the BESS is practically never used in the winter, making the investment less convenient. However, given the present BESS CAPEX, the investment costs are still too high to make the overall project convenient without incentives also for the AMB case, as seen in the analysis of the NPV.

4.6.3 V2G

In this section we analyze a possible scenario for the implementation of V2G. To illustrate this possibility, we have considered a scenario built with AMB data because of its high daily station vehicle flow, and therefore represents a better opportunity for V2G than the Turku city dataset.

About the cost of energy made available by V2G vehicles, a possible rate was not considered, but an economic return for owners was instead assumed equal to the cost of degrading their EV battery pack.

On average, two vehicles per day are supposed participating in the V2G. Their average parking time is around 10 hours in a day. The battery pack is supposed to be equal for all the car and of fixed size of 24 kWh. The minimum threshold for the SOC level is supposed to be 20%. We assume that V2G mode can be performed in two ways: with direct allocation or with time-shifting. In the first case, the EV battery supplies power to the charging station when there is a peak in load demand. In the second case, the energy supplied by the car battery is stored in the BESS to be used later.

Figure 93 shows the results for a PV system of 35 kWp and a BESS of 15 kWh. The first chart refers to power fluxes, while the second bar chart (green) is the power delivered by the vehicles to the grid and the third is the SOC of the stationary battery.

Figure 93: Power fluxes and optimal operation of a CI with a 35 kW PV system and a 15 kWh BESS for AMB and V2G: (a) January, (b) June.

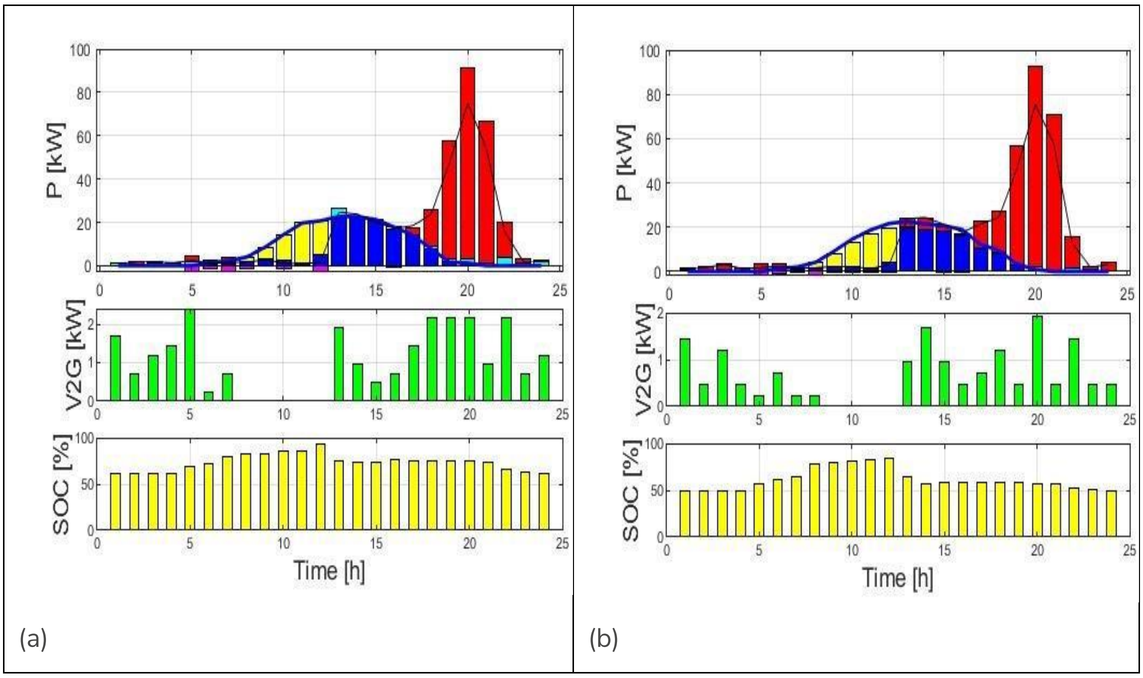

We can see that the contribution of the EV batteries is quite small compared to the level of power at the CI.

Furthermore, for the electro-mobility scenario considered in this numerical simulation, it is convenient to use the V2G but only in direct allocation towards the charging station. The V2G time-shifting mode is still not convenient due to the degradation cost of the stationary storage system, and the greater energy losses related to the further charging / discharging process of the latter compared to the direct allocation mode.

5. Conclusions

The study reported in this paper investigated several topics related to the issues of charging electric vehicle batteries and charging stations. In particular, the following topics of the problem were analysed:

- Battery modeling. The model proposed to simulate the behavior of a battery is an equivalent circuit model. It was built and validated on experimental data of lithium-ion cells. The model was used to evaluate the response of an automotive battery to different charging profiles. The model was also compared with the one proposed by the MatLab software library. The results show the dynamics of recharging are governed by much longer times compared to the battery relaxation making sufficient the use of simplified models compared to the proposed one.
- Recharging strategies. An overview of the main characteristics of different recharging strategies was proposed. Furthermore, a particular time-shifting strategy was proposed based on fuzzy logic, which showed capability of facilitating peak-shaving at the charging station.
- An algorithm was proposed for assessing the technical-economic feasibility of a charging station based on the Net Present Value. In addition, a sensitivity analysis was made for some parameters of the problem. The algorithm was applied to data from the city of Turku and Barcelona. Starting from the obtained results, the average monthly power flows of a selected year were analyzed through a Monte Carlo simulation based on the typical curves of the random input variables. The power flows in presence of vehicles for the vehicle-to-grid were also illustrated.

Results show there are several strategies to implement charging structures that can be integrated with the smart-grid sustainably. The presence of renewable energy sources and stationary storage is a beneficial element for the energy sustainability of the stations. However, economic investment requires an appropriate incentive policy to be convenient, especially in Northern Europe.

Acronyms

Acronym	Meaning
AMB	Municipal area of Barcelona
AC	Alternating current
BESS	Battery energy storage system
BMS	Battery Management system
BoS	Balance of system
BTM	Behind the meter
DOD	Depth of discharge
CI	Charging infrastructure
CP	Charging point
D	Deliverable
DC	Direct current
EC	Eurpean Commission
EMF	Electromotive force
ES	Espana / Spain
ESS	Energy storage system
ETRA	ETRA I+D (project partner)
GA	Grant Agreement
ICT	Information and Communication Technology
IT	Italy
Lcc	Linear correlation coefficient
NMC	Nickel –Manganese-Cobalt
OCV	Open circuit voltage
P	Product
PDF	Probability density function
PV	Photovoltaic
RC	Resistance-capacitor
RES	Renewable energy source
SOC	State of charge
T	Task
USER-CHI	Project Title: innovative solution for USER centric CHarging Infrastructure

Acronym	Meaning
V2G	Vehicle to grid
V2V	Vehicle to vehicle
WP	Work Package

References

[1]. Battery energy storage white paper, SUSCHEM, 2018, http://www.suschem.org/publications (last access: 11/09/2020)

[2]. N. Andrenacci and F. Vellucci, “Batterie per Applicazioni Veicolari”, 2018 (It.), URL: www.simte.enea.it (last access: 22/02/2020)

[3]. P.P. Prosini, “Accumulatori Elettrochimici per Uso Stazionario Accumulatori Elettrochimici per Uso Stazionario”, 2018 (It.) http://simte.enea.it/tecnologie.php?idSettore=2&idBrief=43&idBrief=43#card

[4]. M Doyle, TF Fuller, J Newman, “Modeling of galvanostatic charge and discharge of the lithium/polymer/insertion cell”, Journal of the Electrochemical Society 140 (6), pp. 1526-1533, 1993

[5]. M Doyle, TF Fuller, J Newman, “Relaxation phenomena in lithium-ion-insertion cells,” Journal of the Electrochemical Society, vol. 141, no. 4, pp. 982 – 990, 1994.

[6]. Barreras, J. V., Schaltz, E., Andreasen, S. J., & Minko, T. (2012). Datasheet-based modeling of Li-Ion batteries. In Proceedings of the 2012 IEEE Vehicle Power and Propulsion Conference (pp. 830-835). IEEE Press. https://doi.org/10.1109/VPPC.2012.6422730

[7]. Barai, A., Uddin, K., Widanage, W.D. et al. A study of the influence of measurement timescale on internal resistance characterisation methodologies for lithium-ion cells. Sci Rep 8, 21 (2018). https://doi.org/10.1038/s41598-017-18424-5

[8]. Hongwen He, Rui Xiong, Hongqiang Guo, Shuchun Li, Comparison study on the battery models used for the energy management of batteries in electric vehicles, Energy Conversion and Management,Volume 64, 2012

[9]. http://www.europeanenergyinnovation.eu/Articles/Winter-2016/Costs-and-Economics-of-Electricity-from-Residential-PV-Systems-in-Europe (last access: 22/02/2020)

[10]. Jairo Cervantes, Fred Choobineh, Optimal sizing of a nonutility-scale solar power system and its battery storage, Applied Energy, Volume 216, 2018, Pages 105-115.

[11]. Chen L (2009) Design of duty-varied voltage pulse charger for improving Li-ion battery-charging response. IEEE Trans Industr Electron 56(2):480–487

[12]. Qian Lin, Jun Wang, Rui Xiong, Weixiang Shen, Hongwen He, Towards a smarter battery management system: A critical review on optimal charging methods of lithium ion batteries, Energy, Volume 183, 2019, Pages 220-234.

[13]. P. Y. Kong and G. K. Karagiannidis, “Charging schemes for plug-in hybrid electric vehicles in smart grid: A survey,” IEEE Access, vol. 4, pp. 6846–6875, 2016.

[14]. W. Ma, V. Gupta and U. Topcu, "Distributed Charging Control of Electric Vehicles Using Online Learning," in *IEEE Transactions on Automatic Control*, vol. 62, no. 10, pp. 5289-5295, Oct. 2017, doi: 10.1109/TAC.2016.2636740.

[15]. https://it.mathworks.com/help/physmod/sps/powersys/ref/battery.html

[16]. Tremblay, O., L.A. Dessaint, "Experimental Validation of a Battery Dynamic Model for EV Applications." *World Electric Vehicle Journal*. Vol. 3, May 13–16, 2009.

[17]. Rajab Khalilpour, Anthony Vassallo, Planning and operation scheduling of PV-battery systems: A novel methodology, Renewable and Sustainable Energy Reviews, Volume 53, 2016, Pages 194-208.

[18]. Ramoni, M.O., Zhang, HC. End-of-life (EOL) issues and options for electric vehicle batteries. Clean Techn Environ Policy 15, 881–891 (2013). https://doi.org/10.1007/s10098-013-0588-4
[19]. Liu Y, Hsieh C, Luo Y (2011) Search for an optimal five-step charging pattern for Li-ion batteries using consecutive orthogonal arrays. IEEE Trans Energy Convers 26(2):654–661
[20]. Lazard, 2017. Lazard's levelized cost of storage analysis - version 3.0, u.o.: Lazard
[21]. Belderbos, A., Delarue, E., Kessels, K. & D'haeseleer, W., Levelized cost of storage - introducing novel metrics. Energy economics, September, Volym 67, 2017, pp. 287-299.
[22]. Mayr, F. & Beushausen, H., 2016. Navigating the maze of energy storage costs. PV Tech Power, May, Volym 7, pp. 84-88.
[23]. O. Veneri, L. Ferraro, C. Capasso and D. Iannuzzi, "Charging infrastructures for EV: Overview of technologies and issues," 2012 Electrical Systems for Aircraft, Railway and Ship Propulsion, Bologna, Italy, 2012, pp. 1-6, doi: 10.1109/ESARS.2012.6387434.
[24]. Wajahat Khan, Aqueel Ahmad, Furkan Ahmad & Mohammad Saad Alam (2018) A Comprehensive Review of Fast Charging Infrastructure for Electric Vehicles, Smart Science, 6:3, 256-270, DOI: 10.1080/23080477.2018.1437323
[25]. Matthias, B. & Brearley, D., 2016. Residential Energy Storage economics. SolarPro, july/aug, Issue 9.4.
[26]. https://www.pvxchange.com/en/market-analysis-april-2019-fridays-forever (last access 09/09/2020)
[27]. World Energy Council, 2016. E-storage: Shifting from cost to value, wind and solar applications, London: World Energy Council.
[28]. IRENA, 2017. Electricity storage and renewables: Costs and markets to 2030, Abu Dhabi: International Renewable Energy Agency.
[29]. Vartiainen, E, Masson, G, Breyer, C, Moser, D, Román Medina, E. Impact of weighted average cost of capital, capital expenditure, and other parameters on future utility-scale PV levelised cost of electricity. Prog Photovolt Res Appl. 2020; 28: 439– 453. https://doi.org/10.1002/pip.3189.
[30]. E. Vartiainen, G. Masson, C. Breyer, PV COSTS IN EUROPE 2014-2030, URL: https://etip-pv.eu/publications/etip-pv-publications/?page=2 (latest access: 18/01/2021)
[31]. Fraunhofer ISE (2015): Current and Future Cost of Photovoltaics. Long-term Scenarios for Market Development, System Prices and LCOE of Utility-Scale PV Systems. Study on behalf of Agora Energiewende. URL: https://www.agora-energiewende.de/en/publications/current-and-future-cost-of-photovoltaics/ (latest access: 18/01/2021)
[32]. K. Mongird, V. V. Viswanathan, P. J. Balducci, M. J. E. Alam, V. Fotedar, V. S. Koritarov, B. Hadjerioua, Energy Storage Technology and Cost Characterization Report. United States. 2019.
[33]. https://ec.europa.eu/jrc/en/pvgis
[34]. U. Abronzini et al., "Multi-source power converter system for EV charging station with integrated ESS," 2015 IEEE 1st International Forum on Research and Technologies for Society and Industry Leveraging a better tomorrow (RTSI), Turin, 2015, pp. 427-432, doi: 10.1109/RTSI.2015.7325135.
[35]. Jordan, D.C. and Kurtz, S.R. (2013), D. C. Jordan and S. R. Kurtz. Prog. Photovolt: Res. Appl., 21: 12-29. https://doi.org/10.1002/pip.1182

[36]. https://news.energysage.com/average-solar-panel-size-weight/
[37]. https://www.acea.be/statistics/article/Share-of-diesel-in-new-passenger-cars
[38]. https://www.iea.org/reports/global-ev-outlook-2020#prospects-for-electrification-in-transport-in-the-coming-decade
[39]. Marra, F., Yang, G. Y., Træholt, C., Larsen, E., Rasmussen, C. N., & You, S. (2012). Demand Profile Study of Battery Electric Vehicle under Different Charging Options. In Proceedings of the 2012 IEEE Power & Energy Society General Meeting IEEE. https://doi.org/10.1109/PESGM.2012.6345063
[40]. https://electricrevs.com/2018/03/09/jaguar-and-chevy-have-lg-in-common/
[41]. https://en.wikipedia.org/wiki/Nissan_Leaf#First_generation_(ZE0/AZE0;_2010-2017)
[42]. https://www.mckinsey.com/industries/automotive-and-assembly/our-insights/second-life-ev-batteries-the-newest-value-pool-in-energy-storage# (latest access: 20/02/2021)
[43]. https://www.capgemini.com/2019/04/second-life-batteries-a-sustainable-business-opportunity-not-a-conundrum/#_ftn3 (latest access: 20/02/2021)

-

6. Annex A – Electrochemical energy storage

In the following, we present an overview of the main characteristic for some of the most common chemistries for electrochemical batteries.

6.1 Lithium batteries

Lithium-ion (Li-ion) cells exists in different chemistries with specific power vs. energy characteristics. They have high energy densities (100-265 Wh/kg or 250-670 Wh/L), and can deliver up to 3.6 Volts, 3 times higher than technologies such as Ni-Cd or Ni-MH. [3 A] They also show high efficiency (near 100%) and long life cycle combined with long calendar life.

Li-ion technology is also very versatile, since the cells can be combined to obtain batteries that reach any voltage, power and energy requirement, with power to energy ratios ranging from very high power (i.e. 10kW / kWh) to very high energy.*[1 A]* However, this battery packs require sophisticated control electronics in order to avoid quick aging and safety issues.

In Li-ion cells, the negative electrode (in which the oxidation process takes place during discharge and reduction in charge) is generally based on carbon or graphite. A less common but interesting technology uses lithium titanate. This compound has better performance at extreme temperatures. Moreover, it can extend the duration of the battery since it does not form a solid electrolyte interface (SEI) film or lithium plating when charging at low temperatures or during fast charging. Indeed, lithium titanate batteries can reach up to 7 000 cycles. The main disadvantage of this material is its high cost as well as its low specific energy density of 50 Wh/kg and a low operating voltage range (typically, 1.8 - 2.85V).

The positive electrode (in which the discharge reduction and charge oxidation process take place) is generally based on lithium oxides and transition metals or phosphates. The materials used for the positive electrode can be classified into three categories, namely: layered oxides whose general formula is Li [M] O2; spinel oxides (spinel oxides), whose general formula is Li [M] 2O4, and lithium iron phosphate LiFePO4. In the previous formulas, [M] can represent a transition metal (Co, Mn, Ni.) or even a metal such as Al, Mg, etc.

Typically, the electrolyte is a non-aqueous organic solvent in which lithium salts are dissolved. A separator formed by a porous material, usually a polymeric membrane or ceramic material, physically keeps the two electrodes separated to avoid short-circuits during ionic diffusion. Electrolytes consisting of solid polymers offering greater stability and safety than liquid ones can also be used, but they have a higher impedance and therefore, might have lower performances.

Knowing the several technologies and chemistries behind Li-ion cells, we can say all Li-ion batteries operate with the principle of intercalation, with lithium ions incorporated into the electrode. However, the mathematical description of the battery behavior is complex due to the non-linear effects observed during the discharge and charge phase and to the superimposition of the irreversible changes in the characteristics of the cell components, which are at the basis of the aging processes of the batteries.

6.2 Lead Batteries

Lead batteries have been used for over a century in many industrial applications, from grids to vehicles, and they cover nearly 80% of the total installed capacity of industrial batteries [1 A]. In lead-acid batteries, the electrodes are two flat lead plates, immersed in a pool of electrolyte and with a separator placed between them. The positive electrode is covered with a lead dioxide, while the negative is made of sponge lead. Generally, lead-acid batteries require a longer charging time than other batteries because of the formation of lead sulphate on the negative electrode.

Different kinds of lead-acid batteries are commercialized and they can require some maintenance as in the case of the flooded cells Other types of lead batteries can be maintenance-free, as in the case of the valve-regulated lead-acid (VRLA) batteries (gelled electrolyte, absorbed glass mat). Energy density of lead batteries varies between 30 to 50 Wh/kg, the cell voltage is 2V, and systems can go up to 300 cycles.[2 A]

6.3 Nickel-based Batteries

Nickel-based batteries (also known as alkaline cells) are among the most used electrochemical storage system. They are very robust and reliable when operating in critical environments. They can be easily connected without the need of sophisticated management systems.

Nickel Cadmium (NiCd) was the first type of Ni-based battery. They use nickel hydroxide for the cathode, cadmium as the anode and an alkaline potassium hydroxide as the electrolyte. Standard NiCd cells use a non-aqueous chemical impregnation process for the manufacture of the electrodes. NiCd technology has been used for the accumulation of electrical energy in spacecraft since the beginning of space exploration. It has fast charging capability, long cyclic life (more than 1 000 cycles), good low- and high-temperature performance, long shelf life in any state of charge. The memory effect is one of its major disadvantages together with the high rate of self-discharge at high temperature. NiCd has also a relatively low specific energy density of 45 – 80 Wh/kg . Since cadmium is highly toxic, its use in batteries is now prohibited, with the exception of some medical and military applications.

Nickel Metal Hydrate (NiMH) batteries use nickel hydroxide for the cathode. Hydrogen is used as an active element that is absorbed at the anode. This electrode is made from a metal hydrate, usually lanthanum, and rare earth alloys acting as a solid source of reduced hydrogen. The electrolyte is alkaline, usually potassium hydroxide.

NiMH batteries have higher energy density than NiCd cells, fast charging capacity, long cyclic life, and long shelf life in any phase of charge. There are minimal environmental problems. However, their high current performance is inferior to that of NiCd. The low charge retention, the memory effect, and the higher cost of the anode are the main disadvantages of this type of battery. This technology has been used in computers, cell phones, and other consumer electronics applications, with the possible exceptions of applications where low battery cost is the major constraint. This type of battery was the original choice for hybrid vehicles. However, lithium-ion batteries are gradually occupying the market of electric and plug-in hybrid vehicles, NiMH batteries were an important technology until lithium-ion batteries reached sufficient technological maturity. However, their greater weight, lower energy density, and lower ability to perform deep cycling mean they will not be able to compete with lithium-ion batteries for next-generation electric and plug-in hybrid vehicles. [1 A]

6.4 Sodium Sulphur batteries

Two types of sodium-based batteries are available: sodium-sulfur (NaS) batteries and sodium-nickel chloride (NaNiCl2) batteries. Both operate at an internal temperature above 250 ° C since they use molten sulfur as the positive electrode and molten sodium as the negative electrode. The two electrodes are separated by solid ceramic sodium alumina, which acts as the electrolyte as well.

Sodium-sulfur (NaS) batteries were developed in the early 1980s, and are used exclusively in industrial applications such as electrical storage for grid support and aerospace applications. Test results of sodium-sulfur batteries for electric vehicles in the early 1990s revealed that this technology is not suitable for automotive applications.

Sodium-nickel chloride (NaNiCl2) batteries have been marketed since the 1990s and originally found application in "heavy-duty" electric and hybrid vehicles such as buses, trucks, vans (for example, IVECO Electric EcoDaily fleets in Bologna, Rome, Lyon, Barcelona, Madrid).

So-called Zebra batteries, which operate above 270 °C, use sodium tetrachloraluminate (NaAlCl4), which has a melting point of around 160 °C, as the electrolyte. The negative electrode is molten sodium. The positive electrode is nickel during the discharge and nickel chlorite in the charging phase.

Zebra batteries have a specific energy and power of 90 Wh/kg and 120 W/kg respectively. The electrolyte liquid freezes at 157 °C and the normal operating temperature range is 270 ÷ 350 ° C.

The β-alumina solid electrolyte that was developed for these systems is very stable and are usually metallic sodium and sodium tetrachloroaluminate.

When not in use, Zebra batteries are typically kept with molten electrolyte to be ready for use when needed. However, this imply a certain rate of self-consumption for the battery. If off, the heating process lasts 12 hours and then a charge of 6 ÷ 8 hours is required to reach the fully charged state again. Applications include traction batteries, heavy-duty electric and plug-in hybrid vehicles, buses, trams, railway applications.[1 A]

6.5 Flow batteries

Flow batteries are somewhere in between a conventional battery and a fuel cell. There are dozens of different types of flow batteries but they all operate on the same basic principle: catholyte and anolyte (metallic salts dissolved in liquids) are stored in separate tanks, and pumps are used to circulate the fluids into a stack with electrodes separated by a thin membrane. This membrane allows ion exchange between the anolyte and catholyte to produce electricity. The reverse process is used to charge the battery. In flow batteries, the energy is stored in the electrolyte (compared to the electrodes in conventional batteries), therefore the capacity is proportional to the battery's volume. Moreover, the power produced is dependent on the surface area of the electrodes, while the storage duration is a function of the electrolyte volume. For some technologies, power and energy can be scaled independently, allowing for an easily customizable battery. Besides, the fact that electrodes do not contain active material, leads to more durable and stable performance, and longer lifetimes. Charge and discharge rates are very fast, and they have a wider operational temperature range than lithium batteries. These types of batteries have a limited fire hazard as well as a limited human health risk when exposed to them. The main disadvantage of flow batteries is their large size and their restricted use for only large stationary industrial applications. In addition, the complexity of the system of pumps, sensors, vessels, etc. required, is another obstacle to their usability.[2 A]

Bibliography

[1 A] https://www.eurobat.org/news-publications/position-papers/116-eurobat-paper-battery-energy-storage-for-smart-grids-applicationshttp://www.suschem.org/publications *(last access: 11/09/2020)*

[2 A] N. Andrenacci and F. Vellucci, “Batterie per Applicazioni Veicolari” (It.), URL: www.simte.enea.it *(last access: 09/09/2020)*

[3 A] *Lithium-ion battery, Clean Energy Institute, University of Washington, https://www.cei.washington.edu/education/science-of-solar/battery-technology (last access: 09/09/2020)*

7. Annex B - Aging

Given the very high diffusion of batteries in many applications such as electronic devices, systems for the electric traction of vehicles or renewable storage systems for stationary use, it is extremely important giving a reliable estimate of the duration (life) of the batteries within a working cycle and therefore, to implement an optimal design.

Aging of a battery is the result of its degradation during its lifetime. Since the internal processes of the battery are mostly non-linear, the evolution over time of battery degradation depends on the conditions of its use and storage, as well as on the specific technology to build the cell. In general, aging is classified in two ways:

• Shelf life (more commonly: calendar life) linked to intrinsic degradation even in conditions of non-use and therefore a function of time (as well as storage conditions);

• Cycle life, linked to the use of the battery with certain working cycles. In this case, the lifetime can be expressed with respect to various parameters, such as time, number of cycles, total capacity delivered by the battery, etc.

The fading capacity of a battery depends on its usage profiles and it also depends from the different lithium-ion chemicals used for its manufacturing [1 B]

Therefore, it is evident the study of degradation phenomena turns out to be a complex task as it must provide the development of significant tests and the use of appropriate extrapolation processes to model real-life working conditions and to make aging predictions. Furthermore, the aging and failure mechanisms are the product of several interconnected processes taking place at different time scales and that concern not only the electrodes and active materials but all the battery components.

The process of modeling the ageing phenomenon to predict the battery useful life in real world starting from laboratory tests includes the following steps:

- Definition of typical load and cycles of use;
- Design specific laboratory tests;
- Identification of the cell state of health;
- Description of the ageing through a mathematical model;
- Validation of the model

Different aging modeling approaches exist for lithium-ion batteries, similar to those illustrated in for model how the battery works (see Battery models), and we will not discuss them any further. Instead, we present two approaches that are strictly devoted to aging, namely: the theory of the fatigue for the material and a Markov chain approach.

The first approach relies on the Palmgren–Miner rule. According to this rule, the damage accumulated during a cycle or an interval of operations is added to the pre-existing damages deriving from the previous cycles or intervals of operations. In other words, this rule is equivalent to stating that the total number of cycles that produce a certain damage is given by the sum of the number of cycles performed at a certain stress level weighted by the magnitude of the stress. Furthermore, the sequence in which the various stress levels are applied has no effect on the lifespan. The hypotheses underlying the Palmgren-Miner rule are very stringent and often unsuitable even for certain applications of fatigue theory. They are also very difficult to verify for complex systems. Nonetheless, there are studies showing its applicability to battery packs. [2 B]

In the second approach, the degradation process is represented as a Markov process, in which the probability that the battery degrades increases with the aging process. A Markov process is a stochastic process that satisfies the property of being "memoryless", that is, it represents a process for which it is possible to make predictions about future results based exclusively on its current state and not on past ones. This approach has been proved to be suitable to describe capacity fade in some cases. [3 B][4 B]

However, we have found that, when the level of the stress applied to the battery is close to its limit value, the two approaches fail to describe the capacity fade. This is probably due to the fact that when the applied stress is high, the memory effect cannot be disregarded and the damage accumulates in a non-linear way. Indeed, adding a “memory effect”, the stochastic approach used in the Markov process leads to satisfying results. It should be stressed that, since a memory effect is present, the results is not a Markov process, and should be referred to as a recursive stochastic model.[5 B]

The modified approach has been applied to the results of ageing tests performed on EiG 20Ah cells, which are lithium-ion-polymer batteries with a cathode NMC technology, and a "pouch" structure. The battery cell has been aged following cycles with a depth of discharge equal to DOD = 80% (90% ≤ SOC ≤ 10%) and a continuous discharge current equal to Crate = 3C (the maximum discharge current for this battery is 5C). The charge current is 1C. In Figure 94, we report the test results for the capacity measured as a function of the number of cycles (red line).

Figure 94: Comparison among test results and models outcomes for the capacity fade of a EiG 20Ah cell.

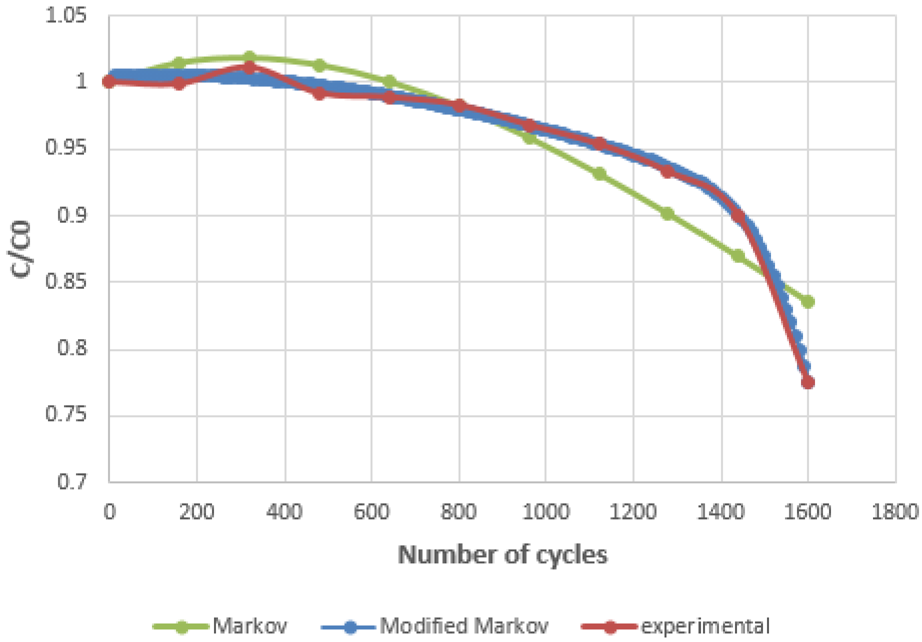

The green line represent the Markov fit to the experimental data. It is clear that it fails to reproduce the capacity fading trend, especially for the kink toward the end of life. On the other hand, the recursive stochastic ("modified Markov") model is able to fit all the characteristic of the experimental curve.

As for fast charging, we analyzed the database available from [6 B], who proposed an early-stage life prediction mode. The dataset contains the result of test on 124 cells aged using 72 different fast-charging conditions and at controlled temperature. The cells are commercial LFP/graphite cells (A123 Systems, model APR18650M1A, 1.1 Ah nominal capacity). They have found that the capacity fade is negligible in the first one hundred cycles and accelerates near the end of life, as we also observed in the EiG 20Ah cells. These data on fast-charges have been created for fast charging protocols that provide both charging up to 80% always with the same current, and with 2 steps at different currents. To compare the effects of fast charging, we calculated a weighted average charging current and compared it with the number of life cycles achieved. A linear correlation coefficient of -0.9 is obtained between current and life span, as shown in Figure 95.

Figure 95: Correlation among lifespan (in number of cycle) and charging current (in C-rate).

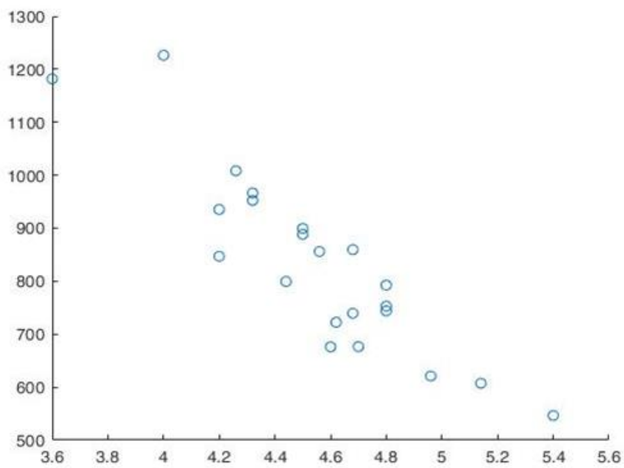

Considering as goodness-of-fit coefficient the R-square coefficient[6], we obtain that the second order polynomial fit gives R-square of 0. 8173, and the linear fit gives R-square of 0.8132. The fitting has been done usign the CurveFitting tool of MatLab. The resulting expressions are:

$C_{loss} = 46.61 * \mathrm{I}_c{}^2 - 822.6 * I_c + 3602$ (b1)

$C_{loss} = -401.6 \ * \ I_c + 2659$ (b2)

Where C_{loss} is the capacity loss and I_c is the average charging current applied. Using this fits, one can predict the capacity loss of a battery that is recharged with a given average current in a certain duty cycle.

[1 B] E. M. Krieger, J. Cannarella, C. B. Arnold, A comparison of lead-acid and lithium-based battery behavior and capacity fade in off-grid renewable charging applications, Energy, Volume 60, 2013, Pages 492-500, ISSN 0360-5442, https://doi.org/10.1016/j.energy.2013.08.029.

[2 B] Chin-Yao Chang, Punit Tulpule, Giorgio Rizzoni, Wei Zhang, Xinyu Du, A probabilistic approach for prognosis of battery pack aging, Journal of Power Sources, Volume 347, 15 April 2017, Pages 57-68, ISSN 0378-7753, https://doi.org/10.1016/j.jpowsour.2017.01.130.

[3 B] Michelusi N, Badia L, Carli R, Corradini L, Zorzi M. Energy management policies for harvesting-based wireless sensor devices with battery degradation. IEEE T Commun 2013;61:4934–47.

[4 B] Risse S, Angioletti-Uberti S, Dzubiella J, Ballauff M. Capacity fading in lithium/sulfur batteries: a linear four-state model. J Power Sources 2014;267:648–54

[5 B] N. Andrenacci, V. Sglavo, F. Vellucci, Modello di invecchiamento per le celle litio-ione applicato a celle NMC invecchiate in ENEA, (in It.), https://www.enea.it/it/Ricerca_sviluppo/lenergia/ricerca-di-

[6] We recall that the better is the fit the closest R-square is to 1.

sistema-elettrico/accordo-di-programma-MiSE-ENEA-2015-2017/trasmissione-e-distribuzione-dellenergia-elettrica/sistemi-di-accumulo-di-energia/report-2017
[6 B] Severson, K.A., Attia, P.M., Jin, N. *et al.* Data-driven prediction of battery cycle life before capacity degradation. *Nat Energy* **4,** 383–391 (2019). https://doi.org/10.1038/s41560-019-0356-8

8. Annex C – Questionnaire

In this appendix, we report the answers received from a questionnaire on charging infrastructure

In Table 1 we reported the AMB questionnaire, which refers to the public charging points (in the street and owned by public administrations) in Barcelona and 35 municipalities around the city, while in Table 2 the results for Turku are reported.

Table 1: Answers to the questionnaire for AMB

Charging infrastructures (CIs)	Your answer		
Which are the most common configurations for charging infrastructures in you city? (answer where apply)	**Type of charger in the CI**	**Power of chargers (typical)**	**Number of charging point for CI**
	slow	2 CPs for 3kW	2 CP
	fast	2 CPs for 43kW + 1CP for 55 kW	3 CP
	Slow+fast	2 CPs for 3kW + 2 CPs for 43kW + 1CP for 55 kW	5 CP
Are there any incentive policies for installing CI in your city?	Yes		
If yes: which ones?	The local administrations (like AMB or Barcelona city council) promote the installation of CI in the streets. In this case, the municipalities act as CPO. The regional and the national governments subsidies this infrastructure (Plan MOVES https://www.idae.es/ayudas-y-financiacion/para-movilidad-y-vehiculos/plan-moves-ii)		
Are there any incentive policies for installing RES in your city?	Yes		

If yes: which ones?[7]	The Consorci Metropolità de l'Habitatge (https://www.cmh.cat/web/cmh/ajuts/programes/programa-habitabilitat-2020) has subsidies programs oriented to the PV panels for housing
Is it allowed to install PV panels near CI in your city?	It is allowed by usually there is not enough space around the CI in urban areas. The common solution is installing PV panels on the roof of the parking lots 
If yes, could you give an estimation of the available area for installing the PV?	It is very difficult/impossible to give an estimation for that.

Table 2: Answers to the questionnaire for the city of Turku.

Charging infrastructures (CIs)	**Your answer**
Which are the <u>most common</u> configurations for charging infrastructures in you city? (answer where apply) In public charging points 22kW AC is most common charger and 50kW DC most common fast charger. In housing (overnight) most common are 3,6kW and 11kW AC chargers.	**Type of charger in the CI** / **Power of the chargers (typical)** / **Number of charging point for CI**: **slow** – 22kW – 2-4 **fast** – 50kW – 1-2 **Slow+fast** – 22+50kW – 2+1
Are there any incentive policies for installing CI in your city? If yes: which ones?	For housing charging points, there is government provided incentive for installing new charging points, up to 45% and 90k€.
Are there any incentive policies for installing RES in your city? If yes: which ones?	For solar energy government incentives are: Private housing: 40 percent of the labor costs of the system Companies: 25 percent of the system Farms: 40 percent of the system
Is it allowed to install PV panels near CI in your city?	Yes

[7] Instead of extended answer, you can link to on-line resources

Charging infrastructures (CIs)	Your answer
If yes, could you give an estimation of the available area for installing the PV?	It depends where CI are build. In downtown there are not that much potential for PV, but outside city there is almost limitless potential. Bad thing is that in Turku there is 3 winter months that are so dark, PV doesn't work. And 70 percent of all energy is produced in June to August.

In Table 3 we report the answer that Qwello GmbH provided for Munich. For this city we did not have data on charging events and therefore we did not performed any analysis in the present work.

Table 3: Answers to the questionnaire for the city of Munich

<table>
<tr><th>Charging infrastructures (CIs)</th><th colspan="3">Your answer</th></tr>
<tr><td rowspan="3">Which are the <u>most common</u> configurations for charging infrastructures in you city? (answer where apply)</td><td>Type of charger in the CI</td><td>Power of the chargers (typical)</td><td>Number of charging point for CI</td></tr>
<tr><td>slow</td><td>11-22 kW</td><td>1169 CPs in total; 2 CPs per pole</td></tr>
<tr><td>fast</td><td>100 kW</td><td>24 in total, 1 CP per pole</td></tr>
<tr><td>Are there any incentive policies for installing CI in your city? If yes: which ones?</td><td colspan="3">No, so far only the city utility provider was allowed to put up CI in larger volume. Recently the Munich tender for 2,700 AC CPs was released. In that the city does not want to pay for any infrastructure. Only governmental grants apply, which could bear up to 40% of the hardware cost</td></tr>
<tr><td>Are there any incentive policies for installing RES in your city? If yes: which ones?</td><td colspan="3">Not with regards to CI, CI must use certified green energy though</td></tr>
<tr><td>Is it allowed to install PV panels near CI in your city?</td><td colspan="3">No. Public space is very limited and valuable. To put up a PV panel on street level is impossible within the city. Only on rooftop level</td></tr>
</table>